

CNS&E

**Current Natural
Sciences &
Engineering**

Peer reviewed, Partially open-access Journal



Picture Courtesy:
Adobe Firefly

“Human Brain Intelligence cannot be Dwarfed by AI (Artificial Intelligence), a Brain Child of Human, but a Remarkable Tool to handle Colossal Data more Efficiently with a Greater Speed, Accuracy using Smart Algorithms Devoid of Emotions & New Science !”

About CNS&E

Current Natural Science & Engineering (CNS&E) Journal publishes new, innovative and cutting-edge research in Natural sciences including physical, chemical, biological, agricultural and environmental sciences, metrology, and other related interdisciplinary fields. Scientific research results in the form of high-quality manuscripts, review articles, mini-reviews, reports, news and short communications are highly welcome.

CNS&E is a partially Open Access, bimonthly, multidisciplinary journal published by the Vigyanvardhan Blessed Foundation (VBF), a non-profit organization working to disseminate science for the betterment of society.

Scope: CNS&E journal has a broad multidimensional scope. It publishes research in the areas of:

- Hydrogen & Renewable Energy
- Environmental Sciences & Hydroelectric Cell
- Green Energy & Earth Sustainability
- Net Carbon Zero & Carbon Footprint Remediation
- Condensed Matter & Nanomaterials
- Health Science & Technology
- Nuclear Science: Health & Society
- Measurement Science & Industrial Research
- Digital & Sustainable Agriculture
- Smart Engineering Materials & Sensors

Publication Policy: The journal maintains integrity and high ethical values. Submitted manuscripts are peer-reviewed and evaluated for novel scientific content irrespective of its origin. The information about a submitted manuscript will be confidential and will not be disclosed other than Chief Editor, editorial staff, corresponding author, reviewers, and the publisher. The journal ensures that any unpublished work must not be used in Editor's, and reviewer's own research without the explicit written consent of the author(s).

Publication Decisions: The Chief Editor of the journal is responsible for deciding the publication or rejection of the submitted manuscript. The Chief Editor may take suggestion with other editors or reviewers in making decision.

Publisher: VB Foundation

CNS&E Editorial Board

Chief Editor

Prof. (Dr.) R K Kotnala,

Former Chairman NABL, Raja Ramanna Fellow DAE &
Chief Scientist, CSIR-National Physical Laboratory

Senior Editors

Prof. A C Pandey

Director, Inter University Accelerator
Centre, New Delhi, India

Prof. K K Pant

Director IIT Roorkee, Uttarakhand, India

Prof. Sanjay Behari

Director, Sree Chitra Tirunal Institute for
Medical Sciences and Technology,
Thiruvananthapuram, India

Prof. R K Sinha

Vice Chancellor, Gautam Buddha
University, G Noida, India

Prof. Bhanooduth Lalljee,

President, Sustainable Agricultural
Organisation, External Professor at the
Mauritius Institute of Education (MIE) and
JSS Academy, Mauritius.

Editors

Dr. Indra Mani

Vice-Chancellor, Vasant Rao Naik
Marathwada Krishi Vidyapeeth,
Maharashtra, India

Prof Ajay Dhar

Associate Director, Academy of Scientific
and Innovative Research, AcSIR,
Ghaziabad-UP, India

Dr A K Srivastava

Director, CSIR-Advanced Materials and
Processes Research Institute, CSIR-
AMPRI, Bhopal

Dr. S K Jha

Outstanding Scientist and Head, Radiation
Protection Section (Nuclear Fuels) Health
Physics Division & Professor, HBNI,
Bhabha Atomic Research Centre, Mumbai.

Dr. Nasimuddin

Principal Scientist, Antenna and Optical
Department, Institute for Infocomm
Research; Agency for Science, Technology,
and Research, Singapore.

Associate Editors

Prof. Kedar Singh

Professor & Dean of School of Physical
Sciences, Jawaharlal Nehru University,
New Delhi, India

Prof Rajesh Punia

Head of Department, Department of
Physics, MDU, Rohtak, India

Dr Jyoti Shah

DST-WoSA, CSIR-National Physical
Laboratory, India

Dr. Rakesh Kr Singh

Academic Head, Aryabhata Center for
Nano Science and Nano Technology,
Aryabhata Knowledge University, Patna,
India

CNS&E Volume 1, Issue 3, May 2024

Table of contents:

S. No.	Title and Author	Page No.
1.	Editorial on Artificial Intelligence	174
2.	Quantum 3.0: Quantum Learning, Quantum Heuristics and Beyond Mrittunjoy Guha Majumdar	175-187
3.	Agrochemical Spray Technology Adoption and Safety Awareness Assessment in Crop Protection in Vineyard Cultivation Dattatray G. Bhalekar, Roaf Ahmad Parray, Indra Mani, Tapan Kumar Khura, Susheel Kumar Sarkar, N V Kumbhare	188-196
4.	MAA encapsulated MoS₂ Quantum Dots as a fluorescent probe for the sensing of flavonoid Shivani Bharti, Kedar Singh	197-203
5.	Chemical footprint of open dumping sites due to electronic and battery waste Umang Singh, Anil Kumar, Deepak Pant	204-210
6.	Investigation of substrate materials laminated CPW-Fed patch antennas: Opportunities and challenges Nupur, Neeraj Agarwal, Santosh Kumar Mishra	211-220
7.	Thermodynamics of a confined macromolecule: An analytical approach P. K. Mishra	221-228
8.	Farmers' Awareness of Millets in the Marathwada region Indra Mani, P. S. Kapse, and P. R. Deshmukh	229-243
9.	A short review on toughened epoxy based nanocomposites for EMI shields Ravi Kant and M. Fahim	244-256

Editor's Message

Artificial Intelligence (AI) Importance - A Brainchild of Humans !*Prof R K Kotnala**Chief Editor, Current Natural Sciences & Engineering ,Journal (CNS&E).**May 11, 2024*

"Human Brain Intelligence cannot be Dwarfed by AI (Artificial Intelligence), a Brain Child of Human, but a Remarkable Tool to handle Colossal Data more Efficiently with a Greater Speed, Accuracy using Smart Algorithms Devoid of Emotions & New Science !"

- R K Kotnala

It is our pleasure to focus on the importance of AI role in science & technology alongwith, how a common man is reaping direct benefit from AI ? The CNS&E journal Vol 1, issue 3 cover page depicts a representative picture (courtesy Adobe) of AI and human brain. No doubt AI is the brainchild of humans as such; hence it can never supersede human brain potential ! Although, it is sure that AI is not only about machine language algorithms as it is the outcome of human imaginations. Thereby, AI is not just about machines but humans intelligence & machines work together, wherein it augments our capabilities to bigger heights. It explicitly means AI is an assistive tool rather than a human intelligence substitute. In short, AI is a remarkable tool to handle Colossal Data more efficiently with a greater speed, accuracy using Smart Algorithms devoid of Emotions & New Science !

No doubt AI is playing a significant transforming role in science and technology and today's documentation tasks to serve masses. It is being used frequently in data analysis, natural language processing, and computer vision, supporting the scientists & engineers in data analysis, improving decision-making on the healthcare tests/measurements. It is well known that AI-powered simulations are being used to model complex systems like weather forecasting, predict disease outbreaks etc. AI-driven robots are assisting in industries automation tasks, also in surgery and space exploration. Besides, it is also being used to analyze huge amounts of data, identify sound/image patterns and is able to predict outcomes. In a wider perspective AI has led to significant advancements in fields such as medicine, engineering, finance, energy and environmental science.

That is why, CNS&E has focussed on the manuscript published in this issue - Quantum 3.0: Quantum Learning, Quantum Heuristics and Beyond.

Quantum learning paradigms address the question of how best to harness conceptual elements of quantum mechanics and information processing to improve operability and functionality of a computing system for specific tasks through experience. It is one of the fastest evolving frameworks, which lies at the intersection of physics, statistics and information processing, and is the next frontier for data sciences, machine learning and artificial intelligence. Progress in quantum learning paradigms is driven by multiple factors.

R K Kotnala

Quantum 3.0: Quantum Learning, Quantum Heuristics and Beyond

Mrittunjoy Guha Majumdar^{1*}

¹Centre of Excellence for Quantum Technology UPES, Dehradun, India

Volume 1, Issue 3, May 2024

Received: 9 April, 2024; Accepted: 25 May, 2024

DOI: <https://doi.org/10.63015/3A-2425.1.3>

**Corresponding Author E-mail: mrittunjoy.majumdar@ddn.upes.ac.in*

Abstract: Quantum learning paradigms address the question of how best to harness conceptual elements of quantum mechanics and information processing to improve operability and functionality of a computing system for specific tasks through experience. It is one of the fastest evolving framework, which lies at the intersection of physics, statistics and information processing, and is the next frontier for data sciences, machine learning and artificial intelligence. Progress in quantum learning paradigms is driven by multiple factors: need for more efficient data storage and computational speed, development of novel algorithms as well as structural resonances between specific physical systems and learning architectures. Given the demand for better computation methods for data-intensive processes in areas such as advanced scientific analysis and commerce as well as for facilitating more data-driven decision-making in education, energy, marketing, pharmaceuticals and healthcare, finance and industry.

Introduction: Quantum 1.0 was the revolutionary utilization of quantum resources for technology, primarily electrical and optical, such as transistors and optical masers, while Quantum 2.0 was about harnessing non-classical elements in the quantum formalism such as entanglement for information processing (1–15). Quantum mechanics have been used for undertaking information processing tasks such as teleportation, superdense coding, remote state preparation, quantum tomography, quantum cryptography and quantum key distribution, circuit-based and measurement-based quantum computing, quantum network coding and quantum internet, quantum random walks and quantum transduction (16–55). What can be called as Quantum 3.0 would be the harnessing of quantum resource and representation theory for a novel computational learning paradigm, along with quantum generalizations of existing classical computational learning models (56,57). This is the next frontier of exploration in the quantum realm and seeks to address the question: can we fundamentally reframe and re-envision learning models when the information-system and/or process is quantum mechanical in nature?

The term ‘machine learning’ was coined by Arthur Samuel in 1959, in the context of a ‘looking-ahead’ algorithm implemented on a classical computer for a game of checkers, realized using a neural net approach with randomly connected switching net as well as an approach involving a highly organized network designed to learn only specific things (58). In 1961, the punched-tape system known as Cybertron K-100 by Raytheon was developed as an early learning system that employed pattern recognition on sound samples, such as those from sonar signals, for learning (59). Basic pattern recognition, storage and referencing were the primary elements that supported the learning framework in the next few decades, such as with the work on feed forward networks with one layer of modifiable weights connecting input units to output units, in what could be called reflexive systems that could discover hidden relationships in data (60, 61). Machine learning addresses the twin questions of what fundamental information theoretic laws govern all learning systems and how could one construct computing systems that can improve their functioning through experience (62). For various applications, training based on a limited set of inputs and outputs obtained from

a system for specific empirical task seems to be more optimum than trying to predict the generalized response of the system in all circumstances.

Learning, in the context of information theory, describes the improvement of a yardstick or performance criterion for a system for a given task. For instance, we could seek to classify Iris flowers into three species: *Iris adriatica*, *Iris taochia* and *Iris kemaonensis* from a defining characteristic such as the cumulative length measurement of their petals and sepals. The yardstick index could be how accurately the classification takes place, and the training could be over a historical sample of irises from a phytologist's collection. We could also employ other criteria that have different penalties for incorrect classification. There are a number of algorithms for machine learning that are applicable to different kinds of datasets and problem types. Machine learning algorithms probe through various candidate models, based on training data and experience, to find the one that is optimum for the selected performance metric. The diversity of machine-learning algorithms can be segregated based on their manner of representation of candidate models (such as decision trees) and their manner of probing through the space of candidate models (such as evolutionary search methods).

The question is whether loading our phytological data into quantum states can make this classification better. We could create a parameterized quantum circuit or ansatz to do this, using a feature map. Any parameterized quantum circuit should be able to generate maximum number of quantum states in the Hilbert space and also have ability to entangle constituent qubits. It turns out that the variational quantum classifiers (VQCs) help classify the irises efficiently, using optimizers such as the constrained optimization by linear approximation optimizer (COBYLA). It is this interface of quantum mechanics and machine learning that provides various possibilities: machine learning with quantum computers, classical learning for quantum mechanical problems

and generalized quantum learning theory. Quantum machine learning brings together the learning capability and scalable nature of machine learning and the speed, efficiency and processing power of quantum computers. There have been several classical learning paradigms that have had quantum analogues proposed and realized: quantum neural networks, quantum reinforcement learning, quantum support vector machines, quantum linear regression, cluster detection and assignment algorithms, quantum principal component analysis and quantum decision tree classifier (63–70). In this comprehensive review of quantum learning paradigms, we will be looking at the spectrum of algorithms and protocols, before moving on to understanding the conceptual shift that this may provide when assessing learning theory from the perspective of quantum phenomenon.

Quantum Patterns: The underlying premise for the utility of the quantum realm for machine learning has to do with the emergence of classically anomalous patterns in data. Among phenomena that are intrinsically quantum in nature, an interesting example is that of quantum revival patterns, where we find superposed and displaced replicas of the initial state of the system (71–74). Quantum Kerr systems have such a kaleidoscopic mode of evolving, which is found to be reproducible based on interference of trajectories in the classical phase space (75). In the quantum-classical limit, where Planck's constant $\hbar \rightarrow 0$, it is seen that observables behave differently, leading to the preservation or disappearance of significant variables and their stochastic tendencies, such as for oscillator coordinate and spin variable respectively (76). Even in the case of skyrmions, we cannot simulate quantum skyrmions on classical supercomputers due to fundamental limitations, particularly around quantum fluctuations (77). Quantum patterns are seen as periodic magnetic formations that are spontaneously formed in antiferromagnetic Bose-Einstein condensate (78). When ultracold atoms form quantum ferrofluids, we find a spontaneous development of coherent

quantum density patterns leading to the formation of a super-solid (79). When nanoscale lead films grown on silicon substrates are annealed to high temperatures, we observe intricate quantum patterns in the energy landscape (80). A beat pattern emerges in the quantum magnetoresistance of polar semiconductors without a centre of inversion symmetry, such as InAs/GaSb, when the carrier concentration is high (81). Patterns are ubiquitous in quantum chemistry, in properties such as chemical hardness and electronegativity (82).

Given the ability of classical computers to both produce and recognize classical statistical data, the extrapolation would be that systems that produce classically atypical data, like in quantum systems, would also be able to recognize such data. This gives us the possibility of harnessing the quantum analogue of complex classical pattern recognition. Pattern recognition compares data input with specific memorized patterns, as it processes this input. Quantum pattern recognition provides a number of advantages over its classical counterpart. For instance, if we assume a Hopfield network approach for pattern recognition, we do so by local optimization, while utilising a quantum approach such as adiabatic quantum computation does so using global optimization (83). A realization of this was using the liquid-state NMR technique, where some of the interesting insights included the possibility of representing a superposition of recognized patterns using a quantum neural register (84). The parallelism inherent in quantum phenomena such as entanglement facilitate the execution of subroutines, even with big data, and this is one of the primary reasons for quantum machine learning, in general, being regarded as being better than its classical counterpart. Among pattern recognition protocols, one-class classification is important due to its applications in areas where detection of abnormal data points vis-a-vis instances of a known class is needed, using techniques such as support vector machines and principal component analysis (85–90). This helps in

addressing problems where we have imbalanced datasets, such as in metaheuristics, medical image datasets, manufacturing, high-energy physics and bioinformatics (91–98). Recently, a semi-supervised quantum one-class classification system known as Variational Quantum One-Class Classifier (VQOCC) was developed using (99). At the centre of this proposition is a quantum autoencoder, which is basically a circuit that undertakes compression of a quantum state onto a lesser number of qubits while retaining the information encapsulated in the initial state (100, 101). Quantum autoencoders have been applied to quantum data compression, quantum error correction, denoising of data and even for preserving entanglement (102–105).

An important question to be addressed here is what can be categorized as a quantum pattern. Is it just an arbitrary pattern of quantum randomness? Is it the byproduct of a quantum process, such as in cold exciton gases? Is it the quantum analogue of classical patterns in nature? Harney and Pirandola defined a quantum pattern as an m -mode coherent state undergoing local kary modulations (106). We can also define patterns in the information dynamics associated with quantum systems, such as in the case of quantum computing and communication systems (107). Examples would include basis encoding, quantum associative memory, amplitude encoding, angle encoding, QRAM encoding, quantum kernel estimator, variational quantum algorithm, variational quantum eigensolver, quantum associative memory, amplitude amplification, phase shift, oracle operations, quantum approximate optimization algorithm and quantum key exchange. Along with information theoretic arrangement and elements as well as quantum data types and quantum data structures, we can also specify entanglement structures to define the notion of quantum patterns (108). There are various kinds of entanglement patterns, from maximally entangled Dicke states to partially entangled cluster states. Even the outcome of measurements successively performed on an

open quantum system have a pattern because of the interaction between system and environment. The pattern encapsulates information on non-Markovian memory effect and the relaxation rates associated with the system (109). The primacy of quantum patterns can also be seen within phases of matter, which can be distinguished by distinct symmetry breaking instances - within the Landau theory, symmetry of ordering of constituents of a physical system differentiates one phase from others. In certain systems, such as chiral spin liquids, even without symmetry breaking, we have different characteristics due to what is known as topological order, which has been posited to describe entanglement in many-body systems (110).

Quantum Algorithmic Resource-Pool: The central question around assessing the possibilities in quantum machine learning is whether we have the algorithmic tools in the quantum domain for the same. A quantum algorithm is a succession of instructions for tackling a problem on a practical quantum computer (111). Cleve et al. highlighted that a common thread underlying all quantum algorithms can be as-certain when “quantum computation is viewed as multiparticle interference” (112). By and large, we have quantum search algorithms, quantum simulations of quantum systems on a quantum computer and algorithms premised on quantum implementations of the Fourier transform like Shor and Deutsch-Josza algorithm. Quantum supremacy or the enhancement of computational ability using quantum systems over that of classical counterparts has heralded the age of noisy intermediate-scale quantum (NISQ) technologies (36, 113). One of the earliest quantum algorithms came with by formulation of an algorithmic solution to a special case of the hidden subgroup problem by Peter Shor (114). Quantum Merlin-Arthur (QMA) completeness of a problem highlights that a supposed solution to it can be verified by a quantum computing system - a condition that has been extended to k unentangled provers in QMA(k) class problems (115, 116). When it

comes to claims of quantum supremacy, we often speak of speedup, resource reduction, scaling and ability to address greater number as well as variety of problems. Quantum speedup can be contextually defined in terms of the asymptotic behavior of the ratio of the times taken by a specific classical and quantum algorithm for a particular problem when the size of the problem is made to be very large (117). Speedup can be provable, like in Grover’s algorithm, while in some cases the enhancement due to the quantum effects is not obvious, like in quantum annealing (118, 119). Quantum resource optimization is seen in realization of randomness processing with quantum Bernoulli factories (120).

The reason for enhancement of computational power, when it comes to machine learning and data analysis, with quantum machine learning arises due to the inherent primacy, within quantum mechanics, of high-dimensional vector spaces and, more importantly, matrix transformations between vectors in such spaces, as is important for data analytics and machine learning methods. The speedup is especially pronounced when the matrices being dealt with have an element of sparseness or are low-rank matrices (121, 122). A classic example arises in a key tool used for machine learning - principal component analysis, which evaluates the eigensystem (and corresponding principal components) of the covariance matrix of data. Using a quantum random access memory, we initialize the vectors for a classical principal component analysis protocol onto quantum states and utilise the density matrix of the states (instead of the covariance matrix), which when exponentiated and operated on by a conditional SWAP operation for the quantum phase algorithm, yields the eigensystem that forms the premise of the principal component analysis (67). The algorithmic scaling is to the order of the square of the logarithm of the size of the system, in query as well as computational complexity. Essentially, the quantum principal component analysis scales exponentially faster than the classical counterpart.

While quantum principal component analysis is an unsupervised method that identifies patterns within higher-dimensional data for the reduction of data complexity with the retention of most of the information, there are various supervised learning algorithms that have had a quantum implementation (123). One such algorithm relates to quantum support vectors. Support vector machines undertake regression and classification using the delineation of feature vectors of the data into distinct classes around a hyperplane that is at maximum distance from the nearest data-points in either classes around it (124). If the data is not separable into distinct classes, we can use the kernel trick to project the data into a higher-dimensional space- a pursuit that by Cover's theorem can help in attaining separability in the data-set (125). Quantum algorithms such as Grover's algorithm are premised on binary classification. Even in cases of machine learning algorithms based on adiabatic quantum evolution, we define our approach in terms of a strong classifier that discerns whether a data-point is correct or erroneous based on a program specification (126). Like in the classical case, the quantum support vector machine relies on the definition of a quantum kernel that we can create by using a quantum feature map $\phi(\vec{x})$ between classical feature vectors \vec{x} and a Hilbert space to help us obtain the kernel $K(\vec{x}_i, \vec{x}_j) = |\langle \phi(\vec{x}_i) | \phi(\vec{x}_j) \rangle|^2$. We can then expand the hyperplane in the general form: $f(\vec{x}) = \sum_i \alpha_i y_i K(\vec{x}_i, \vec{x})$, where α_i denote bounded positive quantities and y_i the data labels. We can then use measures like the Gaussian or Rademacher Complexity to evaluate the classification error, based on this hyperplane definition and the data-set (127). While the quantum support vector machine paradigm defined using Grover's algorithm gives a quadratic speedup, the implementation using the least squares approach provides an exponential speedup over classical algorithms (64). In recent years, we have had quantum support vector machine implementations with the Newton method, amplitude estimation, gradient descent and using quantum annealers

as well as variational quantum-circuitry (128–132).

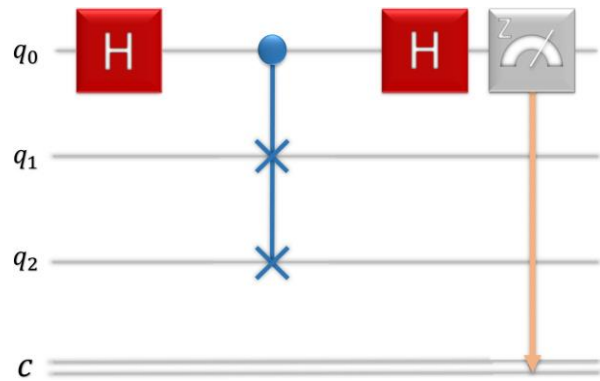


Figure 1: Swap Test

A natural extension of this comes with quantum k-nearest neighbour algorithms. Instead of a hyperplane as in the case of support vector machines, the underlying assumption of k-nearest neighbour methods is that the likelihood of two data-points that are proximal being of the same type is high (133). Labelled training vectors are used as reference for comparison of unlabelled testing vectors to determine k nearest train-state neighbours for the specific testing vector-state, whose label is ascertained using majority voting. In the quantum picture, we use the concept of fidelity of a specific testing state $|\psi\rangle$ with respect to multiple training states $|\phi_j\rangle$: $F_j = |\langle \psi | \phi_j \rangle|^2$. After taking an initial set of candidate neighbour states, we use quantum search algorithms to find other states and corresponding indices till the nearest neighbours are found. The functional way to obtain the fidelity is by using the swap test. In this test (Figure 1), we begin with two quantum states $|a\rangle$ and $|b\rangle$ along with an ancilla qubit initialized to $|0\rangle_{anc}$, on which we apply the Hadamard operation on the ancilla qubit. We thereafter apply a controlled swap operation on the ancilla qubit. A controlled swap operation is a gate where target qubits $|a\rangle$ and $|b\rangle$ are swapped if the control (in this case, the ancilla qubit) is in the state $|1\rangle$. Applying a second Hadamard gate on the ancilla gives us the state $|\chi\rangle = 1/2 |0\rangle_{anc}(|a, b\rangle + |b, a\rangle) + 1/2 |1\rangle_{anc}(|a, b\rangle - |b, a\rangle)$.

The measurement of the state $|0\rangle_{\text{anc}}$ has the associated probability $P(|0\rangle_{\text{anc}}) = 1/2 + 1/2 |\langle a|b\rangle|^2$. The inner product in this expression makes the overlap between the states primary: orthogonality gives us a probability of 0.5 while maximum overlaps gives a unity probability. This method can be used to find the distance between real-valued multi-dimensional vectors with the use of a quantum measurement (69). We can also undertake more rigorous pattern recognition between binary strings $|a_1, a_2, \dots, a_n\rangle$ and $|b_1, b_2, \dots, b_n\rangle$, using an extension of the construction in the k-nearest cluster model by initializing a state $|\psi\rangle = |a_1, a_2, \dots, a_n, b_1, b_2, \dots, b_n\rangle \otimes \sqrt{1/2} (|0\rangle + |1\rangle)_{\text{anc}}$, undertaking a XOR operation between the respective $(a_k, b_k) \forall k$ before storing it in place of the $b_k \forall k$, and finally undertaking a Hadamard operation on the ancilla qubit (134). If we measure the ancilla qubit in the ground state $|0\rangle_{\text{anc}}$, we obtain a resultant state whose amplitude has a scaling characteristic dependent on the Hamming distance between the binary strings.

Quantum Reinforcement Learning and Deep Learning: Going beyond supervised or unsupervised machine learning models, a major area of contemporary research has been in quantum-enhanced reinforcement learning, which is premised on the adaptive evolution of a quantum system based on reinforcement from a classical or quantum environment (135). The system receives percepts from the environment and undertakes actions. Unlike in conventional learning models, the learner in a reinforcement learning model has an influence on the state of the environment around it as much as it is influenced by it, thereby making it impossible to represent the environment in terms of a stationary memory. Both - the system and the environment, are stored as maps with memory, and the history of interactions between the two is the fundamental element in reinforcement learning. In the case of quantum reinforcement learning (QML), this history must be maintained in a quantum setting. In QML, we

define a Hilbert space for the percept and action states- HS and HA respectively.

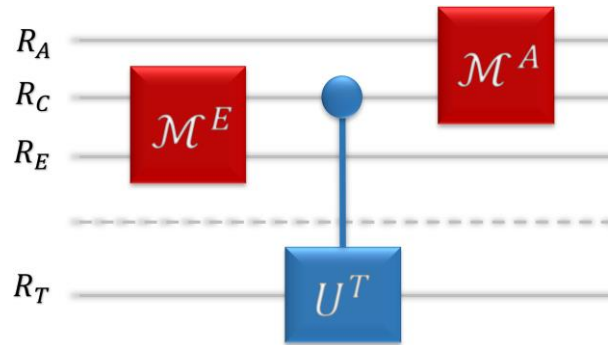


Figure 2: Quantum Reinforcement Learning (QRL) is premised on testing agent-environment interaction where the percept and action states have distinct Hilbert spaces associated with them. The register RT is not controlled by the agent or by the environment.

The agent and environment both have memory registers (RA and RE respectively) to store the histories of the system-environment composite. We can model the interaction with a distinct Hilbert space HC and we can characterize the agent (environment) by a series of Completely Positive Trace Preserving (CPTP) maps $\{M_i^A\}_i$ ($\{M_i^E\}_i$) that acts on a resultant register formed by concatenation of the registers of system-environment interaction RARC (environment-environment interaction RCRE) systems. The performance of the system-environment is assessed against a figure of merit. Dunjko et al showed that a quantum agent will outperform a classical learning agent associated with a classically delineated, controllable epochal environment against a particular figure of merit, if we were to consider a selected classical sporadic testing element (136). The quantum enhancement arises from being able to extract additional attributes from the environment for optimization of a classical agent. Our point of interest is in environments that are quantum in nature and that facilitate the preservation of superposition of percepts and actions.

When we are talking of quantum reinforcement learning, it is imperative to discuss what we mean by quantum accessibility. Quantum accessibility implies the utilization of access of the agent to the

environment for the simulation of an oracle O_q that behaves as follows:

$$|a_1, a_2, \dots, a_k\rangle|x\rangle \xrightarrow{O_q} |a_1, a_2, \dots, a_k\rangle|x \oplus R(a_1, \dots, a_k)\rangle$$

where R is the value of the 'reward' that the agent obtains once it successfully executes the actions a_1, a_2, \dots, a_k , for some auxiliary state $|x\rangle$. In the cumulative process, we see the utilization of a quantum interaction using what is known as oracularization with the environment to undertake effective simulation of access to the oracle (which encapsulates important information about the environment), followed by the usage of this information for determining behavior that is optimum in the given environment. We can attain a greater insight into the oracularization process by understanding the import of an auxiliary state, which usually comprises of percept states $|s_1, s_2, \dots, s_k\rangle$, the reward state $|R\rangle$ and $|e_1, e_2, \dots, e_k\rangle$ that are auxiliary quantum subsystems kept within the environment. For the simulation of the oracle, these states need to be controlled and erased (137). To undertake this, the agent should be able to undertake modification of specific memory components of the environment with what are known as register scavenging and register hijacking operations, followed by a way to 'uncompute' with the implementation of the Hermitian adjoint of the net unitary (map) that the environment implements. There are two primary kinds of reinforcement learning paradigms with specific quantum realizations: value-based, like in the case of Q-learning, which is premised on the learning of a value function that guides how the system environment makes decisions at each time step, as well as policy-gradient methods that optimizes a policy (function) $\pi(a|s; \theta)$ using the parameter θ (138–141). An important concept in this regard is meta-learning, wherein the learning agent undertakes the identification of its meta-parameter configuration that is optimum so as to be able to facilitate the optimization of performance. This parameter meta-learning is done by having the learning agent monitor its performance, and utilising a metaparameter register as well as techniques like adaptive Bayesian quantum estimation (142). The

reduction of the agent-environment interaction to a unitary oracular query is not feasible when we consider memory effects. In general, the oracular element may vary temporally and in such scenarios amplifying amplitude using Grover-type methods may be a possible approach to undertake reinforced learning in reward spaces that have an increasing monotonicity in the success probability.

Deep learning has also seen a quantum expansion in recent years. Deep learning is premised on using artificial neural networks for discovering the representations required for the detection and classification of features from raw data (143, 144). The basic unit of a neural network is a perceptron or a single artificial neuron. Gallant described one of the first perceptron-based connectionist models where each cell i computes a single activation u_i , which may be input to other cells or be an output of the network (145). Ricks et al. gave one of the earliest quantum neural network models based on implementation of quantum circuitry with gates whose weights are evolved through learning using quantum search as well as piecewise weight allocation (146). In each step, we have a density operator for the qubits representing the hidden states, which can be extracted with any output ancillaries using a partial trace operator and fed forward to the next layer of the neural network where the unitary transformations that encapsulate the action of perceptrons can be applied. There have been recent works on Bayesian approaches being implemented using quantum algorithms to learn Gaussian processes to train neural networks that are arbitrarily deep, with a quantum matrix inversion protocol being the core routine (147). In the quantum convolutional neural network presented by Cong et al (148), the modeling of the convolutional layer is in terms of a unitary transformation (on the state density of the input) that is quasi-local and is applied in error correction and phase recognition in quantum systems. The forward pass of the convolutional neural network can be computed as a convolutional product using quantum algorithmic tools even as gradient descent

methods can give us an idea about what are the relevant network parameters in the quantum context (149). There have also been hybrid models with quantum layers in the network where we undertake local transformation of the data with several random quantum circuits in the set bounded-error quantum polynomial time (150). Recently, quantum methods were used for physiological application such as for body part recognition using Hybrid Quantum Convolutional Neural Networks, although in this case the classical counterpart was found to have a greater validation accuracy by 0.5% (151).

Quantum Natural Language Processing, Quantum Advantage and the Path Forward Language is one of the earliest forms of representative evolution for humankind. Notwithstanding the tale of the Tower of Babel or the Gigantomachy myth, the diversity and complexity of language is of prime interest for computational representation and processing. Natural language processing is all about harnessing computational methods for the learning and production of content in human languages. We have come a long way from simply analysing the disparate linguistic forms and recognizing speech patterns to the creations of dialogues, translating speech from speech as well as the identification of emotional response of users towards services and products. The synchronic model of language aligns with the psycholinguistic understanding which highlights that language is dynamic (152). In any speech-based natural language processing (NLP) system, we have computation based on phonetic, phonemic and prosodic rules, besides the morphemic analysis which is as relevant for other kinds of NLPs as well (153–155). Higher levels of natural language processing include the lexical, the syntactic, the semantic, the discourse-oriented and the pragmatic (156). When it comes to natural language processing, we can have quantitative statistical approaches like the Hidden Markov models, connectionist approaches that are based on inter-related fundamental processing units as well as symbolic approaches that lay emphasis on the

logic or rules that a linguistic framework encapsulates. Zeng and Coecke were among the first to give us a quantum version of natural language processing when they employed the closest vector problem for sentence similarity identification within the distributional compositional categorical (DisCoCat) model given by Coecke, Sadrzadeh and Clark (157–159). In the compositional distribution model, meanings are encapsulated in quantum states while quantum measurements give us the grammatical structure for a specific sentence and context (160). The embedding of the language in the vector space of quantum systems naturally leads to word-correlations represented by the vector geometry, even as we map diagrams formed from parsing of sentences to quantum variational circuits. Essential quantum properties such as superposition helps us in the modelling of uncertainties in the language while phenomena like entanglement help us in describing how semantics and syntax are composed and distributed. Recently, natural language processing experiments have been practically realized for over 100 sentences on the Noisy Intermediate-Scale Quantum (NISQ) computing system provided by IBM Quantum (161).

When we speak about quantum natural language processing, in particular, and machine learning, in general, the elephant in the room is: how much of an advantage do we obtain using quantum systems over classical ones? The 'quantum native' view of quantum natural language processing which posits that the vector-landscape provided by quantum systems is better suited for the linguistic-syntactic, semantic and pragmatic elements, is preliminary and unsubstantiated by practical realizations, with a critical shortcoming being the primary reliance on quantum RAMs, which are expensive and not yet empirically implemented. More broadly, there are many aspects of quantum computing that are often off-set by machine learning paradigms.

For instance, the size of inputs is usually small, such as in fault-tolerant algorithms, while there

could high-dimensional tensorial structures with numerous entries in machine learning. The problems in machine learning can be highly unstructured and complex while problems studied in quantum computing are structured, often with elements of regularity and periodicity. Theory is defined and delineated in quantum computing problems while empiricism is preeminent in machine learning, with modelling and interpolations being important in the latter. Quantum computing can have absolute benchmarks like the scaling of run-time while machine learning have more constructivist benchmarks between disparate models. Quantum advantage can be spoken of in terms of solvability, expressivity of the class of the model, size of training sample needed, generalizability and how the optimization landscape is structured (162–171). Due to the need to be able to capture the system dynamics in terms of quantum systems and circuitry, we can only gauge performance of machine learning algorithms in specific selected contexts and examples, with this selectivity preventing any generalizability of performance-based advantage, if any. Such constraints also exist for readout and loading of data, when it comes to quantum examples. Performance parameters are also highly contextual and it is not straight-forward to assess if any 'quantum advantage' is due to the specific way in which we have selected benchmarking thresholds and hyper-parameters or whether they are actually observations made structurally. There may be a need to move towards studying Quantum 3.0, the revolution of quantum learning theory, as a paradigm in itself, without needing to resort to bylines towards 'quantum advantage' and 'quantum supremacy'. For example, classical intractability of kernels being bypassed using quantum tools can be an interesting pursuit but given that such kernels are not found to be utilizable in realizable machine learning, such an approach has no practical relevance. Today, we have moved beyond kernel methods with even more efficient ones like data re-uploading and explicit models (172, 173). We now have quantum machine learning models that have features that preserve privacy as well as those

that take into consideration the impact of decoherence (174, 175). The future is bright for quantum machine learning, even as the intersection of quantum mechanics, learning theory and information processing is explored to find novel methods of deploying artificial intelligence.

Competing Interests: The Author declares no Competing Financial or Non-Financial Interests.

Author Contributions: The author formulated the premise, undertook the analysis and wrote the paper.

References and Notes:

1. N. Bloembergen, Y.-R. Shen, *Physical Review* 133, A37 (1964).
2. T. L. Paoli, J. E. Ripper, *Physical Review A* 2, 2551 (1970).
3. K. Lehovec, *Physical Review* 75, 1100 (1949).
4. R. Hall, *IRE Transactions on Electron Devices* 7, 1 (1960).
5. D. Deutsch, *Proceedings of the Royal Society of London. A. Mathematical and Physical Sciences* 400, 97 (1985).
6. R. P. Feynman, *Optics news* 11, 11 (1985).
7. A. Peres, *Physical review A* 32, 3266 (1985).
8. W. H. Zurek, *Physical Review Letters* 53, 391 (1984).
9. P. Benioff, *Journal of statistical physics* 22, 563 (1980).
10. D. P. DiVincenzo, *Science* 270, 255 (1995).
11. A. Barenco, et al., *Physical review A* 52, 3457 (1995).
12. P. W. Shor, *Physical review A* 52, R2493 (1995).
13. D. P. DiVincenzo, *Physical Review A* 51, 1015 (1995).
14. P. W. Shor, *Proceedings 35th annual symposium on foundations of computer science (Ieee, 1994)*, pp. 124–134.
15. J. I. Cirac, P. Zoller, *Physical review letters* 74, 4091 (1995).
16. D. Bouwmeester, et al., *Nature* 390, 575 (1997).

17. A. Furusawa, et al., *science* 282, 706 (1998).
18. S. Pirandola, J. Eisert, C. Weedbrook, A. Furusawa, S. L. Braunstein, *Nature photonics* 9, 641 (2015).
19. M. Guha Majumdar, *Pramana* 95, 200 (2021).
20. C. Wang, F.-G. Deng, Y.-S. Li, X.-S. Liu, G. L. Long, *Physical Review A* 71, 044305 (2005).
21. X. S. Liu, G. L. Long, D. M. Tong, F. Li, *Physical Review A* 65, 022304 (2002).
22. A. Harrow, P. Hayden, D. Leung, *Physical review letters* 92, 187901 (2004).
23. C. H. Bennett, et al., *Physical Review Letters* 87, 077902 (2001).
24. B. Dakic', et al., *Nature Physics* 8, 666 (2012).
25. C. H. Bennett, P. Hayden, D. W. Leung, P. W. Shor, A. Winter, *IEEE Transactions on Information Theory* 51, 56 (2005).
26. Y. Xia, J. Song, H.-S. Song, *Journal of Physics B: Atomic, Molecular and Optical Physics* 40, 3719 (2007).
27. T. Jullien, et al., *Nature* 514, 603 (2014).
28. S. T. Flammia, D. Gross, Y.-K. Liu, J. Eisert, *New Journal of Physics* 14, 095022 (2012).
29. N. Gisin, G. Ribordy, W. Tittel, H. Zbinden, *Reviews of modern physics* 74, 145 (2002).
30. G. Brassard, N. Lutkenhaus, T. Mor, B. C. Sanders, *Physical review letters* 85, 1330 (2000).
31. V. Scarani, et al., *Reviews of modern physics* 81, 1301 (2009).
32. P. W. Shor, J. Preskill, *Physical review letters* 85, 441 (2000).
33. D. Gottesman, H.-K. Lo, N. Lutkenhaus, J. Preskill, *International Symposium on Information Theory, 2004. ISIT 2004. Proceedings. (IEEE, 2004)*, p. 136.
34. A. Steane, *Reports on Progress in Physics* 61, 117 (1998).
35. J. L. O'brien, *Science* 318, 1567 (2007).
36. J. Preskill, *Quantum* 2, 79 (2018).
37. M. G. Majumdar, *Journal of Quantum Information Science* 8, 139 (2018).
38. B. Yurke, J. S. Denker, *Physical Review A* 29, 1419 (1984).
39. M. Hayashi, K. Iwama, H. Nishimura, R. Raymond, S. Yamashita, *STACS 2007: 24th Annual Symposium on Theoretical Aspects of Computer Science, Aachen, Germany, February 22-24, 2007. Proceedings* 24 (Springer, 2007), pp. 610–621.
40. C. Simon, *Nature Photonics* 11, 678 (2017).
41. H. J. Kimble, *Nature* 453, 1023 (2008).
42. S. Wehner, D. Elkouss, R. Hanson, *Science* 362, eaam9288 (2018).
43. M. G. Majumdar, S. S. Garani, *Quantum Information Processing* 20, 1 (2021).
44. Y. Aharonov, L. Davidovich, N. Zagury, *Physical Review A* 48, 1687 (1993).
45. J. Kempe, *Contemporary Physics* 44, 307 (2003).
46. B. C. Travaglione, G. J. Milburn, *Physical Review A* 65, 032310 (2002).
47. N. Shenvi, J. Kempe, K. B. Whaley, *Physical Review A* 67, 052307 (2003).
48. M. G. Majumdar, C. Chandrashekar, *Journal of Physics B: Atomic, Molecular and Optical Physics* 55, 045501 (2022).
49. N. Lauk, et al., *Quantum Science and Technology* 5, 020501 (2020).
50. M. T. Rakher, L. Ma, O. Slattery, X. Tang, K. Srinivasan, *Nature Photonics* 4, 786 (2010).
51. M. Mirhosseini, A. Sipahigil, M. Kalaei, O. Painter, *Nature* 588, 599 (2020).
52. M. Wu, E. Zeuthen, K. C. Balram, K. Srinivasan, *Physical review applied* 13, 014027 (2020).
53. R. W. Andrews, et al., *Nature physics* 10, 321 (2014).
54. T. Bagci, et al., *Nature* 507, 81 (2014).
55. M. G. Majumdar, C. Chandrashekar, *Physics Letters A* p. 128829 (2023).
56. J. Biamonte, et al., *Nature* 549, 195 (2017).
57. V. Dunjko, H. J. Briegel, *Reports on Progress in Physics* 81, 074001 (2018).
58. A. L. Samuel, *IBM Journal of research and development* 3, 210 (1959).
59. R. Scharff, *The how and why Wonder Book of Robots and Electronic Brains (Wonder, 2017)*.

60. N. J. Nilsson, *The mathematical foundations of learning machines* (Morgan Kaufmann Publishers Inc., 1990).
61. R. O. Duda, P. E. Hart, et al., *Pattern classification and scene analysis*, vol. 3 (Wiley New York, 1973).
62. M. I. Jordan, T. M. Mitchell, *Science* 349, 255 (2015).
63. T. Menneer, A. Narayanan, *Tech. Rep. R329* (1995).
64. P. Rebentrost, M. Mohseni, S. Lloyd, *Physical review letters* 113, 130503 (2014).
65. M. Schuld, I. Sinayskiy, F. Petruccione, *Physical Review A* 94, 022342 (2016).
66. S. Lu, S. L. Braunstein, *Quantum information processing* 13, 757 (2014).
67. S. Lloyd, M. Mohseni, P. Rebentrost, *Nature Physics* 10, 631 (2014).
68. S. Lloyd, *IEEE transactions on information theory* 28, 129 (1982).
69. S. Lloyd, M. Mohseni, P. Rebentrost, *arXiv preprint arXiv:1307.0411* (2013).
70. K. A. McKiernan, E. Davis, M. S. Alam, C. Rigetti, *arXiv preprint arXiv:1908.08054* (2019).
71. R. Vasseur, S. Parameswaran, J. Moore, *Physical Review B* 91, 140202 (2015).
72. R. W. Robinett, *Physics reports* 392, 1 (2004).
73. C. F. e Silva, A. E. Bernardini, *Physical Review A* 107, 042220 (2023).
74. M. Berry, I. Marzoli, W. Schleich, *Physics World* 14, 39 (2001).
75. G. M. Lando, R. O. Vallejos, G.-L. Ingold, A. M. O. de Almeida, *Physical Review A* 99, 042125 (2019).
76. S. Dumitru, E. I. Verriest, *International Journal of Theoretical Physics* 34, 1785 (1995).
77. V. V. Mazurenko, I. A. Iakovlev, O. M. Sotnikov, M. I. Katsnelson, *Journal of the Physical Society of Japan* 92, 081004 (2023).
78. J. Kronja"ger, C. Becker, P. Soltan-Panahi, K. Bongs, K. Sengstock, *Physical review letters* 105, 090402 (2010).
79. J. Hertkorn, et al., *Physical Review Research* 3, 033125 (2021).
80. P. Czochke, H. Hong, L. Basile, T.-C. Chiang, *Physical review letters* 93, 036103 (2004).
81. A. Rowe, J. Nehls, R. Stradling, R. Ferguson, *Physical Review B* 63, 201307 (2001).
82. M. V Putz, *Current Physical Chemistry* 1, 111 (2011).
83. T. Szandała, *Procedia Computer Science* 71, 68 (2015).
84. R. Neigovzen, J. L. Neves, R. Sollacher, S. J. Glaser, *Physical Review A* 79, 042321 (2009).
85. D. M. J. Tax (2002).
86. S. S. Khan, M. G. Madden, *The Knowledge Engineering Review* 29, 345 (2014).
87. S. S. Khan, M. G. Madden, *Artificial Intelligence and Cognitive Science: 20th Irish Conference, AICS 2009, Dublin, Ireland, August 19-21, 2009, Revised Selected Papers 20* (Springer, 2010), pp. 188–197.
88. H. Hoffmann, *Pattern recognition* 40, 863 (2007).
89. B. Scho"lkopf, R. C. Williamson, A. Smola, J. Shawe-Taylor, J. Platt, *Advances in neural information processing systems* 12 (1999).
90. J. C. Platt, J. Shawe-Taylor, A. J. Smola, R. C. Williamson, et al., *Technical Report MSR-T R-99-87*, Microsoft Research (MSR) (1999).
91. F. S. Gharehchopogh, *Artificial Intelligence Review* 56, 5479 (2023).
92. L. Gao, L. Zhang, C. Liu, S. Wu, *Artificial intelligence in medicine* 108, 101935 (2020).
93. B. Krawczyk, M. Woz'niak, F. Herrera, *2014 IEEE Symposium on Computational Intelligence and Data Mining (CIDM)* (IEEE, 2014), pp. 337–344.
94. X. Du, *Journal of Process Control* 83, 1 (2019).
95. J. Lee, Y. C. Lee, J. T. Kim, *Journal of Manufacturing Systems* 57, 357 (2020).
96. M. A. Md Ali, N. Badrud'din, H. Abdullah, F. Kemi, *International Journal of Modern Physics A* 35, 2050131 (2020).
97. E. J. Spinosa, A. C. de Carvalho, *Advances in Bioinformatics and Computational Biology: Brazilian Symposium on Bioinformatics, BSB 2005, Sao Leopoldo, Brazil, July 27-29, 2005. Proceedings* (Springer, 2005), pp. 54–64.

98. M. Yousef, M. D. Sacar Demirci, W. Khalifa, J. Allmer, *Advances in bioinformatics* 2016 (2016).
99. G. Park, J. Huh, D. K. Park, *Machine Learning: Science and Technology* (2022).
100. J. Romero, J. P. Olson, A. Aspuru-Guzik, *Quantum Science and Technology* 2, 045001 (2017).
101. A. Pepper, N. Tischler, G. J. Pryde, *Physical review letters* 122, 060501 (2019).
102. C.-J. Huang, et al., *Physical Review A* 102, 032412 (2020).
103. D. F. Locher, L. Cardarelli, M. Müller, *Quantum* 7, 942 (2023).
104. D. Bondarenko, P. Feldmann, *Physical review letters* 124, 130502 (2020).
105. F. Zhou, et al., *Applied Physics Letters* 121, 134001 (2022).
106. C. Harney, S. Pirandola, *PRX Quantum* 3, 010311 (2022).
107. F. Leymann, *Quantum Technology and Optimization Problems: First International Workshop, QTOP 2019, Munich, Germany, March 18, 2019, Proceedings 1* (Springer, 2019), pp. 218–230.
108. S. Perdrix, *Electronic Notes in Theoretical Computer Science* 170, 125 (2007).
109. I. Luchnikov, S. Vintskevich, D. Grigoriev, S. Filippov, *Physical review letters* 124, 140502 (2020).
110. X.-G. Wen, *Science* 363, eaal3099 (2019).
111. A. Montanaro, *npj Quantum Information* 2, 1 (2016).
112. R. Cleve, A. Ekert, C. Macchiavello, M. Mosca, *Proceedings of the Royal Society of London. Series A: Mathematical, Physical and Engineering Sciences* 454, 339 (1998).
113. B. M. Terhal, *Nature Physics* 14, 530 (2018).
114. P. W. Shor, *SIAM review* 41, 303 (1999).
115. S. P. Jordan, D. Gosset, P. J. Love, *Physical Review A* 81, 032331 (2010).
116. Y.-K. Liu, M. Christandl, F. Verstraete, *Physical review letters* 98, 110503 (2007).
117. T. F. Rønnow, et al., *science* 345, 420 (2014).
118. V. Vedral, *Foundations of Physics* 40, 1141 (2010).
119. E. Crosson, D. Lidar, *Nature Reviews Physics* 3, 466 (2021).
120. R. B. Patel, T. Rudolph, G. J. Pryde, *Science advances* 5, eaau6668 (2019).
121. A. W. Harrow, A. Hassidim, S. Lloyd, *Physical review letters* 103, 150502 (2009).
122. B. D. Clader, B. C. Jacobs, C. R. Sprouse, *Physical review letters* 110, 250504 (2013).
123. M. Schuld, F. Petruccione, *Supervised learning with quantum computers*, vol. 17 (Springer, 2018).
124. M. A. Hearst, S. T. Dumais, E. Osuna, J. Platt, B. Scholkopf, *IEEE Intelligent Systems and their applications* 13, 18 (1998).
125. F. Samuelson, D. G. Brown, *The 2011 International Joint Conference on Neural Networks (IEEE, 2011)*, pp. 1020–1026.
126. K. L. Pudenz, D. A. Lidar, *Quantum information processing* 12, 2027 (2013).
127. D. Anguita, S. Ridella, F. Riviaccio, R. Zunino, *Neural Networks* 16, 763 (2003).
128. R. Zhang, J. Wang, N. Jiang, H. Li, Z. Wang, *Neural Networks* 151, 376 (2022).
129. R. Zhang, J. Wang, N. Jiang, Z. Wang, *Information Sciences* 635, 25 (2023).
130. H. Li, N. Jiang, R. Zhang, Z. Wang, H. Wang, *International Journal of Theoretical Physics* 61, 92 (2022).
131. D. Willsch, M. Willsch, H. De Raedt, K. Michielsen, *Computer physics communications* 248, 107006 (2020).
132. M. Ezawa, *Scientific Reports* 12, 6758 (2022).
133. P. Cunningham, S. J. Delany, *ACM computing surveys (CSUR)* 54, 1 (2021).
134. M. Schuld, I. Sinayskiy, F. Petruccione, *Contemporary Physics* 56, 172 (2015).
135. D. Dong, C. Chen, H. Li, T.-J. Tarn, *IEEE Transactions on Systems, Man, and Cybernetics, Part B (Cybernetics)* 38, 1207 (2008).
136. V. Dunjko, J. M. Taylor, H. J. Briegel, *2017 IEEE International Conference on Systems, Man, and Cybernetics (SMC) (IEEE, 2017)*, pp. 282–287.
137. V. Dunjko, Y.-K. Liu, X. Wu, J. M. Taylor, *arXiv preprint arXiv:1710.11160* (2017).
138. C. J. Watkins, P. Dayan, *Machine learning* 8, 279 (1992).

139. A. Skolik, S. Jerbi, V. Dunjko, *Quantum* 6, 720 (2022).
140. S. M. Kakade, *Advances in neural information processing systems* 14 (2001).
141. J. Yao, M. Bukov, L. Lin, *Mathematical and Scientific Machine Learning (PMLR, 2020)*, pp. 605–634.
142. L. J. Fiderer, J. Schuff, D. Braun, *Prx Quantum* 2, 020303 (2021).
143. Y. LeCun, Y. Bengio, G. Hinton, *nature* 521, 436 (2015).
144. I. Goodfellow, Y. Bengio, A. Courville, *Deep learning (MIT press, 2016)*
145. S. I. Gallant, et al., *IEEE Transactions on neural networks* 1, 179 (1990).
146. B. Ricks, D. Ventura, *Advances in neural information processing systems* 16 (2003).
147. Z. Zhao, A. Pozas-Kerstjens, P. Rebentrost, P. Wittek, *Quantum Machine Intelligence* 1, 41 (2019).
148. I. Cong, S. Choi, M. D. Lukin, *Nature Physics* 15, 1273 (2019).
149. I. Kerenidis, J. Landman, A. Prakash, *International Conference on Learning Representations*.
150. M. Henderson, S. Shakya, S. Pradhan, T. Cook, *Quantum Machine Intelligence* 2, 2 (2020).
151. P. Gohel, A. Chakraborty, K. R. JV, 2022 *IEEE International Conference on Quantum Computing and Engineering (QCE) (IEEE, 2022)*, pp. 831–832.
152. J. Barr, *Synchronic or Diachronic?* (Brill, 1995), pp. 1–14.
153. T. Cho, *Language and Linguistics Compass* 10, 120 (2016).
154. S. Yolchuyeva, G. Ne'meth, B. Gyires-To'th, *arXiv preprint arXiv:2004.06338* (2020).
155. S. C. Kak, *International Journal of Approximate Reasoning* 1, 117 (1987).
156. V. Raskin, *Machine translation: Theoretical and methodological issues* pp. 42–58 (1987).
157. W. Zeng, B. Coecke, *arXiv preprint arXiv:1608.01406* (2016).
158. N. Wiebe, A. Kapoor, K. M. Svore, *Quantum information and computation* 15, 318 (2015).
159. S. Clark, B. Coecke, M. Sadrzadeh, *Proceedings of the Second Quantum Interaction Symposium (QI-2008) (Citeseer, 2008)*, pp. 133–140.
160. R. Guarasci, G. De Pietro, M. Esposito, *Applied Sciences* 12, 5651 (2022).
161. R. Lorenz, A. Pearson, K. Meichanetzidis, D. Kartsaklis, B. Coecke, *Journal of Artificial Intelligence Research* 76, 1305 (2023).
162. Y. Liu, S. Arunachalam, K. Temme, *Nature Physics* 17, 1013 (2021).
163. J. Liu, et al., *Machine Learning: Science and Technology* 4, 025003 (2023).
164. J. J. Meyer, et al., *PRX Quantum* 4, 010328 (2023).
165. E. Abedi, S. Beigi, L. Taghavi, *Quantum* 7, 989 (2023).
166. S. Arunachalam, R. De Wolf, *The Journal of Machine Learning Research* 19, 2879 (2018).
167. L. Banchi, J. Pereira, S. Pirandola, *PRX Quantum* 2, 040321 (2021).
168. Z. Krunić, F. F. Flo'ther, G. Seegan, N. D. Earnest-Noble, O. Shehab, *IEEE Transactions on Quantum Engineering* 3, 1 (2022).
169. S. F. Ahmad, R. Rawat, M. Moharir, 2021 *International Conference on Computational Intelligence and Knowledge Economy (ICCIKE) (IEEE, 2021)*, pp. 345–349.
170. J. R. McClean, S. Boixo, V. N. Smelyanskiy, R. Babbush, H. Neven, *Nature communications* 9, 4812 (2018).
171. X. Ge, R. Wu, H. Rabitz, *Complex System Modeling and Simulation* 1, 77 (2021).
172. A. Pe'rez-Salinas, A. Cervera-Lierta, E. Gil-Fuster, J. I. Latorre, *Quantum* 4, 226 (2020).
173. V. Havlíček, et al., *Nature* 567, 209 (2019).
174. W. M. Watkins, S. Y.-C. Chen, S. Yoo, *Scientific Reports* 13, 2453 (2023).
175. H. Liao, I. Convy, Z. Yang, K. B. Whaley, *Quantum Machine Intelligence* 5, 7 (2023).

Agrochemical Spray Technology Adoption and Safety Awareness Assessment in Crop Protection in Vineyard Cultivation

Dattatray G. Bhalekar¹, Roaf Ahmad Parray^{*2}, Indra Mani², Tapan Kumar Khura², Susheel Kumar Sarkar³, N V Kumbhare²

¹Department of Biological Systems Engineering, Washington State University, Prosser, Washington (USA) -99164-1035

^{2*}Division of Agricultural Engineering, ICAR-IARI, New Delhi

³Indian Agricultural Statistics Research Institute, New Delhi.

Volume 1, Issue 3, May 2024

Received: 10 January, 2024; Accepted: 21 February, 2024

DOI: <https://doi.org/10.63015/9S-2407.1.3>

*Corresponding Author Email: rouf.engg@gmail.com

Abstract: A study was conducted in the Jalna district of Maharashtra to assess the adoption pattern of spray technology, and safety awareness among grape growers. The respondents were selected through random sampling and data was collected through a structured interview. The study revealed that among marginal landholders (< 1 ha) back-pack type sprayer was mostly in operation with an adoption level of 75%. In small landholders (1-2 ha), horizontal triplex pump (HTP) sprayers with an adoption level of 51.85% followed by tractor-operated air-blast sprayers (40.75%) were prevalent pesticide spraying technologies. More than 2/3rd (76.00%) of medium landholders (2-4 ha) had adopted tractor-operated air blast sprayers. For the application of plant growth regulators, 62.5% of small farmers, 81.8% of medium, and 100% of farmers had adopted electrostatic sprayers. The number of chemical sprays per season varied from 25 to 100, making grapes one of the major pesticide-consuming crops. Capacity, efficiency, cost, and availability of sprayers on a custom hiring basis were the four major factors affecting the adoption of spraying technologies.

KEYWORDS: *Air-blast sprayer, Custom hiring, Electrostatic sprayer, Plant growth regulator.*

1. Introduction: Agriculture is the mainstay of the Indian economy and contributes about 18.8% of the Gross Value Added (GVA) of the country (Economic Survey of India, 2021-22). Since Independence, India has witnessed tremendous growth in agriculture- 5 times increase in grain production, 9 times in horticultural production, 12 times in fish production, and 9.5 times in milk production [1] Horticulture has become a key driver for economic development in many of the states in the country and it contributes 30.4% to the gross domestic product (GDP) of agriculture [2]. Among horticultural crops, India has emerged as one of the major grapes growing countries in the world. India ranks first with average grape productivity of 22.32 tonnes ha⁻¹ against the global average productivity of 9.32 tonnes ha⁻¹.

Grape production has increased by about 195% from 1057 thousand tonnes in 2000-01 to 3125 thousand tonnes in 2019-20 [3]. In India, about 0.14 million hectares of grape cultivation produces 3.12 million tonnes of grapes annually. India is the only country in the world, where table grapes are available during April-May [4] Grapes occupy the prominent position in exports with 188.2 thousand tonnes valued at ₹1,89,99 million [5]. In India, Maharashtra State (MS) is the largest producer of grapes, accounting for up to 78.3% of the country's total grape production followed by Karnataka and Tamil Nadu. Maharashtra has an estimated grapes cultivation area of 0.09 million hectares with an annual production of 774000 tonnes in 2015 [6]. For the production of quality grapes with sustainable yields especially in tropical climates, farmers

often use pesticides to control diseases like downy mildew, powdery mildew, and insect pests such as thrips, jassids, and mealybugs therefore, pesticide consumption in grape farms is on the higher side. Due to the widespread use of pesticides, their toxic residue has been reported in various environmental matrices [7].

The precision chemical and growth regulator application in vineyard cultivation demands mechanization in crop protection operations. Specialty crop spray application methods have advanced significantly in recent years in terms of better control and lower costs with improved spray performance and reduced off-target drift. Recently, the use of sensor-based control volume [8] and electrostatic spray technology [9] has shown improved spray deposition compared to conventional sprayers. To develop and disseminate different technologies for vineyard cultivation, it is essential to analyse the existing technology adoption pattern among different farmers and develop scale neutral technologies for widespread adaptability. A survey was conducted in the grape-growing Jalna district (Marathwada region) of Maharashtra (India) to understand spraying technology adoption patterns and worker health safety awareness among grape-growing farmers of India. The primary aim of the study was to investigate the adoption pattern of spray technology and safety practices across diverse land holdings within the study area. The overarching goal was to pinpoint potential interventions that could enhance the mechanization of spraying operations specifically within vineyards in the Marathwada region.

2. Experimental Procedure

A study was conducted in major grape-cultivating villages of the Jalna district (MS, India). Five villages namely, Kadwanchi (19.9199°N, 75.9986°E), Dharkalyan (19.8868° N, 76.0218° E), Nandapur (19.9064° N, 75.9754° E), Gondgaon (19.9376°N, 75.9289°E), and Thar (19.9139° N, 75.9608° E)

were selected randomly from this region (fig.1) for this study.



Fig.1 Satellite image of the study area

Further, from each village 14 farmers were selected randomly, thus making a total sample size of 70 farmers. The basic information about cropping patterns, cultivation practices, major grape cultivation regions, etc. of Jalna district was taken from District Agriculture Offices and *Krishi Vigyan Kendra* (KVK), Jalna, MS. The data were collected by the researcher by interviewing the respondents with the help of a pre-tested standard interview questionnaire. The collected data were compiled, tabulated, and analysed using statistical tools.

In order to validate the effect of spraying technology on growth of grape clusters, a pilot study was conducted at ICAR-Indian Agricultural Research Institute, New Delhi. The study employed three distinct treatment methods for the application of the plant growth hormone Gibberellic acid (GA3) at a concentration of 40 ppm. The three methods utilized were:

Sensor-Based Control Volume Sprayer (SB)

This treatment involved the use of a sensor-based control volume sprayer, which likely leveraged advanced technology for precise and controlled spraying of the Gibberellic acid on the berry clusters.

Conventional Hand Dipping (DP)

The conventional hand dipping method implied manually immersing berry clusters in a solution containing Gibberellic acid. This traditional

method may involve direct contact with the solution and manual labor.

Manual Compressed Air Sprayer

This treatment utilized manual compressed air sprayer (Model No: B0BKTCQG5H, 5 L, compressed air sprayer, Saiagro Ltd., India) to facilitate the spraying of the Gibberellic acid solution onto the berry clusters.

Statistical Analysis

In order to assess the effectiveness of the Plant Growth Regulator (PGR) application method on the growth of clusters, a statistical analysis of variance (ANOVA) was conducted at a significance level of $\alpha = 0.05$. The cluster and berry growth datasets were normalized using cube- root transformation. All the statistical analysis was performed in RStudio programming software (version: 2022.12.0+353, public-benefit corporation, USA).

3. Results and Discussion

The major observations inferred from the survey data are presented below,

I. Educational status of respondents

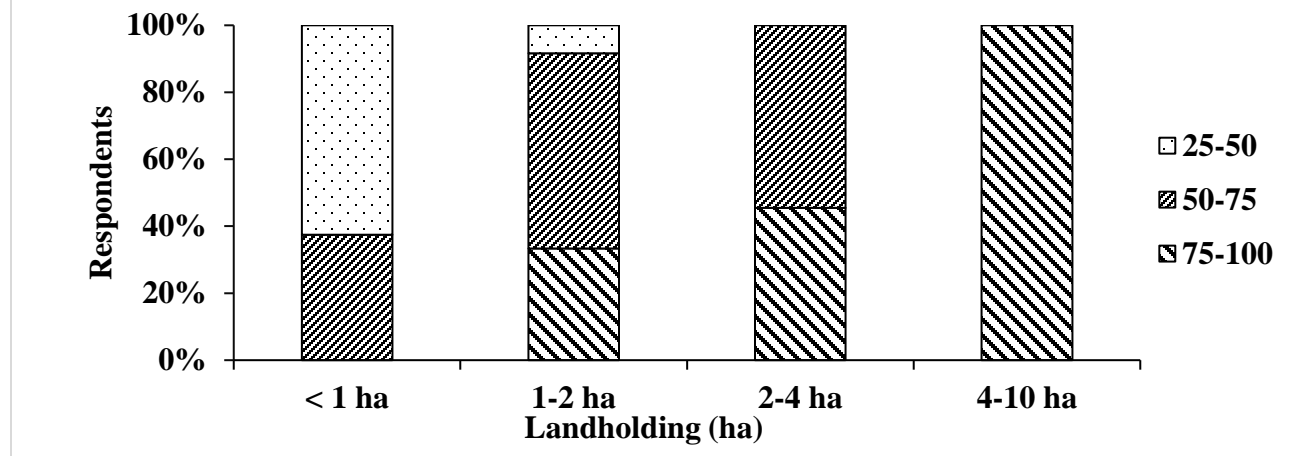
The educational status of the respondents shows that the majority of farmers (41.43%) had completed their secondary education whereas farmers without any formal education were 2.85%. The respondents who had completed their primary and higher secondary levels were 20 and 25.72% respectively. Farmers who had received education up to graduation level were around 10%. Based on the information provided by the farmers it was observed that all the respondents belonged to the age group of 25 years to 60 years [10][11]. The inclusion of educational status and age-related data is essential because psychological factors play a crucial role in understanding how individuals perceive and adopt new technologies. Those with higher education levels may be more open to embracing new technologies due to a better

understanding of their benefits. The age of farmers aligns with the Innovation Diffusion Theory, which suggests that the adoption of innovations follows a pattern, with younger individuals often adopting new technologies earlier than older individuals. Understanding this pattern is crucial for designing interventions that consider the varying needs of different age groups.

II. Technology adaptation pattern among different landholding categories

Grapes are highly vulnerable to various diseases throughout the season from fruit setting to harvesting and hence require frequent chemical applications. Fig. 2 shows the frequency of chemical application including the growth regulator sprays per season varied from 25 to 100, making grapes one of the major pesticide-consuming crop. However, the frequency of sprays varied with landholding. It was observed that sometimes 2-3 sprays were done during a single day depending upon the disease incidence and weather conditions. Spray frequency for marginal farmers ranged from 25-50 sprays per season. The spray frequency was 50-75 sprays per season for 40% of small and 51.5% of medium landholding farmers. All the respondents from the large landholding category reported a higher spray frequency of 75-100 per season. A major factor affecting the frequency of spraying among the different categories was the type of technology and man-hours requirement for spray applications. Mostly, marginal and small farmers were using the small capacity sprayers hence, more man-hours were required which resulted in reduced spray frequency. However, large landholding farmers had adopted high-capacity tractor-operated sprayers with fewer man-hour requirements, hence, the increased frequency was observed.

Fig. 2. Frequency of chemical applications among the different landholding category



Based on the details provided by respondents, it was observed that three different types of sprayers were adopted by the farmers of the surveyed region. These were backpack-type sprayers, engine-driven stationary type (horizontal triplex pump [HTP]), and tractor PTO-driven airblast sprayers (fig 3a) (also

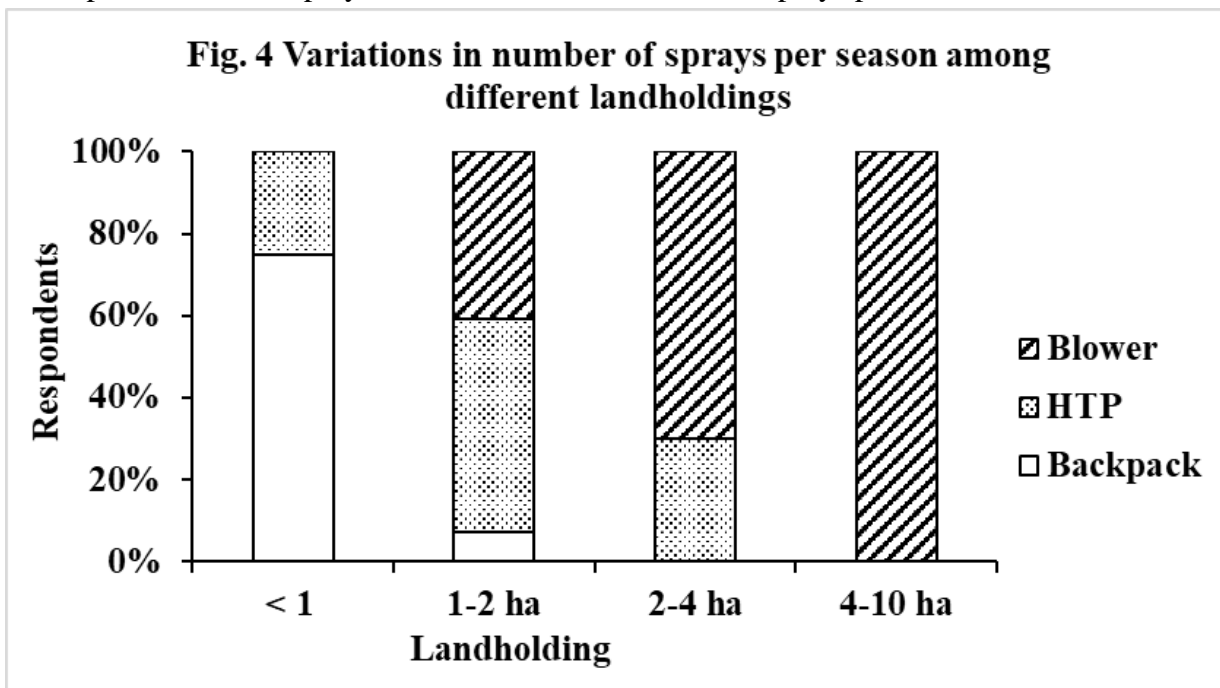
known as blowers locally). Farmers with landholding less than one hectare were using backpack sprayers (fig 3b) such as battery-operated knapsack sprayers and backpack-type power sprayers; with few being HTP. Farmers of the small landholding category (1-2 ha) were mainly using HTP with a tank capacity of 200



Fig. 3 Spray application technologies adopted in vineyard cultivation a) airblast sprayer, b) backpack sprayer, c, d) Horizontal triplex pump with hand spray gun, e) hand dipping

liters (fig. 3c,d). A fraction of them had adopted tractor-operated air-blast type sprayers, whereas very few were using backpack sprayers. Growers of medium and large landholding categories (2-4 ha) preferred high-volume tractor-operated airblast sprayers.

Plant growth regulators (PGR) are essential for the uniform growth of grape berries. Better productivity can be obtained by precise plant growth regulator applications. Respondents reported that grapes usually require about four to six PGR sprays per season.



Graphical representation of adopted spraying technology by the respondents of different landholding categories (Fig.3) indicates that about 75% of marginal landholding grape growers were using back-pack type sprayers and 25% had adopted HTP type sprayers. In case of small landholding category, the adoption of different spraying technology was like HTP sprayers (51.85%), tractor-operated airblast sprayers (40.75%) and 7.5% using backpack sprayers. In medium landholding grape growers, 76% had adopted airblast sprayers. It was observed that as the landholding increased, the adoption of tractor-operated sprayers also increased. It could potentially be due to the affordability of tractor-operated sprayers among large land-holding farmers. 12] highlighted that age, annual income, education, social involvement, usage of information sources, land ownership, knowledge, and socio-economic level were shown to be correlated with the adoption of improved technologies.

Significant variation in the adoption of plant growth regulator spraying technology was also observed among the different categories of landholding farmers. Farmers of marginal landholdings majorly were using the traditional hand-dipping method of PGR application in which every grape cluster was dipped manually into a conical pot full of chemicals (fig. 3e).

In small land-holding farmers, four different modes of PGR application i.e. hand dipping, horizontal triplex pump, blower, and electrostatic sprayer were prevalent with adoption levels of 8.55%, 16.45%, 12.5%, and 62.5%, respectively (Fig.4).

In case of medium landholding category, 81.8% grape growers were using electrostatic sprayers and remaining (18.2%) were using a blower. All large landholding farmers had adopted electrostatic sprayers for the precise application of plant growth regulators. One major

observation was the farmers' perception of the need for the application of an optimum concentration plant growth regulator. Less concentration was reported to be ineffective in grape cluster development, while overdose caused adverse effects on the quality of the grape cluster. Although 67.15% of farmers were using electrostatic sprayers, however, only 7.15% of farmers owned electrostatic sprayers while the majority of farmers were using electrostatic sprayers on a custom-hire basis. Therefore, custom hiring services had a great role to play in technology adoption due to the affordability of high-cost sprayers by most farmers.

III. Factors affecting the adoption of spraying technology in vineyards

The major focus of the study was to elicit information on different factors affecting the selection of spray equipment for pesticide management in grape orchards. [13] reported 80% of variation in agricultural mechanization could be attributed to four major factors-land holding, family income, custom hiring service availability, and education. The adoption or non-adoption of spraying technologies was mainly related to three major factors- cost, efficiency, and availability of sprayers.

- (i) **Efficiency and capacity of spraying:** A majority (57%) of farmers responded that the efficiency and capacity of a sprayer for grape cultivation was a major factor in the selection of a sprayer. However, most of such farmers were of medium and large land holding categories, therefore adoption of high-cost air-blast type sprayers and the electrostatic sprayer was economically feasible for them.
- (ii) **Cost of sprayer:** Cost is one of the major factors affecting the adoption of machinery among resource-poor farmers. Among the total surveyed grape growers, 31% reported that cost of operation was a major concern for the adoption of efficient and high-capacity sprayers like air-blast type sprayers and electrostatic sprayers. Most of the farmers in this category were marginal, small, and

medium landholding category. For such farmers, the purchase of machinery like air-blast type sprayers and electrostatic sprayers was against economics of scale due to fewer annual use hours. Many farmers in this category were availing of custom hiring services for the use of high-cost machinery for spraying in their orchards. Farmers of the marginal and small categories were adopting manual backpack sprayers.

- (iii) **Ease of availability:** Custom hiring of agricultural machinery plays an important role in machinery dissemination [14] . Out of the total surveyed farmers, 11 percent reported the non-availability of machinery on a custom hiring basis as a major constraint in the adoption of sprayers for pesticide and growth regulator application in grapes. Most of the farmers reported non-availability of sprayers a major concern were medium land holders. [15]while studying farm power-machinery status and custom-hiring opportunities reported the need for facilitation of high-cost machines through custom hiring centers, *Krishi Vigyan Kendra*, and through private-public partnerships to improve the mechanization status of the country.

IV. Safety awareness and health issues associated with pesticide application in the vineyard

Variations in the level of safety precaution during pesticide application were observed in selected respondents. During the survey, farmers were asked for the type of protective measure they follow while pesticide spraying in grape orchards. All three types of respondents i.e., those not following any safety precaution during spraying of hazardous pesticides, farmers with partial precaution (covering the nose and mouth with proper clothing), and farmers with full precautions (safety goggles, shoes, and personal protective kit) were observed (Table 1).

The data relating to protective measures followed by grape growers while spraying

indicates that about 87.5% of farmers of marginal landholding were not following any protective measure, whereas, as a fraction of them were using partial precaution while spraying. In the case of small and medium farmers about 62.5% and 48.5%, respectively were not following any safety precautions while spraying in a vineyard. The safety awareness was found quite satisfactory in large landholding farmers with 60% taking partial precaution and 40% following full precaution in pesticide application. This was because of the reason that most of the large land-holding farmers had higher education and were voluntarily involved in training related to agriculture. [16] revealed education level and lack of training related to pesticide use among major factors certain factors affecting the safety awareness of farmers in pesticide application practices in India.

Table 1 Safety measures pattern observed in selected respondents

Level of precautions	% Respondents among different landholdings			
	< 1 ha	1-2 ha	2-4 ha	4-10 ha
No Precautions	10.0	21.4	22.8	
Partial Precautions	0	3	6	0.00
Full Precautions	1.43	0	0	4.29
	0.00	2.86	4.29	2.86

V. Health issues related to pesticide application reported by the farmers

Pesticides act as plant-protection agents to control most dreadful diseases in agriculture. However, exposure to pesticides continuously for a bit longer period causes a range of human health-associated issues. From the surveyed area, headache was the most common problem reported by about 41.42% of the grape growers. Most of these farmers were observed to apply pesticides without any protective measures. The next major health issue faced by about 25.71%

of farmers was breathing problems after pesticide spraying. Other 12.85% and 5.71% farmers had experienced eye problems and nausea, respectively during pesticide spraying in grape orchards. It was found that farmers of all age groups were equally susceptible to the health effects due to unsafe pesticide application practices. However, 14.28% cent of farmers who were following either complete or partial protective measures while spraying did not report any major health issues. The major reason behind health issues was improper information about the chemical composition of sprayed pesticides due to lack of awareness. Given that farmers were observed applying pesticides without protective measures, the risk of dermal issues becomes a significant concern. The use of appropriate personal protective equipment (PPE) like gloves, long-sleeved clothing, and other protective gear is crucial to minimize direct skin contact and mitigate the potential health risks associated with pesticide exposure. It is recommended to raise awareness among farmers about the importance of using PPE and providing them with proper training on safe pesticide handling practices to reduce the occurrence of dermal issues and other health-related problems. [17] reported that middle-aged group farmers mostly being illiterate are dependent on others for reading information given on pesticide bottles or instructions provided by agriculture extension departments. Thus, the availability of information in the local language may sensitize the people to better follow up on necessary protocols during pesticide application to avoid health hazards.

Effect of spraying technology on growth characteristics of grape cluster

The analysis of variance (ANOVA) revealed a significant difference in cluster length ($F_{2,99} = 4.84, p = 9.84 \times 10^{-3}$) based on the application method. However, no significant differences were observed in cluster width ($F_{2,99} = 1.39, p = 0.25$) when considering the application method as the main effect. The change in cluster

length (Mean \pm Std. Error) observed in the selected plant growth application methods were as: Sensor-Based (SB) Sprayer: 16.89 ± 1.72 mm; Hand Dipping (DP): 16.66 ± 1.55 mm; Conventional Manual Sprayer (CS): 7.63 ± 0.94 mm. On the other hand, the maximum growth in cluster width was observed in the SB method (16.23 ± 1.84 mm), followed by DP (11.12 ± 1.28 mm) and CS (8.55 ± 1.77 mm), respectively. The cluster growth was comparable between the SB and DP methods, while the least growth was observed in the CS method (Figure 5). This change in cluster growth may be attributed to potential influence of higher atomization and increased spray deposition on clusters under control volume conditions, particularly in the SB method (Dattatray *et al.*, 2023)

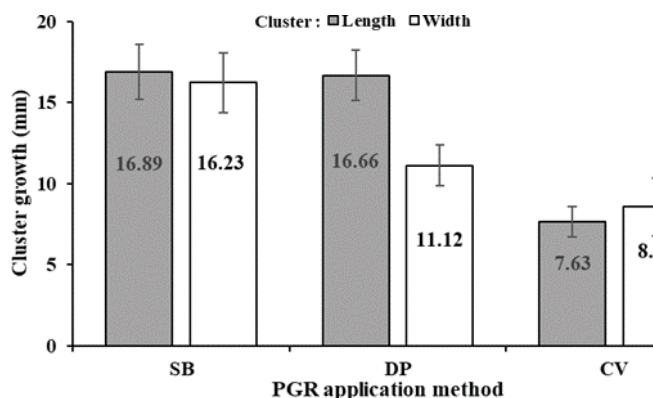


Figure 5 Effect of PGR application methods on cluster growth

4. Conclusions: The study's key findings highlight that the adoption of farm machinery for pesticide and plant growth regulator application in grape cultivation is significantly influenced by the size of land holdings. Large land-holding farmers tend to embrace advanced technologies like tractor-operated air-blast sprayers and electrostatic sprayers, whereas such technologies see limited use among small land-holding farmers. To bridge this gap and promote the widespread adoption of advanced and precise equipment, there is a proposed strategy of making such machinery available on a custom

hiring basis. This approach aims to increase accessibility to innovative technologies, ultimately reducing input costs and minimizing environmental impact. The study underscores the necessity for developing affordable spraying technologies customized to the needs of small and marginal farmers. This is critical to make farmers with limited land holdings reap the benefits associated with advanced and efficient spraying technologies. Moreover, the low adoption pattern of precautionary measures among farmers requires specialized training programs to educate farmers about the importance of implementing proper protection measures during pesticide application. This proactive approach will enhance awareness and promote safer practices, addressing health concerns associated with pesticide exposure. Overall, the study suggests a multifaceted approach to improve the adoption of advanced agricultural machinery and enhance safety measures during pesticide application, catering to the diverse needs of farmers with varying land holdings. The findings on the specific effects of different PGR application methods on grape cluster dimensions, highlighted the potential advantages of sensor-based spraying technology in promoting cluster elongation.

5. References:

1. Goverdhan, M.; Latheef Pasha, M.; Sridevi, S.; Kumari, P. Integrated farming approaches for doubling the income of small and marginal farmers. *International Journal of Current Microbiology and Applied Sciences* 2018, 7(3), 3353-3362.
2. Surendran, V. Horticultural sector in India: retrospect and prospect. *Journal Impact Factor* 2014, 5(4), 66-72.
3. Indian Annual Budget for Year 2021-2022 published by Government of India. 2022. [Online] Available: <https://www.indiabudget.gov.in/economicsurvey/doc/eschapter/echap07.pdf>

4. Adsule, P. G.; Upadhyay, A.; Sharma, A. K.; Satisha, J.; Yada, D. S. Vision – 2050 NRC for Grapes, Pune, and Perspective Plan National Research Centre for Grapes (Indian Council of Agricultural Research) Pune pp: 3. [Online] Available: <https://nrcgrapes.icar.gov.in/NRCG%20%20old%20website%20as%20on%2031-05-2019/zipfiles/NRC-Grapes%20Pune%20Vision%202050%20July%202015.pdf>
5. Glance, H. S. A. A. Horticulture Statistics Division Department of Agriculture. Cooperation & Farmers' Welfare Ministry of Agriculture and Farmers' Welfare Government of India. 2018.
6. Ghosh, D.; Chakraborty, C.; Dasgupta, R. A survey on Indian grapes at Sangli, Maharashtra, India. *International Journal of Current Microbiology and Applied Sciences* 2017, 6, 1904-1911.
7. Pujeri, U. S.; Pujar, A. S.; Hiremath, S. C.; Yadawe, M. S. Status of pesticide residue in grapes of Bijapur (Karnataka). *Recent Research in Science and Technology* 2010, 2(2), 100-102.
8. Bhalekar, D. G.; Parray, R. A.; Mani, I.; Kushwaha, H.; Khura, T. K.; Sarkar, S. K.; Lande, S. D.; Verma, M. K. Ultrasonic sensor-based automatic control volume sprayer for pesticides and growth regulators application in vineyards. *Smart Agricultural Technology* 2023, 4, 100232.
9. Salcedo, R.; Llop, J.; Campos, J.; Costas, M.; Gallart, M.; Ortega, P.; & Gil, E. Evaluation of leaf deposit quality between electrostatic and conventional multi-row sprayers in a trellised vineyard. *Crop Protection* 2020, 127, 104964.
10. Chatterjee, D.; Acharya, S. K.; Mondal, S. Socio-psychological Determinants for Technology Socialisation of Jute Production in West Bengal. *Indian Journal of Extension Education* 2022, 58(3), 175-178.
11. Mondal, D.; Bandyopadhyay, A. K. Adoption of jute production technology in West Bengal. *Econ Aff* 2014, 59, 701-709.
12. Mishra, B. P.; Kanwat, M.; Gupta, B. K.; Meena, N. R.; Mishra, N. K.; Kumar, P. S. Correlates of adoption of improved apiculture practices in Arunachal Pradesh. *Indian Journal of Extension Education* 2020, 56(2), 51-54.
13. Parray, R. A.; Khura, T. K.; Lande, S. D. Factors affecting Agricultural Mechanization- A case study from Aligarh Division of Uttar Pradesh. *Agricultural Engineering Today* 2019, 43(4), 1-5.
14. Pabba, A. S.; Naik, R. Adoption of Climate Resilient Agricultural Technologies by Farmers in Nalgonda district of Telangana State. *Indian Journal of Extension Education* 2022, 58(2), 30-34.
15. Parray, R. A.; Indra, M.; Adarsh, K.; Khura, T. K.; Lande, S. D. Pilot study of farm power-machinery status and custom-hiring opportunities in rice (*Oryza sativa*)-wheat (*Triticum aestivum*) cropping system. *Indian Journal of Agricultural Sciences* 2016, 86(2), 167-172.
16. Abhilash, P. C.; Singh, N. Pesticide use and application: an Indian scenario. *Journal of Hazardous Materials* 2009, 165(1-3), 1-12.
17. Mubushar, M.; Aldosari, F. O.; Baig, M. B.; Alotaibi, B. M.; Khan, A. Q. Assessment of farmers on their knowledge regarding pesticide usage and biosafety. *Saudi Journal of Biological Sciences* 2019, 26(7), 1903-1910.

MAA encapsulated MoS₂ Quantum Dots as a fluorescent probe for the sensing of flavonoid

Shivani Bharti, Kedar Singh*

School of Physical Sciences, Jawaharlal Nehru University, New Delhi, 110067

Volume 1, Issue 3, May 2024

Received: 27 March, 2024; Accepted: 8 May, 2024

DOI: <https://doi.org/10.63015/10S-2423.1.3>

Corresponding Author: kedar@mail.jnu.ac.in

Abstract: Transition metal dichalcogenide (TMDs) quantum dots (QDs) have attracted widespread attention among scientific community as fluorescent nanomaterial. Among TMDs, MoS₂ has received particular interest due to its novel and intriguing optical properties. In this work hydrothermal method is used to prepare aqueous soluble MoS₂ QDs using Molybdenyl acetylacetonate and thiourea as Mo and S precursors, respectively. The solubility of unfunctionalized MoS₂ is poor in water and organic solvent, therefore thioglycolic acid is used as surfactant for surface functionalization and to enhance the aqueous solubility & stability. These functionalized QDs have been synthesized at pH 11 using hydrothermal method and explored their structural and optical properties. The as synthesized QDs are characterized using TEM, XRD, FTIR, UV-Vis and PL spectroscopy. The morphological shape of as prepared QDs is spherical with size 4-6.5 nm. The MAA encapsulated MoS₂ QDs are further explored as fluorescent probe for the sensitive sensing of flavonoid Quercetin.

Keywords: Colloidal, fluorescent, transition metal dichalcogenides, flavonoid

Introduction: Szent-Gyorgyi are the first to isolate and identify bioflavonoids[1]. Bioflavonoids are the important class of bioactive molecules with effective antimicrobial, anti-inflammatory, antibacterial, antitumor and anticancer properties[2, 3]. Anthocyanidins, flavans, flavonols, anthoxanthins, and flavanones are the five subclasses of bioflavonoids. Quercetin is one of the flavonols mainly found in leafy vegetables, herbs, vegetables, seeds, red wine and fruits. The chemical structure of Quercetin consists of catechol ring and hydroxyl (-OH) groups at position 3',4', 3, 5 and 7 which makes it a potential material for numerous biomedical applications like anti-blood platelet, anti-carcinogenic, radical scavenger, expanding blood vessels because of antioxidant properties[4]. As Quercetin is an important antioxidant which plays important role for treating numerous diseases and also present in the daily diet of human. In spite of the high dietary intake of Quercetin, only 0.4-1% is

excreted in urine[5]. Thus, it is necessary to develop a sensitive and selective probe for the sensing of Quercetin in biological samples and pharmaceutical drugs.

The luminescent properties of metallic nanostructures, Quantum dots (QDs) and organic fluorescent dyes are used to detect analytes in the fluorescence-based methods. The unique properties of QDs like high quantum yield, broad absorption spectrum, good extinction coefficient, narrow and tunable emission spectra have fascinated researcher's interest worldwide. QDs possess excellent optical properties and have been widely utilized for the detection of toxic molecules, ions, small molecules, and biomacromolecules[6-8]. MoS₂ QDs have attracted more interest because of their high solubility in an aqueous medium and the presence of large number of active edge atoms. The synthesis of MoS₂ QDs has been explored by using several methods including liquid exfoliation, lithium intercalation and hydrothermal[9]. The tunable emission

properties of MoS₂ QDs makes them a potential material for sensing applications. MoS₂ nanostructure owing to their unique structures, high stabilities, low toxicity and high surface to volume ratio make them extremely attractive in the field of biosensing[10, 11]. There is still a critical need for the development of facile and widely accessible synthesis methods for the preparation of fluorescent MoS₂ QDs for biological applications. Ideally, these methods should synthesize small size, low polydisperse and colloidal nanoparticles with stability in a broad range of pH and various ionic buffers. For biological applications, there should be different functional groups available on the surface of nanostructure for surface modification with biomolecules such as peptides, proteins or drugs[12]. Most importantly the synthesized nanostructure should be stable and do not agglomerate in biological media i.e., intracellular environment and demonstrate an improved quantum yield.

In this manuscript, we have synthesized functionalized water soluble MoS₂ QDs using hydrothermal approach. Mercaptoacetic acid (MAA) encapsulated MoS₂ QDs were further utilized for the sensitive and selective sensing of Quercetin. The optical properties of synthesized MAA capped MoS₂ QDs have been explored using UV-Visible spectroscopy, and Photoluminescence (PL) spectroscopy. The structural and morphological characteristics have been studied using X-Ray diffraction (XRD), Transmission electron microscopy (TEM) and Fourier Transform Infrared spectroscopy (FT-IR), and. The sensing of Quercetin has been done based on the variation in the emission signal of MAA encapsulated MoS₂ QDs.

2. Experimental Section

2.1. Chemicals and reagents: The chemicals and reagents utilized in all the investigations are of analytical grade and have been used without any further purification. Mercaptoacetic acid [HSCH₂CO₂H], and Molybdenyl acetylacetonate [MoO₂(acac)₂] were procured

from Sigma Aldrich. Thiourea [CH₄N₂S] and Sodium hydroxide [NaOH] were purchased from Fisher Scientific. BOROSIL glassware is used for all the synthesis procedure. For the cleaning of the glassware chromic acid was used, followed by rinsing with DI water, ethanol, and acetone step by step and dried before using.

Synthesis of MoS₂ nanostructures: The current methodology utilizes hydrothermal method to synthesize MAA encapsulated MoS₂QDs. Thiourea and Molybdenyl acetylacetonate are used as precursors for S and Mo, respectively. Mercaptoacetic acid (MAA) is used as surfactant and for the functionalization of nanostructures. Firstly, 3.5 mM of Molybdenum acetylacetonate is dissolved in 60 ml DI followed by the addition of 96 µl of MAA. The above solution is stirred for 20 minutes at 100 °C. After cooling down the solution for some time the pH was set to 11 using 1 M NaOH solution. To the above prepared solution, add 15 mM of thiourea. After 15 minutes of magnetic stirring, the solution was transferred to 100 ml Teflon tube and sealed. The temperature of the stainless-steel autoclave was maintained at 220 °C for 24 hours. The supernatant containing QDs were collected after centrifugation.

2.3. Characterizations: Electronic absorption spectra were recorded using U-3900 Spectrophotometer-LABINDIA and emission spectra using F-4700 FL Spectrophotometer-LABINDIA. De-Ionized water was used as solvent to record the absorption and emission characteristics of the samples. Structural measurement of as prepared sample was done using a TEM; JOEL 2100F, high resolution transmission electron microscope (200 kV) (TEM). For TEM measurements, 5-10 µL QDs sample was drop casted over carbon support film of a 300 mesh Cu grid and let the sample dry for some time. Fourier transform infrared (FTIR) spectrum was recorded with FTIR spectrometer (Shimadzu 8400, Japan) utilizing KBr pellets in the range from 4000 cm⁻¹– 400 cm⁻¹. XRD was recorded using Rigaku mini-Flex 600, Japan, 1.54 Å°. The sample was dried at 50°C and then

XRD spectra was recorded. Zeta potential was measured using Malvern.

3. Results and Discussion: MoS₂ QDs are synthesized by one pot hydrothermal method using Molybdenyl acetylacetonate, Thiourea and MAA. In the synthesis process MAA and Thiourea could work as reducing agent due to the existence of various functional groups and as a source of S precursor, respectively. MAA will also work as a surface encapsulation agent and provide carboxyl groups over MoS₂ QDs surface which enhances the aqueous stability and solubility of synthesized QDs. Figure 1 (a) shows the TEM micrograph of MAA encapsulated MoS₂ QDs. The micrograph shows that the particles do not show any agglomeration and are well dispersed in aqueous media. The obtained size ranges from 4 nm – 6.5 nm with spherical morphology. The XRD pattern shown in Figure 2 (b) shows no obvious diffraction peaks, which may be due to their very small size. These small size QDs hardly have layer-layer interaction between each other. Bulk MoS₂ shows a diffraction peak at $2\theta = 14.4^\circ$

corresponding to the (002) plane[13]. However, its absence in the MoS₂ QDs XRD spectra reveals the lack of interlayer action in synthesized QDs. Figure 2 (c) depicts the FT-IR spectrum of MAA encapsulated MoS₂ QDs. The presence of surface passivated groups over MoS₂ QDs surface is confirmed by FT-IR spectra. The characteristic peak at 3452 cm⁻¹ illustrates the O-H bond of the adsorbed H₂O[14]. The characteristic band at 1635 cm⁻¹ is due to the stretching of C=O bond present in the stabilizing agent MAA. A sharp peak corresponding to the stretching of S-H group of MAA lies in the region 2550 cm⁻¹ – 2670 cm⁻¹. However, the absence of S-H in the MAA encapsulated MoS₂ QDs indicates the binding of the S atom of S-H group of the MAA to the Mo atoms lying on the surface of MoS₂ QDs. In the fingerprint region, the absorption band at 463 cm⁻¹ arises due the stretching of Mo-S bond[15].

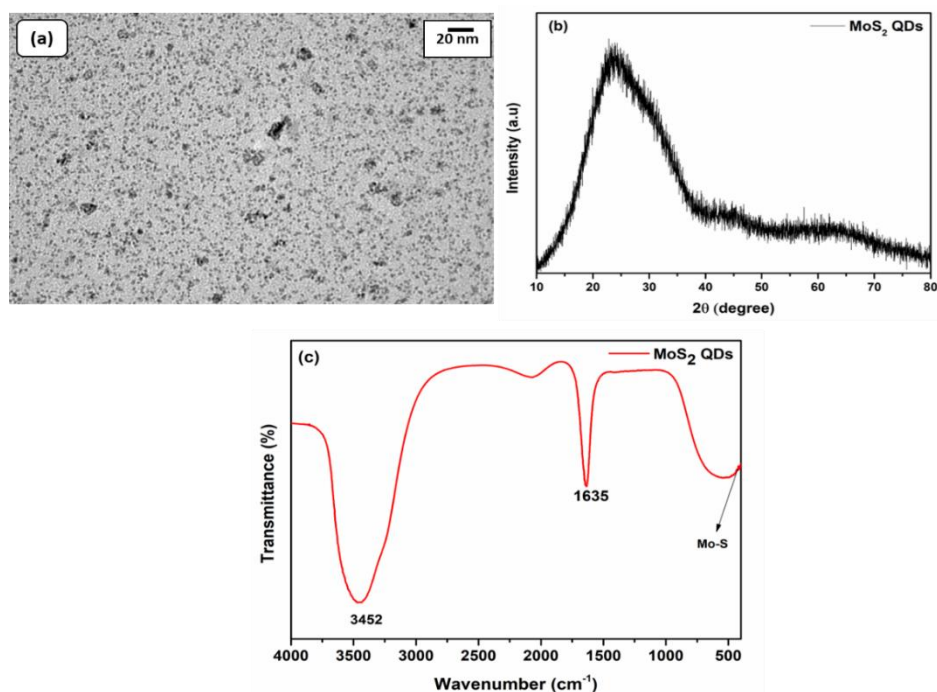


Figure 1: (a) TEM micrograph of MAA encapsulated MoS₂ QDs, (b) XRD spectrum of MoS₂ QDs and (c) FT-IR spectrum of MoS₂ QDs.

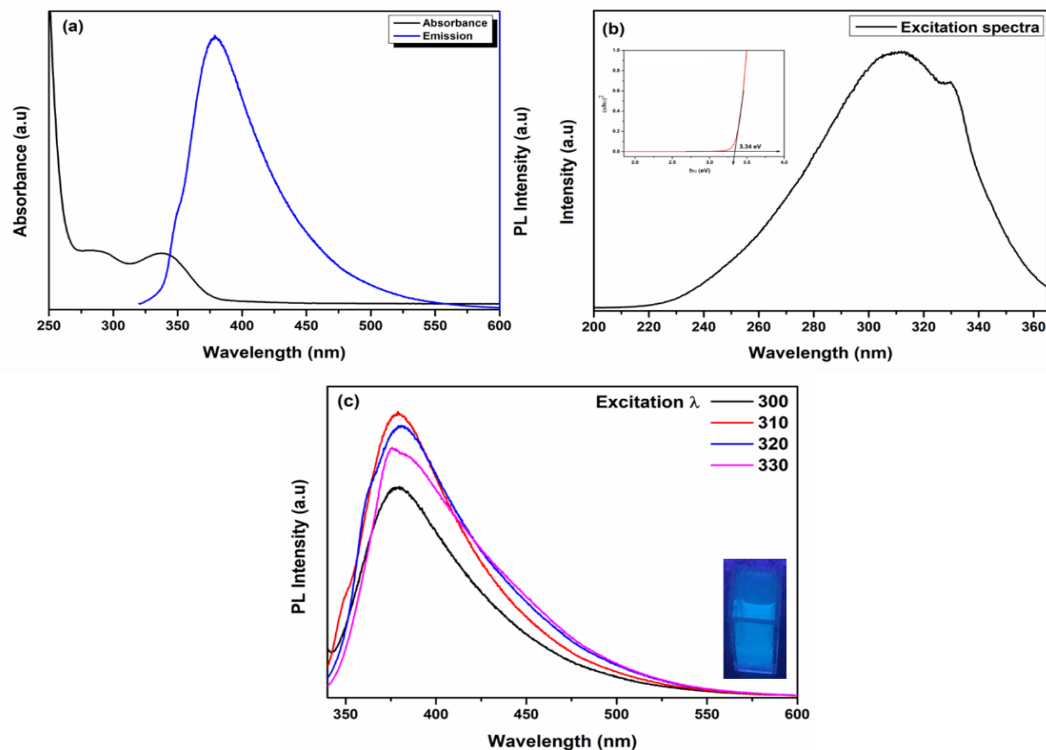


Figure 2: (a) Absorption and emission spectra (b) excitation spectra (inset shows the tauc plot) and (c) excitation dependent emission spectra of MAA capped MoS₂ QDs.

The optical characteristics of MAA encapsulated MoS₂ QDs are explored using UV-Visible and PL spectroscopy. Figure 2 (a) illustrates the absorption and emission spectra of prepared MoS₂ QDs. It has been reported that low dimensional or MoS₂ QDs show strong blue shift in the absorption peak when the dimension of the nanostructure reduced to less than 50 nm because of the quantum confinement effect [16]. The shoulder absorption peak observed at 340 nm can be ascribed to the direct transitions from the deep valence band to the conduction band in MoS₂ QDs. The absence of peaks in the higher wavelength region i.e. 600 nm–700 nm shows the absence of 2D MoS₂ with large lateral dimensions[17]. Also because of the strong quantum confinement effect the band gap of the QDs is enhanced, which is calculated using Tauc's relation[18]. Using Tauc's relation a graph is plotted between $(\alpha h\nu)^2$ i.e. square of the absorption energy and E as shown in inset in Figure 2(b). By extrapolating the tangent, the obtained bandgap is 3.34 eV which is much

larger than monolayer MoS₂ i.e. 1.9 eV and bulk MoS₂ with band gap 1.2 eV[19].

The excitation spectrum of MAA capped MoS₂ QDs (Figure 2(b)) illustrates an intense peak at ~310nm. Also, the emission spectrum shows a strong emission peak at 380 nm when excited at 310 nm. PL investigation is commonly used to explore the transition properties, carrier migration, and trapping properties. The higher emission intensity reveals the higher recombination rate of e-h pairs[20]. Also, the as synthesized MAA capped MoS₂ QDs show bright blue color when seen using UV lamp with 365 nm wavelength light, while they reflect light greenish color when observed with daylight. When as synthesized QDs are excited with different excitation wavelengths (300 nm- 330 nm) as shown in Figure 2(c), the emission spectra show a slight shift in the emission peak of ~ 2-3 nm. This excitation dependent emission spectrum is due to the polydisperse nature of the QDs[21]. Zeta potential was measured to know

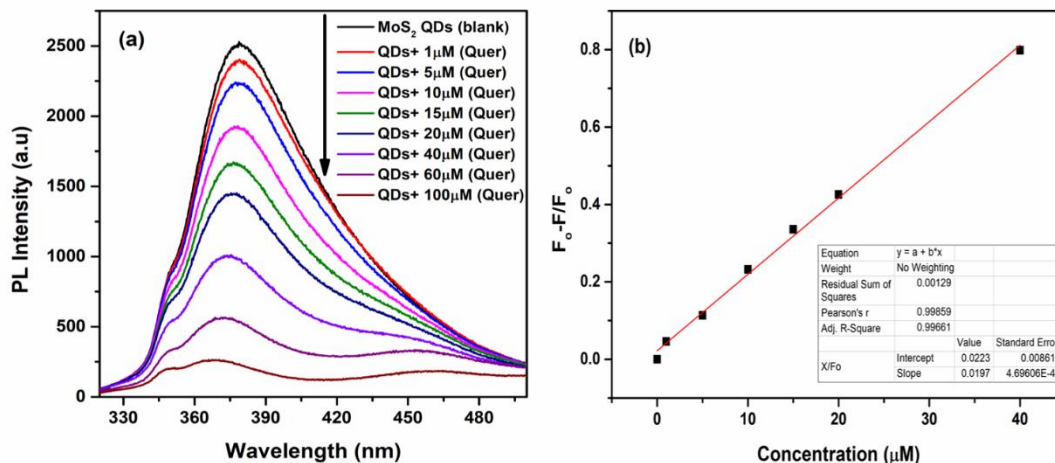


Figure 3: (a) PL spectra (λ_{exc} = 310 nm) of MAA encapsulated MoS₂ QDs in the presence of variable concentration of Quercetin (0-100 μ M) and (b) Plot showing the relative fluorescence intensity (F_o-F/F_o) vs the concentration of analyte Quercetin.

the colloidal stability of MAA capped MoS₂ QDs in aqueous media. Zeta potential was found to be -31.2 mV. The results suggest that synthesized QDs are highly stable in aqueous media.

Sensing of Quercetin: To explore the luminescence properties of QDs towards the detection of Quercetin, we have done the fluorescence titration experiment. For sensing experiment, we have diluted 100 μ L QDs in 3 mL solvent and then different concentration of Quercetin (1 μ M-100 μ M) are added to it. All the samples are incubated for 10 minutes so that MoS₂ QDs-Quercetin complex can completely react with an effective reduction in emission intensity. The excitation wavelength for all the samples is set to be 310 nm. From the emission spectra, it has been observed that there is quenching in the PL of QDs after adding Quercetin. The Quenching of QDs i.e., reduction in the emission intensity as the concentration of Quercetin increases from 1 μ M - 100 μ M. The fluorescence quenching efficiency is analyzed using Stern-Volmer equation[22]:

$$\frac{F_o - F}{F_o} = K_{S-V}[Q] + 1$$

Where F_o and F are the emission intensities of QDs in the absence and presence of Quercetin

respectively. $[Q]$ is the molar concentration of Quercetin and K_{S-V} is the quenching constant.

The quenching of emission of QDs may result from the strong complex formation between MoS₂ QDs and Quercetin. The formed complex Quercetin-MoS₂QDs might prevent the non-radiative electron to hole transfer and enhances the release of decreasing recombinant fluorescence, resulting in reduction of concentration of fluorescent molecule. It was observed that PL quenching was linear when the concentration of quencher was low i.e. till 40 μ M, while the linearity disrupts when concentration increases from 60- 100 μ M. Notably when the concentration of Quercetin reaches to 100 μ M, the emission intensity of the MoS₂ QDs quenches almost completely. The sensitivity of the fluorescent probe calculated using the slope from Figure 3(b) is $1.97 \times 10^4 M^{-1}$, which is good for sensing quercetin.

4. Conclusions: In the present manuscript water soluble MAA capped MoS₂ QDs are synthesized using one pot hydrothermal method. The prepared QDs shows high intensity PL emission at 380 nm with excitation wavelength 310 nm. The as prepared MoS₂ QDs shows the excitation dependent PL spectra because of the polydispersity of the synthesized QDs. FTIR confirms the functionalization of MoS₂ QDs

with mercaptoacetic acid successfully. The as prepared MAA encapsulated QDs exhibit spherical morphology with size 4-6.5 nm with intense blue emission. The high negative zeta potential confirms the colloidal stability of QDs in aqueous media. The fluorescence results and stability of synthesized MAA encapsulated MoS₂ QDs show that they can be further utilized as fluorescent tag for biomedical applications. We have utilized MoS₂ QDs as fluorophore for the sensitive sensing of Quercetin in aqueous medium with sensitivity of $1.97 \times 10^4 M^{-1}$.

Acknowledgements: Shivani Bharti is grateful to Dr. D. S. Kothari Postdoctoral Fellowship (F.4-2/2006 (BSR)/PH/20-21/0188), UGC for the financial support. We are thankful to AIRF, Jawaharlal Nehru University, New Delhi for using the characterization Instruments.

References

- Unusan N (2020) Proanthocyanidins in grape seeds: An updated review of their health benefits and potential uses in the food industry. *J Funct Foods* 67:103861. <https://doi.org/https://doi.org/10.1016/j.jff.2020.103861>
- Kopustinskiene DM, Jakstas V, Savickas A, Bernatoniene J (2020) Flavonoids as Anticancer Agents. *Nutrients* 12:. <https://doi.org/10.3390/nu12020457>
- KANADASWAMI C, LUNG-TA LEE, PING-PING HLEE, et al (2005) The Antitumor Activities of Flavonoids. *In Vivo (Brooklyn)* 19:895
- Hostetler GL, Ralston RA, Schwartz SJ (2017) Flavones: Food Sources, Bioavailability, Metabolism, and Bioactivity. *Advances in Nutrition* 8:423–435. <https://doi.org/https://doi.org/10.3945/an.116.012948>
- Andres S, Pevny S, Ziegenhagen R, et al (2018) Safety Aspects of the Use of Quercetin as a Dietary Supplement. *Mol Nutr Food Res* 62:1700447. <https://doi.org/https://doi.org/10.1002/mnfr.201700447>
- Wegner KD, Hildebrandt N (2015) Quantum dots: bright and versatile in vitro and in vivo fluorescence imaging biosensors. *Chem Soc Rev* 44:4792–4834. <https://doi.org/10.1039/C4CS00532E>
- Hai X, Feng J, Chen X, Wang J (2018) Tuning the optical properties of graphene quantum dots for biosensing and bioimaging. *J Mater Chem B* 6:3219–3234. <https://doi.org/10.1039/C8TB00428E>
- Li L, Wang T, Zhong Y, et al (2024) A review of nanomaterials for biosensing applications. *J Mater Chem B* 12:1168–1193. <https://doi.org/10.1039/D3TB02648E>
- Guo Y, Li J (2020) MoS₂ quantum dots: synthesis, properties and biological applications. *Materials Science and Engineering: C* 109:110511. <https://doi.org/https://doi.org/10.1016/j.msec.2019.110511>
- Yadav V, Roy S, Singh P, et al (2019) 2D MoS₂-Based Nanomaterials for Therapeutic, Bioimaging, and Biosensing Applications. *Small* 15:1803706. <https://doi.org/https://doi.org/10.1002/smll.201803706>
- Zhang J, Zhang X, Bi S (2022) Two-Dimensional Quantum Dot-Based Electrochemical Biosensors. *Biosensors (Basel)* 12:. <https://doi.org/10.3390/bios12040254>
- Zeng S, Yong K-T, Roy I, et al (2011) A Review on Functionalized Gold Nanoparticles for Biosensing Applications. *Plasmonics* 6:491–506. <https://doi.org/10.1007/s11468-011-9228-1>
- Wu P-R, Zhang W, Liu Z, Cheng Z-L (2019) A novel preparation method for MoS₂ nanosheets with good tribology performance by the combination of

- expansion and freeze exfoliation. *Ceram Int* 45:1730–1736. <https://doi.org/https://doi.org/10.1016/j.ceramint.2018.10.055>
14. Jain S, Bharti S, Bhullar GK, Tripathi SK (2022) Synthesis, characterization and stability study of aqueous MPA capped CuInS₂/ZnS core/shell nanoparticles. *J Lumin* 252:119279. <https://doi.org/https://doi.org/10.1016/j.jlumin.2022.119279>
 15. Sharma P, Mehata MS (2020) Colloidal MoS₂ quantum dots based optical sensor for detection of 2,4,6-TNP explosive in an aqueous medium. *Opt Mater (Amst)* 100:109646. <https://doi.org/https://doi.org/10.1016/j.optmat.2019.109646>
 16. Xu B, Su Y, Li L, et al (2017) Thiol-functionalized single-layered MoS₂ nanosheet as a photoluminescence sensing platform via charge transfer for dopamine detection. *Sens Actuators B Chem* 246:380–388. <https://doi.org/https://doi.org/10.1016/j.snb.2017.02.110>
 17. Zhang F, Wang M, Zhang L, Su X (2019) Ratiometric fluorescence system for pH sensing and urea detection based on MoS₂ quantum dots and 2, 3-diaminophenazine. *Anal Chim Acta* 1077:200–207. <https://doi.org/https://doi.org/10.1016/j.aca.2019.06.001>
 18. Khabiri G, Aboraia AM, Soliman M, et al (2020) A novel α -Fe₂O₃@MoS₂QDs heterostructure for enhanced visible-light photocatalytic performance using ultrasonication approach. *Ceram Int* 46:19600–19608. <https://doi.org/https://doi.org/10.1016/j.ceramint.2020.05.021>
 19. Rai DP, Vu T V, Laref A, et al (2020) Promising optoelectronic response of 2D monolayer MoS₂: A first principles study. *Chem Phys* 538:110824. <https://doi.org/https://doi.org/10.1016/j.cchemphys.2020.110824>
 20. Murali A, Sarswat PK, Free ML (2020) Minimizing electron-hole pair recombination through band-gap engineering in novel ZnO-CeO₂-rGO ternary nanocomposite for photoelectrochemical and photocatalytic applications. *Environmental Science and Pollution Research* 27:25042–25056. <https://doi.org/10.1007/s11356-020-08990-z>
 21. Lin H, Wang C, Wu J, et al (2015) Colloidal synthesis of MoS₂ quantum dots: size-dependent tunable photoluminescence and bioimaging. *New Journal of Chemistry* 39:8492–8497. <https://doi.org/10.1039/C5NJ01698C>
 22. Baride A, Engebretson D, Berry MT, Stanley May P (2013) Quenching of coumarin emission by CdSe and CdSe/ZnS quantum dots: Implications for fluorescence reporting. *J Lumin* 141:99–105. <https://doi.org/https://doi.org/10.1016/j.jlumin.2013.03.027>

Chemical footprint of open dumping sites due to electronic and battery waste

Umang Singh^a, Anil Kumar^b, Deepak Pant^{a*}

^a School of Earth and Environmental Sciences, Central University of Himachal Pradesh, Dharamshala, Kangra, Himachal Pradesh-176215

^b Forest Ecology and Climate Change Division, Himalayan Forest Research Institute, Shimla, India

Volume 1, Issue 3, May 2024

Received: 16 March, 2024; Accepted: 13 May, 2024

DOI: <https://doi.org/10.63015/3E-2422.1.3>

*Corresponding Author Email: dwpant2003@gmail.com

Abstract: Leachate from open dumping sites is found to be a major threat towards carcinogenic chemical footprint. The present study was conducted to evaluate the supply of various chemicals from electronic and battery (E&B) waste in dumping sites. Various types of E&B waste from household sources are regularly mixed with municipal solid waste (MSW). This study reports the presence of various types of primary and secondary pollutants in MSW from E&B waste. The major organic compounds found in the leachate were various phthalates, pyrrolidone and succinimide derivatives which may be due to the presence of e-toys and battery waste in the landfill. Intrusion of leachate containing these toxic compounds into river and groundwater systems leads to health implications like reproductive and developmental disorders, endocrine disruption and even cancer. It is concluded that a proper E&B waste management is necessary to ensure human and ecological health.

Introduction: Electronic toys and batteries (E&B) are commonly used in every household and due to some bad practices and limitations in the municipal segregation system, dumped in municipal solid waste (MSW). E&B waste contains a variety of organic and inorganic pollutants, causing various health implications (Table 1) like carcinogenesis, reproductive and developmental disorders, mutagens, endocrine disruptors, neurotoxins, etc. This position is made worse in case of open dumping in the hilly regions, where leachate from open dumps is carried by various seasonal rivers and ultimately supplies various contaminants to the river and groundwater bodies [1].

E&B waste has been reported to be a cause of many disorders like childhood lymphoma [2], neurotoxicity [3], bioaccumulation [4], possible respiratory disorders [5], etc. E&B waste contains various POPs, PCBs, PBDEs, PAHs, heavy metals, toxic additives, etc. which are detrimental for environmental and public health [6,7]. E&B is responsible behind the leaching of inorganic contaminants like heavy metals such as Pb, Cr, Mn, Fe, Co, Ni, Cu, and Cd [8], and organic contaminants like phthalates [9], etc. The above pollutants may increase the risk of cancer to mankind if not managed properly [10,11]. E-waste contains

Table 1: Toxic substances present in E&B waste

Toxic substance	Presence in e-waste	Health impacts
As	LEDs, solar cells, photovoltaic devices, trace contaminant or impurity in components like semiconductors, circuit boards, displays	Carcinogen, skin lesions, cardiovascular diseases, respiratory problems, neurological disorders
Azo dyes	E-toys	Mutagenic, toxic
Ba	CRTs, X-ray tubes, semiconductors, ceramic capacitors	Gastrointestinal effects, cardiovascular effects, respiratory effects, neurological effects, renal effects, developmental effects
Be	Beryllium-copper alloys, connectors, springs, switches, and electrical contacts, X-ray windows and detectors, beryllium oxide (BeO) ceramics, electrical insulation, beryllium-aluminum alloys, semiconductors, microelectronic packaging	Carcinogen, acute and chronic beryllium diseases, skin sensitization
Bisphenol A	Plastic casings, e-toys, epoxy resins, PCBs, cables, wiring	Endocrine disruptor, immuno-suppressant downregulate antioxidant genes, genotoxic, cytotoxic
Cd	Ni-cad batteries used in cordless power tools, camcorders, household appliances, etc., conductors in electronics, pigments in paints and coatings, stabilizers in plastics, electroplating of steel, iron, and copper	Kidney damage, bone damage, respiratory effects, carcinogenic, cardiovascular effect, reproductive and developmental effect
Co	Lithium-ion batteries, magnets, alloys, plating, semiconductors	Carcinogenic, reproductive and developmental effects, respiratory effects (irritation, coughing, wheezing, shortness of breath, and chest tightness), skin irritation, cardiovascular effects, hematological effects, neurological effects, thyroid dysfunction
Cr	HDD, chromium plating, sensors and detectors	Respiratory Effects, skin irritation, cancer risk, systemic toxicity
Cu	Excellent electrical conductivity and corrosion resistance, used in PCBs, wiring and cables, connectors and terminals, coils and inductors, electromagnetic shielding	Gastrointestinal distress, liver damage, neurological effects, kidney damage, hemolytic anemia, hepatic encephalopathy
Fe	Structural component, wiring, connectors, transformers inductors, magnet, storage media, for thermal management	Gastrointestinal symptoms (like nausea, vomiting, abdominal pain, and diarrhea), organ damage, hemochromatosis, iron poisoning, hemolytic anemia
Flame retardants (BFR)	E-toys, plastic casings, PCBs, cables, wiring	Endocrine, neurological, reproductive, immune and cardiovascular systems
Hg	CFLs, batteries, thermostats, electrical switches and relays	Neurological effects, cardiovascular effects, renal effects, developmental effects, reproductive effects, immune system effects, dermatological effects
Li	Li-ion batteries, ceramics and glasses production for electronic displays, touch screens, and other electronic components	Gastrointestinal Symptoms, neurological effects, cardiovascular effects, renal effects, thyroid dysfunction, interference with nucleic acids synthesis
Mn	Magnets, ceramics, semiconductors, batteries, capacitors, plating and surface treatments	Behavioral and cognitive effects, neurological effects, reproductive and

		developmental effects, respiratory effects, hepatic effects, cardiovascular effects, impaired iron absorption
Ni	Batteries (Ni-Cd, NiMH, LIB), electroplating, magnetic alloys, connectors and terminals, PCBs, Thermal Conductors	Carcinogenic, allergic contact dermatitis, asthma, lung damage, systemic effects, reproductive and developmental effects, hypersensitivity reactions
N-methyl-2-pyrrolidone	Lithium-ion batteries, paint and coatings	Irritant (skin, eyes, respiratory system), potentially carcinogenic, affect CNS, reproductive toxicity, developmental toxicity, hepatotoxic, nephrotoxic
PAHs	Plastics, coatings and adhesives, rubber, combustion byproduct	Alters immunological responses, diarrhea, inflammation, affected the intestinal epithelium, transformation of microfold cell (M cell), carcinogenic risk, respiratory effects, cardiovascular effects, reproductive and developmental effects, immune system effects, neurological effects, skin effects
Pb	Soldering electronic components, lead acid batteries, paint, PCBs, CRTs, lead weights in electronics	Neurological effects, developmental effects, hematological effects, renal effects, cardiovascular effects, gastrointestinal effects, reproductive effects, skeletal effects
PBDEs (Polybrominated diphenyl ethers)	PCBs, plastic casings, connectors and components, cables and wiring	Carcinogen, neurotoxin, reproductive toxin, endocrine disruptor, developmental toxin, effects on immune system
PCBs (Polychlorinated Biphenyls)	Capacitors, transformers, insulating fluids, flame retardants	Carcinogenic, neurotoxic, reproductive toxin, endocrine disruption, immune system effects, lung damage
Phthalates	E-toys, cables, wiring, plastic casings and housings, packaging materials, adhesives, sealants	Reproductive and developmental disorders, endocrine disruption, liver damage, kidney damage, metabolic disorders, neurotoxicity, asthma, allergies
PVC	Insulation, wiring, cable conduits and ducts, electronic enclosures, housings, PCBs, antistatic packaging, heat shrink tubing, seals, gaskets	Brain cancer, hormonal imbalances, reproductive and developmental problems, allergies in children, hardening of connective tissue throughout the body
Se	Photovoltaic cells, photocopying, printing, rectifiers, semiconductors, photovoltaic detectors, X-ray imaging	Selenosis, cancer risk, gastrointestinal disturbances, skin and hair problems, neurological symptoms, respiratory distress, hypersensitivity reactions, impaired thyroid function
Styrene butadiene rubber	Lithium-ion batteries, adhesives, sealants, rubber components, cable insulation, protective coatings	Irritant (skin, eyes, respiratory system), potentially carcinogenic, adverse reproductive and developmental effects
REE	Permanent magnets, fluorescent lighting, led lighting, catalysts, glass and ceramics, batteries (Ni-MH, EV-LIBs)	Radioactive contamination, gastrointestinal disorders, organ damage, developmental abnormalities

over 1000 potentially toxic substances which are of serious environmental and public health concern when disposed [6]. E-waste has been recognised as the major component of MSW lately [6]. India is receiving scrap gadgets from western nations¹³ and stood fourth in global e-waste generation [12]. Supplementary to the generation rate, India also receives scrap gadgets from western nations [13].

E&B waste recycling is quite challenging due to complex dismantling and structure, heterogeneity of waste, material diversity, resource recovery challenges, collection and sorting challenges, lack of proper infrastructure, limited public awareness and involvement, etc. [12,14]. Exposure to the e-waste toxins regularly result in poor health and unsafe environment for the workers. Various studies confirm that the indigestion, inhalation and dermal contact with these toxins during E&B waste handling by the informal sector gives rise to occupational hazards which include cellular toxicity by heavy metals, DNA mutations, tumorigenesis, impaired cognition in children, asthma, lung dysfunction, immune dysfunction, altered cell expression, liver and kidney damage, cancer, etc. Generation of E&B waste is increasing day by day, hence investigation on the health and environmental effects of E&B waste is the need of the hour. This paper reports various pollutants from the above type of waste with a policy recommendation so that a proper 3R (reduce, reuse and recycle) can be developed with requisite government partnership.

Material and methods: Samples of leachate were collected from Kangra open landfill site. Kangra is a municipality situated in Kangra district in the Indian state of Himachal Pradesh. It is located at 32°06'11"N 76°16'24"E. The landfill site is situated at a height from where precipitation mixes with the leachate and carries the contaminants downhill to the seasonal rivers.

Leachate samples were collected, stored in cooler boxes at 4°C and analyzed within 24

hours. pH, Electrical Conductivity (EC), Ultraviolet-Visible (UV-Vis) and Fourier Transform InfraRed (FTIR) analysis were performed. pH was calculate using a digital pH meter and EC by using CDM210 conductivity meter. UV-Vis analysis was done using a UDB650 red tide spectrometer with a wavelength range between 200-800 nm. FTIR spectrometry was performed using Bruker alpha instrument with an absorption band ranging between 400 to 4000 cm^{-1} . For UV-Vis analysis, sample dilution was performed with Type-1 water. Samples with 10, 50, 100, 500 and 1000 times dilution were analyzed and best result was obtained at 100 times dilution.

Results and discussion: pH of the leachate samples ranged from 7.5-8.5 and EC readings were between 4.5-8 mS cm^{-1} . UV-Vis analysis showed an absorbance range between 200-300 nm while FTIR showed absorbance bands between 3500-2800 and 1750-700 cm^{-1} . The result confirmed the presence of CH aromatic group, C=O group, C=C group, CH aliphatic bending group, O-H group, C-N bond in the leachate samples [15]. Evidence of a variety of possible compounds were found, among them, presence of various phthalates and pyrrolidone derivatives in the samples were selected to depict the source of the contaminants in the leachate to the presence of e-toys and battery waste in the landfill. These compounds also show their presence in other e-wastes like circuit boards, semiconductors, insulating materials, cable insulation, gaskets, seals, wiring, etc.

Compounds found in the leachate reasonably consist of phthalic acid derivatives which can be identified by the presence of UV and IR peaks around 225-228 nm and 3000, 1750 and 1300 cm^{-1} [16] respectively (Figure 1 and 2), suspected for the presence of phthalates in the leachate. Phthalates are widely used in a variety of plastic products as plasticizers and can cause reproductive and developmental disorders, endocrine disruption, liver damage, kidney damage, metabolic disorders, neurotoxicity,

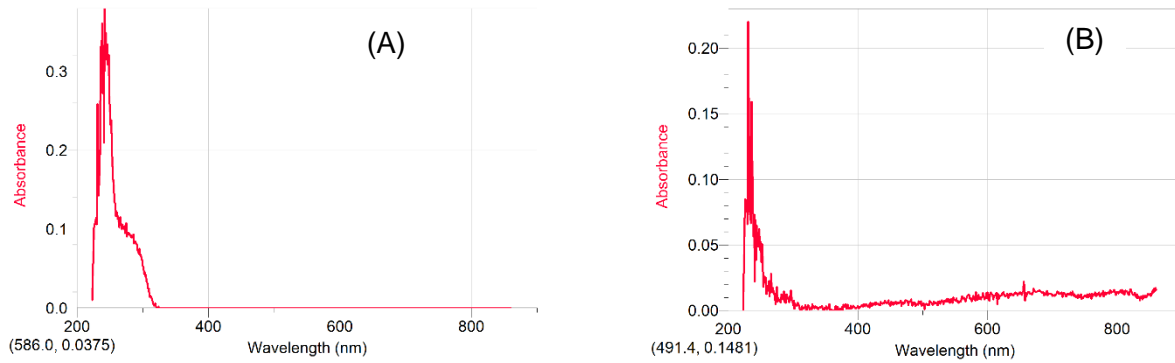


Figure 1: UV-Vis absorbance vs wavelength graph of leachate sample (A) at 100 times dilution; (B) at 500 times dilution

asthma, allergies, etc. These readily leach into the water systems and show common occurrence in wastewater, landfill leachates and groundwater. The source of these compounds in the leachate was traced to the possible presence of e-toys in the waste site.

Compounds succinimide and pyrrolidones derivatives in the leachate can be identified due to the presence of characteristic UV-Vis bands below 450 nm [17] and in the leachate sample identifies, between 230-240 nm and IR absorption bands around 1700, 1300-1400 cm^{-1} [18] (Figure 1 and 2). N-methyl pyrrolidone (NMP) is used as a solvent in paints and electronics industry. It is also used as a solvent in lithium-ion batteries (LIB). NMP is an irritant, potentially carcinogenic, reproductive toxin, developmental toxin, hepatotoxin, nephrotoxin and affects the CNS. The source of pyrrolidones in the leachate was traced to the

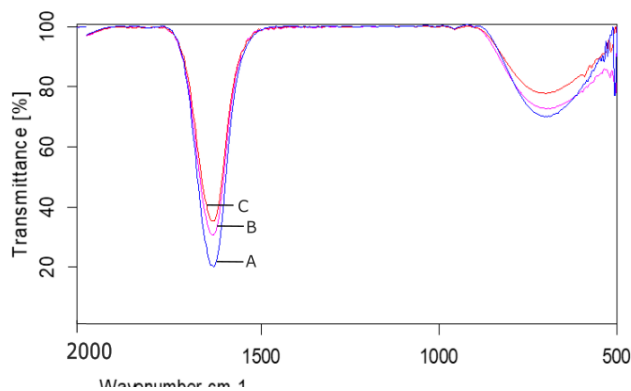


Figure 2: FTIR analysis of leachate samples A, B and C

possible presence of LIB waste in the dumping site.

Policy recommendation: Although the e-waste and battery waste management rules of India include aspects for the solution of E&B waste problems like the development of inventory by record maintenance at the end of every manufacturer, producer, refurbisher and recycler, collection of e-waste, labor safety monitoring, encouragement to put up facilities, public awareness and EPR, the rules require more stringent measures for their proper implementation as a lot of work is still lacking. Despite the E-waste management rules, which support recyclers and refurbishers, the number of registered recyclers are still very less. There are a total of 569 registered recyclers nationwide as on 08-06-2023 as reported by the CPCB. This task will only work through a stronger partnership with the informal sector as they have a widespread network and have an easier channel for collection. Besides, 90% of collection and 70% of recycling is handled by them [19]. Consumer engagement in proper E&B waste management is also very less due to the lack of awareness.

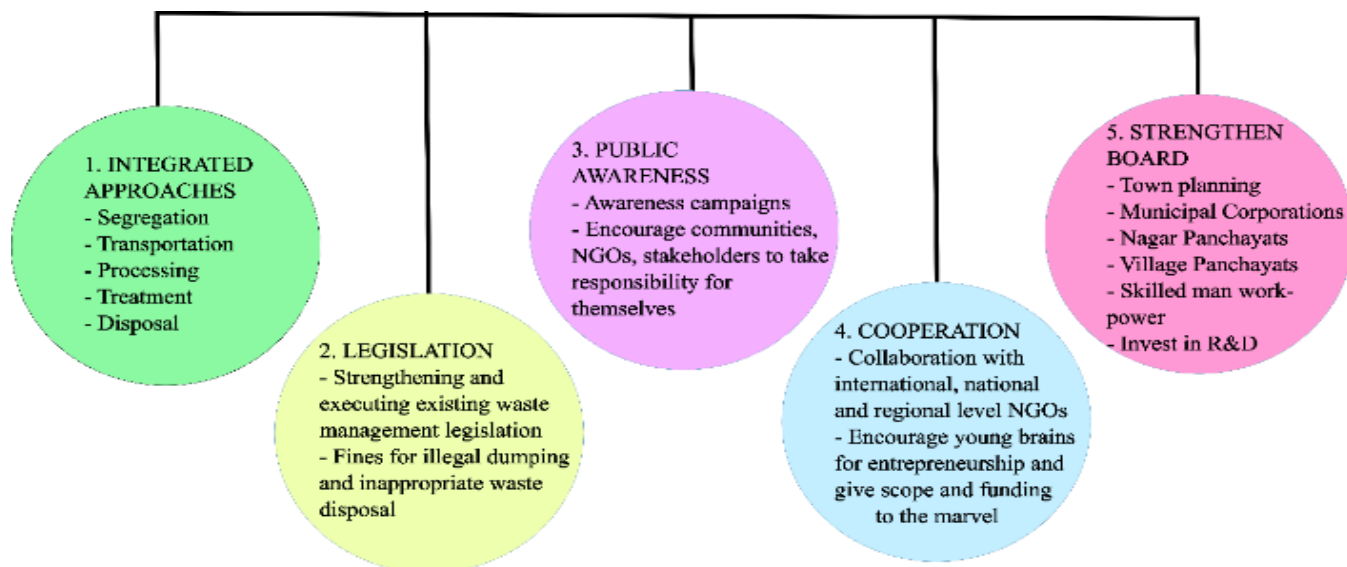


Figure 3. Waste management goals and approach

The government should provide policy incentives and awareness campaigns to promote effective management of E&B waste among the public. E&B waste often ends up in disposal sites without undergoing crucial treatment and is disposed off on open land without proper safety or environmental controls in the small towns. Additionally, burning E&B waste in open areas is also an issue of concern as it releases many toxic formulations, which are of concern to human health. To address these issues, it is essential to implement management rules for waste collection through segregation, transport, processing, treatment, and disposal procedures more stringently. The government should engage with local people and stakeholders respectfully and collaboratively to consider their participation and the role of communities in the waste management phenomenon. However, inadequate infrastructure for proper disposal sites, lack of adequate disposal facilities, and lack of skilled man workpower in India, makes this process very tedious. Therefore, State governments must strengthen town planning commissions, municipal corporations, and Nagar Panchayats to improve waste management practices (Figure 3). They should also continuously evaluate the waste

management mechanisms employed at regional scales by the concerned authorities.

Conclusion: This study was conducted to detect the sources of various toxic compounds present in the leachate of an open dumping site. The analysis of compounds showed their possible source to be from e-toys and battery waste which was mixed with other solid waste. Compounds found in the leachate are detrimental to human health and ecological health and most of them are possible carcinogens. Proper awareness, management and disposal of E&B waste is hence necessary, considering their toxic nature. Public awareness and participation in WEEE waste is also required.

References

1. Y. Wang, F. Wang, Z. Cheng, Q. Su & Y. Cao, Health risk cause of water around landfill in hilly area and prevention and control countermeasures. *J. Environ. Manage.* **346**, 119019 (2023).
2. J. Davis & Y. Garb A strong spatial association between e-waste burn sites and childhood lymphoma in the West Bank, Palestine. *Int. J. Cancer* **144**, 470–475 (2019).
3. J. G. Dórea Neurodevelopment and exposure to neurotoxic metal(loid)s in environments

- polluted by mining, metal scrapping and smelters, and e-waste recycling in low and middle-income countries. *Environ. Res.* **197**, 111124 (2021).
4. W. Li & V. Achal, Environmental and health impacts due to e-waste disposal in China – A review. *Sci. Total Environ.* **737**, 139745 (2020).
 5. O. N. Avenbuan *et al.* A contemporary review of electronic waste through the lens of inhalation toxicology. *Inhal. Toxicol.* **33**, 285–294 (2021).
 6. O. A. Alabi, Y. M. Adeoluwa, X. Huo, X. Xu & A. A. Bakare, Environmental contamination and public health effects of electronic waste: an overview. *J. Environ. Health Sci. Eng.* **19**, 1209–1227 (2021).
 7. A. Sobianowska-Turek, W. Urbańska, A. Janicka, M. Zawisłak & J. Matla, The Necessity of Recycling of Waste Li-Ion Batteries Used in Electric Vehicles as Objects Posing a Threat to Human Health and the Environment. *Recycling* **6**, 35 (2021).
 8. D. Dutta, S. Goel & S. Kumar, Health risk assessment for exposure to heavy metals in soils in and around E-waste dumping site. *J. Environ. Chem. Eng.* **10**, 107269 (2022).
 9. U. Kotowska, J. Kapelewska & R. Sawczuk, Occurrence, removal, and environmental risk of phthalates in wastewaters, landfill leachates, and groundwater in Poland. *Environ. Pollut.* **267**, 115643 (2020).
 10. A. Giuliani, M. Zuccarini, A. Cichelli, H. Khan & M. Reale, Critical Review on the Presence of Phthalates in Food and Evidence of Their Biological Impact. *Int. J. Environ. Res. Public Health* **17**, 5655 (2020).
 11. P. Aendo, R. Netvichian, P. Thiendedsakul, S. Khaodhiar & P. Tulayakul, Carcinogenic Risk of Pb, Cd, Ni, and Cr and Critical Ecological Risk of Cd and Cu in Soil and Groundwater around the Municipal Solid Waste Open Dump in Central Thailand. *J. Environ. Public Health* **2022**, 1–12 (2022).
 12. S. Arya & S. Kumar, E-waste in India at a glance: Current trends, regulations, challenges and management strategies. *J. Clean. Prod.* **271**, 122707 (2020).
 13. P Thakur & S. Kumar, Evaluation of e-waste status, management strategies, and legislations. *Int. J. Environ. Sci. Technol.* **19**, 6957–6966 (2022).
 14. V. Pérez-Belis, M. D. Bovea & A. Simó, Consumer behaviour and environmental education in the field of waste electrical and electronic toys: A Spanish case study. *Waste Manag.* **36**, 277–288 (2015).
 15. Libretexts. Infrared Spectroscopy Absorption Table. *Chemistry LibreTexts* https://chem.libretexts.org/Ancillary_Materials/Reference/Reference_Tables/Spectroscopic_Reference_Tables/Infrared_Spectroscopy_Absorption_Table (2020).
 16. Informatics, N. O. of D. A. (n.d.). 1,2-Benzenedicarboxylic acid. <https://webbook.nist.gov/cgi/cbook.cgi?ID=C88993&Type=IR-SPEC&Index=1>
 17. S. P. Ogilvie *et al.* Considerations for spectroscopy of liquid-exfoliated 2D materials: emerging photoluminescence of N-methyl-2-pyrrolidone. *Sci. Rep.* **7**, 16706 (2017).
 18. Informatics, N. O. of D. A. 2-Pyrrolidinone, 1-methyl-. <https://webbook.nist.gov/cgi/cbook.cgi?ID=C872504&Mask=80>.
 19. Ministry of Electronics and Information Technology Government of India. CIRCULAR ECONOMY IN ELECTRONICS AND ELECTRICAL SECTOR ACTION PLAN. www.meity.gov.in https://www.meity.gov.in/writereaddata/files/Circular_Economy_EEE-MeitY-May2021-ver7.pdf (2021)

Investigation of substrate materials laminated CPW-Fed patch antennas: Opportunities and challenges

Manish Kumar¹, Yamiko D. Banda¹, Ftema W. Aldbea², Serguei V. Savilov³, Sandeep Kumar Singh^{*1}

¹Department of EECE, SUSET, Sharda University, Greater Noida, 201310, India.

²Physics Department, Faculty of Science, Sebha University, Libya

³Department of Chemistry, Lomonosov Moscow State University, Moscow, 119991, Russia

Volume 1, Issue 3, May 2024

Received: 10 April, 2024; Accepted: 22 May, 2024

DOI: <https://doi.org/10.63015/10S-2426.1.3>

*Correspondence Author Email: sandeepsingh.ec@sharda.ac.in

Abstract: This article investigates the design of antennas fed by coplanar waveguide (CPW) utilizing different substrate materials and techniques. The article illustrates the impact of several materials such as FR-4, Rogers, Arlon, etc on electrical properties such as impedance bandwidth (IBW), reflection coefficient ($|S_{11}|$), and gain. The article also examines the effects of design approaches such as including stubs, slots, arrays, etc on antenna $|S_{11}|$ parameters. The resonance frequencies (fr) of the suggested antennas may be modified by manipulating the electrical dimension, the dielectric constant of the substrate materials, and their respective thicknesses. The structure of the Flame-Retardant fiberglass epoxy (FR-4) proposed antenna covers an operating frequency range of 3.3 to 10.1 GHz. It can operate at six distinct frequency bands, making it appropriate for applications including C-band (4-8 GHz), X-band (8-12 GHz), 5G (3.5-6.0 GHz), and 6G (7-20 GHz). The antenna designed and simulated using computer simulation software (CST) electromagnetic simulator.

Keywords: Substrate Material, FR-4, Rogers RT5880, Arlon AD600, CPW-fed

1. Introduction: Antennas are essential for wireless communication systems. Demand for affordable, flexible, low-profile, and small broadband antennas has grown rapidly in the past two decades. Multiple antennas are required for transceiver services, but it's challenging to incorporate them into a single mobile device due to size constraints. Communication technologies must be carefully kept apart. A multi-band circularly polarized (CP) antenna is needed to overcome this limitation. It is used to make independent data transmission and reception, remove fading or multipath shortcomings, tolerate adverse weather conditions, achieve accurate polarization between antennas, and has proven to be highly robust in varied electromagnetic environments. The advantage of this approach is its simplicity, which allows it to be easily

redesigned for multiple frequency bands. The redesign technique is simple, requiring simply a recalculation of the chosen physical dimensions followed by electromagnetic-based parameter modification. The slot antennas with a coplanar waveguide feed increase bandwidth and reduce antenna size. CPW feed offers wideband, high impedance bandwidth, reduced radiation loss, and ease of integration with active elements. To cover radio frequency identification (RFID), global navigation satellite system (GNSS), wireless local area network (WLAN), and worldwide interoperability for microwave access (WiMAX) frequency ranges of interest, a wideband compact CPW-fed circularly polarized antenna is provided [1-6].

A large axial ratio bandwidth (ARBW) is achieved by coupling three CP modes together with an asymmetric CPW structure [7]. The modified coplanar ground plane to accomplish dual operating bands that include S-Band, C-Band, WiMAX, WLAN, 4th generation mobile network (4G), 5th generation mobile network (5G), ultra-wideband (UWB), and X-band communications. A CPW-fed UWB flexible composite antenna is used for wireless personal area network (WPAN) applications. The CPW-fed antennas on high-permittivity substrates are designed to achieve high gain for industrial, scientific, and medical (ISM) applications. The antenna array showed good impedance matching when tested in conformal conditions and has the potential for wearable applications [8-10].

CPW-fed antennas are suitable for various wireless applications, including 5G, and can be optimized for 6G by achieving the desired gain, directivity, efficiency, and bandwidth. Design techniques like defected ground structure (DGS), frequency selective surface (FSS), Metamaterials, arrays, and multiple-input-multiple-output (MIMO), can further improve these characteristics. This article will explore parametric studies using different design techniques with various substrate materials and appropriate thicknesses to

optimize the antennas for several radio frequency (RF) and wireless application. A dielectric material is very important for the operating frequency range. The thicker substrate with lower dielectric constants carries more efficiency and a wider impedance bandwidth but results in a larger antenna. Hence, high-dielectric constant substrate techniques to allow appropriately small antenna sizes have been analyzed for RF and microwave applications. The different types of substrate materials and their properties are tabulated in Table 1. The resonance frequencies are dependent on the substrate area, thickness, and dielectric constant. Fundamental resonance frequencies are moved towards the low-frequency band at a higher dielectric constant with low substrate thickness. Thus, substrates with the high dielectric constants ensure the antenna miniaturization [11-14].

This article reviews various design techniques for CPW-fed antennas, focusing on substrate materials and their thickness. The article is presented in four sections. In section 2, comparative studies and design techniques have been discussed. In section 3, the proposed work and in section 4, comparative outcomes are given.

Table 1: Properties of substrate materials

Material	Dielectric Constant (ϵ_r)	Loss Tangent ($\tan\delta$)	Specific Heat (J/g·K)	Thermal Conductivity (W/mK)	Moisture Absorption (%)	Surface Resistivity (M Ω)
Silicon	11.9	0.0010	1.01	100-150	0.02	-
Polyethylene Terephthalate (PET)	1.80	0.0005	1.17	0.256	-	-
Taconic CER-10	10.0	0.0035	-	0.63	0.02	1.1 \times 10 ⁹
Arlon	3.20	0.0038	0.90	0.24	0.06	1.6 \times 10 ⁹
Rogers RT/Duroid 5880	2.20	0.0009	0.96	0.71	-	3 \times 10 ⁷
Rogers RT/Duroid RO3006	6.15	0.0020	0.86	0.61	0.02	1 \times 10 ⁵
Rogers RT/Duroid RO4003	3.38	0.0027	0.93	0.64	0.04	4.2 \times 10 ⁹
FR-4	4.2 - 4.6	0.0200	0.95	0.16	0.25	4 \times 10 ⁶

2. Comparative Study and Design Techniques:

The selection of design techniques and selecting a suitable antenna is crucial for RF system performance, including bandwidth and communication range. Researchers have proposed various techniques [1-14] to increase antenna bandwidth and gain, and reduce the size of the antenna. These methods modify parameters like bandwidth, gain, directivity, efficiency, and impedance bandwidth, allowing antennas to work in various applications like RFID, WLAN, Wi-Fi, Wi-Max, WPAN, ISM, IMT bands, GNSS, S-band, C-band, X-band, Ku, Ka-band, 5G, high-performance radio local area network (HiperLAN), unlicensed national information infrastructure (U-NII), and work in multiple bands simultaneously. It also shows the applicability of antennas to work in multiple bands at the same time. This paper introduces mathematical modeling for antenna design, focusing on determining dimensions and optimizing performance. Geometries enhance parameters like return loss, bandwidth, gain, and radiation pattern. The antenna's size is crucial for wideband purposes, with resonant frequency, radiation pattern, and input impedance controlled by patch length and width. Basic calculations for antenna dimensions are provided using formulae [3]. The L and W of the patch antenna can be calculated by using the equations (1–5).

2.1. Calculation of the width (W)

$$W = \frac{1}{2fr\sqrt{\mu_0\epsilon_0}} \sqrt{\frac{2}{1+\epsilon_r}} \tag{1}$$

$$W = \frac{c}{2fr} \sqrt{\frac{2}{1+\epsilon_r}} \tag{2}$$

where, $c = \frac{1}{\sqrt{\mu_0\epsilon_0}}$ is the velocity of light in the free space, μ_0 is the permeability of free space, ϵ_0 is the permittivity of free space, ϵ_r is the relative permittivity of the substrate, and f_r is the resonant frequency.

2.2. Actual length of the patch (L)

$$L = L_{eff} - 2\Delta L \tag{3}$$

$$L = \frac{1}{2fr\sqrt{\mu_0\epsilon_0}\sqrt{\epsilon_{reff}}} - 2\Delta L \tag{4}$$

$$L = \frac{c}{2fr\sqrt{\epsilon_{reff}}} - 2\Delta L \tag{5}$$

where, ΔL is the incremental length due to Fringing field, and ϵ_{reff} is the relative effective dielectric constant. The effective dielectric constant can be calculated by using the equation (6), and the effective length (L_{eff}) can be calculated using equation (7).


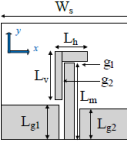





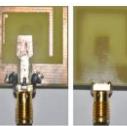
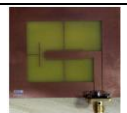
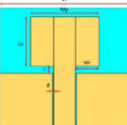
$$\epsilon_{reff} = \frac{\epsilon_r+1}{2} + \frac{\epsilon_r-1}{2} \left(\frac{1}{\sqrt{1+\frac{12h}{w}}} \right) \tag{6}$$

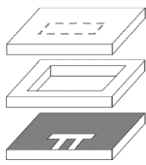
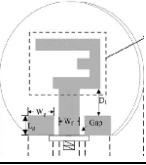
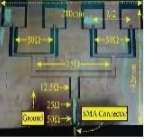

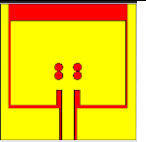
$$L_{eff} = \frac{c}{2fr\sqrt{\epsilon_{reff}}} \tag{7}$$

2.3. Effects of adding stubs, slots, strips, cutting corners, and arrays:

Recent ultra-wideband antenna structure designs have used various techniques to achieve CP radiation on a microstrip antenna, as seen in Table 2. These approaches include cutting corners, slot-loading, branch line loading, adding slits, arcs, asymmetrical feeding, arrays, spiral stubs, and so on. These approaches permit CP radiation, efficient impedance matching, and effective gain across a wider frequency range, with potential biomedical, wearable, and industrial applications.

Table 2. Summary of comparative performance of referred CPW-Fed antennas with various substrate materials

Antenna Design Techniques	Antenna Structure	Antenna Area (mm ²)	Substrate Material (ϵ_0)	IBW (%) (at > -10dB)	Peak Gain (dBi)	Applications	Ref.
Annular Ring Slot, Cutting corner, Slot loading		25 × 24	FR4 (4.4)	56.27%	3.7-4.6	UWB	[1]
L-shaped Strip		35×22.5	Rogers RO4003C (3.38)	89%	3.3	Wideband (3.2-8.4 GHz)	[2]
Square Ring slits, Cross shaped tuning stub		50×50	FR4 (4.4)	91.12%	5.7	WLAN, WiMAX, IMT	[3]
Inverted L-shaped strip, square slot		26×26	Rogers Duroid RT5880 (2.2)	104%	3.4-4.4	C-Band	[4]
Square slot, spiral stub		20×30	FR4 (4.4)	38.89%	3.5	5G Network	[5]
Asymmetrical rectangle slots		88×89.9	Rogers RO3006 (6.5)	129.5%	5.0	RFID, WLAN, Wi-MAX, GNSS	[6]
L-shaped strip		60×80	FR4(4.4)	100%	3.7	Sub-6 band	[7]
Inverted L-shaped strip		24.5×20	FR4(4.6)	-	4.33-4.80	Wi-MAX, WLAN, 4G/5G, X-band	[8]
L-shaped Stubs		50×50	Rogers (2.2)	95%	10.2	IMT, GSM	[9]
Rectangular patches		27.2×26.4	Jute (2.36)	101.3%	2.0	WPAN	[10]

Top layer: Inverted Patch, Bottom layer: CPW-fed and ground plane		4×2.83/ 4.4×2.6	Taconic CER (10)/ Silicon (11.9)	-	6	ISM 24-GHz band	[11]
Inverted E-shaped monopole		490	Ceramic (8.5)	60.45%	4.4	ISM, HIPERLAN, UNII and WiMAX	[12]
Arrays		280×192	Polyethylene Terephthalate (PET) (1.8)	-	10	ISM	[13]
Split-ring resonator (NB-SRR), MIMO antenna		47.4 × 31.7	FR4(4.4)	30.10%, 8.83%	5	Sub-6 GHz 5G	[14]
Rectangular patch with circular slits		32×32	FR4(4.3)	5.73%, 4%, 17.9%,18.2% ,9.2%,6.3%	2.8	5G, C-Band, X-Band	Proposed Antenna

3. Antenna Design: In this section, the work examines the characteristics of three antennas: Antenna-1 focuses on the impact of dielectric substrate materials on patch antenna design based on three materials (Rogers RT5880, FR-4, and Arlon AD600) with permittivity values of 2.2, 4.3, and 6.15 and substrate thickness of 1.6 mm as shown in Figure 1(b). Antenna-2 shown in Figure 1(c) is based on FR-4 substrate material with a permittivity value of 4.3 and substrate thickness values of 1.30 mm, 1.60 mm, and 2 mm, respectively, for analyzing the |S11| parameter. The CPW-Fed antenna is shown in figure 1(d). The antenna dimensions for antenna-1, 2, and antenna-3 is 32×32mm². The structural design parameters of patch are shown in figure 1(a). The proposed work aims to understand the effects of these substrate materials and thicknesses on antenna performance metrics, particularly resonant frequencies, which are essential for optimal antenna operation. The antennas are designed

for the efficient transmission and reception of high-frequency electromagnetic waves.

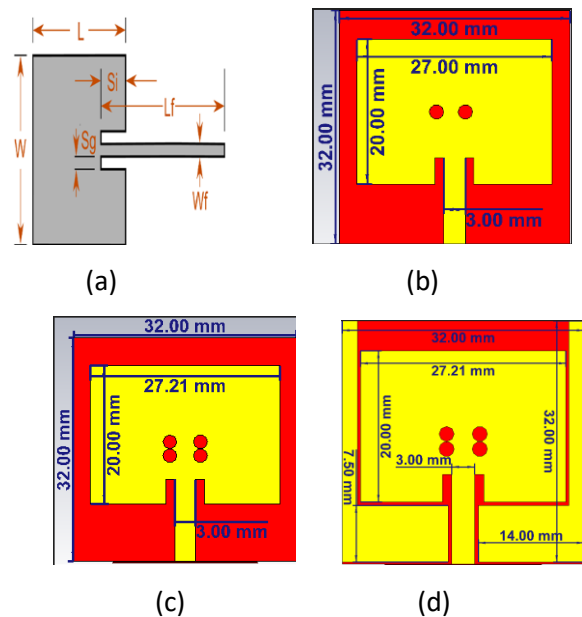


Fig.1: Structure of antennas: (a) Structural design parameter of patch, (b) Antenna-1 (with 2-slits), (c)

Antenna-2 (with 4-slits), and (d) Antenna-3 (4-slits with CPW-Fed)

Table 3. Optimal structural design parameter list of proposed Antenna-3

Design Parameter	Values (mm)	Description
h	2.00	Substrate Thickness
W	27.21	Radiating Stub Width
L	20.00	Radiating Stub Length
Si	3.61	Insert Length of Feed Line
Sg	1.20	Insert Feed Gap
Lf	8.24	Feed Line Length
Wf	3.00	Feed Line Width
R	1.00	Circular slit radius

3.1. Performance of Antenna-1 with various substrate materials: The performance of the proposed antennas utilizing various materials is comprehensively analyzed. The simulation results for Antenna-1 laminated with RT/Duroid, FR-4, and Arlon (see Figure 2) are depicted in Table 4. The simulation results for Antenna-1, as depicted in Figure 2, reveal resonant frequencies (f_r) for Roger RT5880, 6.75 GHz at -20 dB and 9.80 GHz at -20 dB for dual band application. For FR-4 laminated Antenna-1, the resonance frequencies are 4.95 GHz at -45 dB, 7.20 GHz at -12 dB, 8.85 GHz at -26 dB, and 9.90 GHz at -31 dB obtained for quad-band applications. Similarly, in the case of Arlon laminated Antenna-1, the resonance frequencies (f_r) are 4.15 GHz at -28 dB and 7.25 GHz at -21 dB for dual-band applications. Here, the FR-4 based substrate (Antenna-1) provides quad bands in comparison to other substrates. For this structure, the FR-4 dielectric material is appropriate with proper impedance matching, as illustrated in Figure 2.

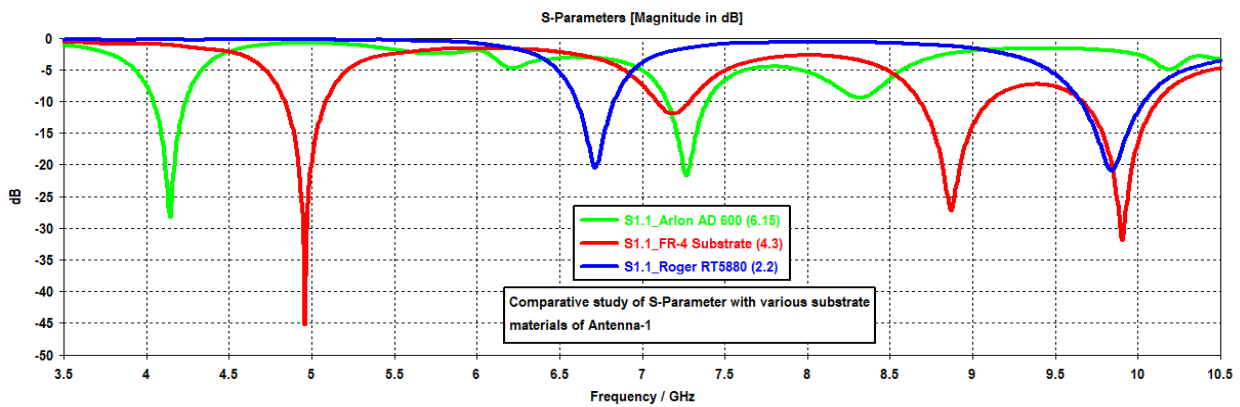


Fig. 2: Optimized reflection coefficient |S11| Parameter: Antenna-1 based on different substrate materials.

Table 4. Performance comparison of proposed Antenna-1 with various substrate materials

Antenna Design Technique	Substrate Material (ϵ_r)	Substrate Thickness (h, mm)	Resonating Frequencies (f_N), GHz				Frequency Bands ($ S_{11} \leq -10$ dB)
			f_{N1} (-dB)	f_{N2} (-dB)	f_{N3} (-dB)	f_{N4} (-dB)	
Two circular strips on the radiating stub	Roger RT5880 (2.2)	1.6	6.75 (20)	9.80 (20)	-	-	2
	FR-4 Glass/Epoxy	1.6	4.95 (45)	7.20 (12)	8.85 (26)	9.90 (31)	4

	(4.3)						
	Arlon AD600 (6.15)	1.6	4.15 (28)	7.25 (21)	-	-	2

3.2. Performance of Antenna-3 (proposed) with various substrate thicknesses: The impact of substrate material (FR4) and their respective thicknesses on antenna performance, specifically |S11| parameters, is thoroughly examined in this section. The selection of FR-4 in antenna-2 is based on the highest number of bands it provides in comparison to Rogers RT5800 and Arlon AD600 given in Table 4. The findings for antenna-3 are illustrated in Figure 3, providing valuable insights into how resonance frequencies are influenced by substrate thickness and dielectric constant. By analyzing the |S11| parameters across different substrate materials and thicknesses, a comprehensive understanding of their effects on antenna performance is gained. The simulation result revealing resonant frequencies (fr) at thicknesses of substrate 1.30, 1.60, and 2 mm is shown in Table 5. This proposed work (Antenna-3) offers multi-operating resonance frequencies (fr) for substrate thickness 1.30 mm at 3.51 GHz (3.46-3.60 GHz), 5.20 GHz (5.10-5.24 GHz), 6.60 GHz (6.51-6.81), 9.10 GHz (8.70-9.20), and 9.85 GHz (9.65-10.05). For substrate thickness 1.60 mm, at 3.50 GHz (3.44-3.58 GHz), 5.10 GHz (5.04-5.17 GHz),

6.55 GHz (6.48-6.77), 8.70 GHz (8.60-9.20), and 9.65 GHz (9.50-9.90). Similarly for substrate thickness 2 mm, at 3.49 GHz (3.38-3.59 GHz), 4.95 GHz (4.89-5.10 GHz), 6.36 GHz (5.84-6.99), 7.70 GHz (7.01-8.43), 9 GHz (8.49-9.28), and 9.95 GHz (9.50-10.13). Optimized results for antenna-2 (without CPW-Fed) and antenna-3(with CPW-Fed) at the thickness h=2 mm, is shown in figure 4. The results for antenna-2 at 3.48 GHz (3.37-3.56 GHz), 5.20 GHz (5.03-5.19 GHz), 6.65 GHz (6.22-7.01), 7.35 GHz (7.15-7.55), and 9.55 GHz (9.39-9.79). The result for antenna-3 (with CPW-Fed) on substrate thickness 2 mm, at 3.49 GHz (3.39-3.59 GHz), 4.99 GHz (4.89-5.09 GHz), 6.42 GHz (5.85-7.00), 7.73 GHz (7.03-8.44), 8.88 GHz (8.47-9.29), and 9.81 GHz (9.50-10.12). Here the advantage of using CPW-Fed (antenna-3) is that there is a considerable increase in the bandwidth (B.W) as compared to the antenna-2 (without CPW-Fed) with an increase in number of bands from five to six as shown in Table 6. The gain of antenna-2 and antenna-3 are shown in figure 5. The antenna-2 has the peak gain of 4.8 dBi and for antenna-3 is 2.8 dBi. The value of gain is reduced in antenna-3 as compared to antenna-2.

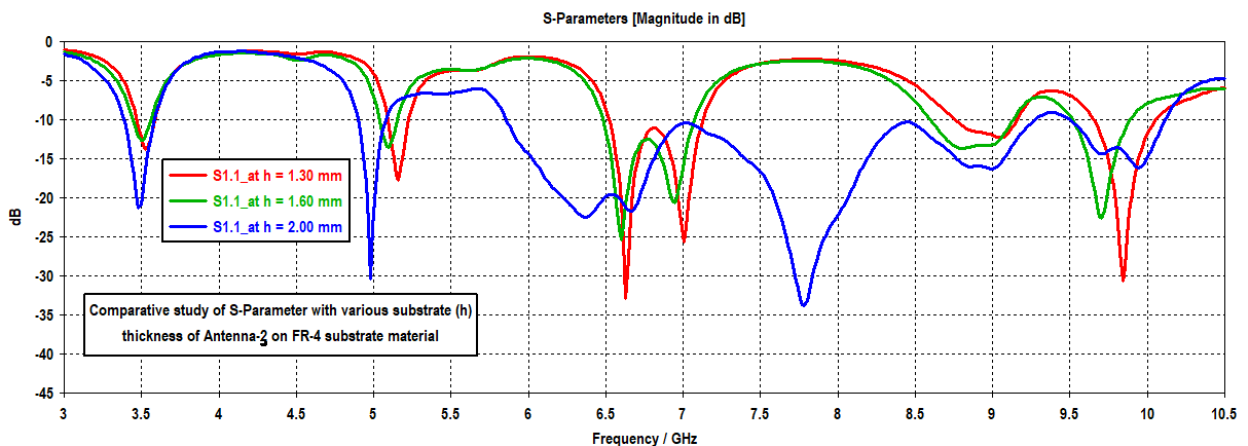


Fig. 3: Optimized |S11| Parameter: CPW-Fed antenna-3 based on different substrate thickness.

Table 5. Performance comparison of proposed antenna-3 on FR-4 material on 4-slits CPW-Fed antenna with different substrate thicknesses

Antenna Design Technique/ Substrate Material (ϵ_r)	Substrate Thickness (mm)	Resonating Frequencies (f_N), GHz						Frequency Bands ($ S_{11} \leq -10$ dB)
		f_{N1} (-dB)	f_{N2} (-dB)	f_{N3} (-dB)	f_{N4} (-dB)	f_{N5} (-dB)	f_{N6} (-dB)	
CPW-Fed with four circular strips/ FR-4 Glass/Epoxy (4.3)	1.30	3.51 (14)	5.20 (17)	6.60 (33)	-	9.10 (12)	9.85 (30)	5
	1.60	3.50 (13)	5.10 (14)	6.55 (25)	-	8.70 (14)	9.65 (23)	5
	2.00	3.49 (21)	4.95 (30)	6.36 (22)	7.70 (34)	9.00 (16)	9.95 (16)	6

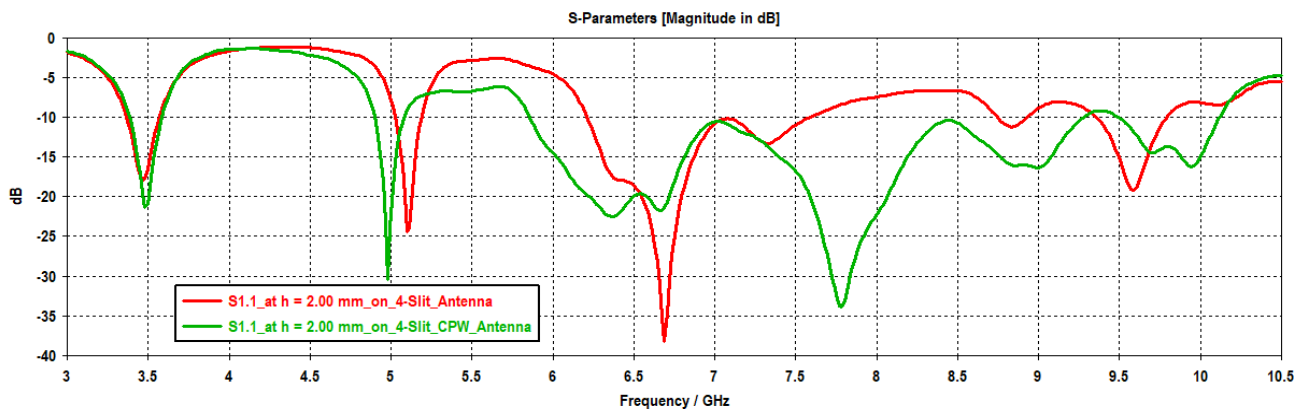


Fig. 4: Optimized |S11| Parameter: Antenna-2 (without CPW) and antenna-3(with CPW-Fed) at thickness, h=2 mm on FR-4 taken on 4-slits.

Table 6. Performance comparison of proposed Antenna-2 and Antenna-3 using FR-4 with same thickness, h=2mm.

Antenna Design Technique/ Substrate Material (ϵ_r)	Substrate Thickness (2 mm)	Resonating Frequencies (f_N), GHz and IBW, (GHz)						Frequency Bands ($ S_{11} \leq -10$ dB)
		f_{N1} (IBW)	f_{N2} (IBW)	f_{N3} (IBW)	f_{N4} (IBW)	f_{N5} (IBW)	f_{N6} (IBW)	
CPW-Fed with four circular strips/ FR-4 Glass/Epoxy (4.3)	Without CPW	3.48 (0.19)	5.20 (0.16)	6.65 (0.79)	7.35 (0.40)	-	9.55 (0.40)	5
	With CPW	3.49 (0.20)	4.95 (0.20)	6.36 (1.15)	7.70 (1.41)	9.00 (0.82)	9.95 (0.62)	6

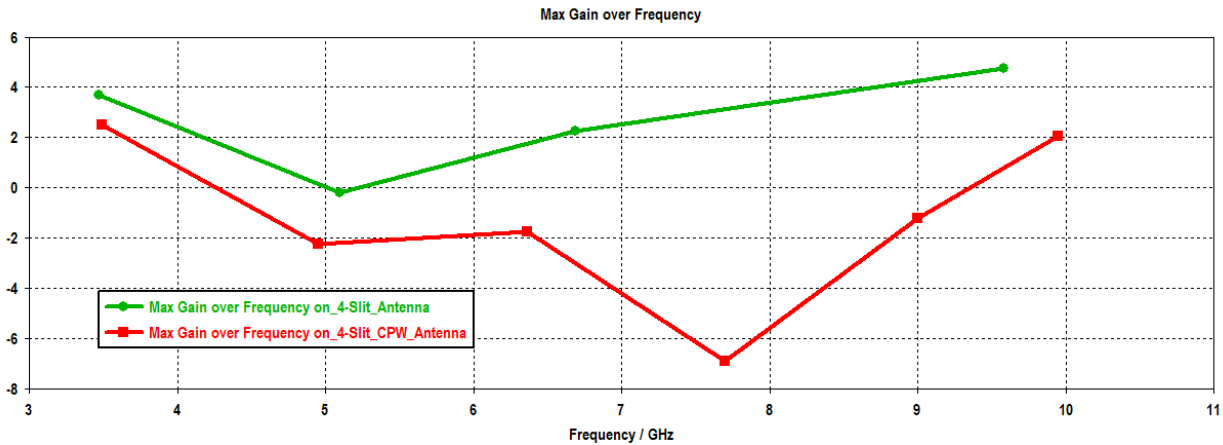


Figure 5. Gain of antenna-2 and antenna-3 at different frequencies.

4. Comparative Outcomes: This article reviews various design techniques for CPW-fed antennas, focusing on substrate materials. Thicker substrates offer more efficiency and wider IBW for a lower dielectric constant. High dielectric constant substrates favor small antenna sizes. The antennas' low profile, simple structure, and broadband impedance characteristics make them suitable for wideband RF communication applications. An Antenna-2 and 3, using two circular slits and four circular slits are used for improving the impedance bandwidth as shown in Table 4 and Table 5. The achieved $|S_{11}|$ results for Antenna-1 and Antenna-2, shows a shift of fundamental resonance frequencies towards the low-frequency band especially in case of increasing in the value of dielectric constant, as shown in Table 4 enabling effective miniaturization of around 60% in between using the substrate material of dielectric constant 2.2 to 6.15. The proposed 4-slit CPW-Fed antenna-3 offers six frequency bands promising potential for enhancing advancements in next-generation wireless technologies in terms of efficiency, bandwidth, and versatility.

5. Conclusions: This article explores the design of coplanar waveguide (CPW)-fed antennas using different substrate materials, thicknesses, and techniques. It investigates how materials like FR4, Rogers, and Arlon affect electrical parameters like as impedance

bandwidth, $|S_{11}|$, and gain. The research also investigates how design techniques such as stubs, slots, strips, arrays, etc affect antenna parameters. The FR-4 suggested antenna has a frequency range of 3.3 to 10.1 GHz and can operate at six frequencies. The proposed antenna has a peak gain of 2.8 dBi. The antennas' low profile, simple construction, and broadband impedance make them ideal for wideband RF and wireless communication applications. The proposed antenna has the potential to increase efficiency, bandwidth with the challenges to achieve the significant gain in next-generation wireless technology applications.

Acknowledgements: Authors are thankful to our EECE department for constant support and funding our research.

Conflict of Interest: Authors declare No conflicts of interest.

6. References:

- [1] Ma, Z.-H. *et al.*, 'Design of planar microstrip Ultra-wideband circularly polarized antenna loaded by annular-ring slot', *International Journal of Antennas and Propagation*, 2021, pp. 1–10.
- [2] Ullah U. and Koziel S. 'A geometrically simple compact wideband circularly polarized antenna', *IEEE Antennas and Wireless*

- Propagation Letters, 2019, 18(6), pp. 1179–1183.
- [3] Singh S.K., Sharan T. and Singh A.K. ‘Enhancing the axial ratio bandwidth of circularly polarized open ground slot CPW-fed antenna for Multiband Wireless Communications’, *Engineered Science*, 202, 1 Vol. 17, pp. 274-284.
- [4] Midya M., Ghosh A. and Mitra M. ‘Meander-line-loaded circularly polarized square-slot antenna with inverted-l-shaped feed line for C-band applications’, *IET Microwaves, Antennas & Propagation*, 2021, 15(11), pp. 1425–1431.
- [5] Seyyedrezaei, S.F. et al. ‘A novel small size CPW-fed slot antenna with circular polarization for 5G application’, *Progress in Electromagnetics Research C*, 2020, 106, pp. 229–238. [6] Gharaati, A. et al. ‘A low-profile wideband circularly polarized CPW slot antenna’, *AEU - International Journal of Electronics and Communications*, 2021, 129, p. 153534.
- [7] Qiu, B. and Li, Y. ‘Asymmetric CPW-fed wideband circularly polarized antenna for sub-6 GHz Application’, *IEEE 3rd International Conference on Electronic Information and Communication Technology (ICEICT)*, 2020.
- [8] Alam Md. M. et al. A dual-band CPW-fed miniature planar antenna for S-, C-, WiMAX, WLAN, UWB, and X-band applications. *Scientific Reports*, 2022, 12(1).
- [9] Singh, S.K., Sharan, T. and Singh, A.K. Investigating the S-parameter ($|S_{11}|$) of CPW-fed antenna using four different dielectric substrate materials for RF multiband applications. *AIMS Electronics and Electrical Engineering*, 2022, 6(3), pp. 198–222.
- [10] Saad, M.F. et al. ‘CPW-UWB flexible composite antenna using jute textile for WPAN applications’, *2020 IEEE International RF and Microwave Conference (RFM)*, 2020.
- [11] Aditya S. et al. (2004) ‘High-gain 24-GHz CPW-fed microstrip patch antennas on high-permittivity substrates’, *IEEE Antennas and Wireless Propagation Letters*, 2004, 3, pp. 30–33.
- [12] Chen Y. and Hsu C. ‘Inverted-E shaped monopole on high-permittivity substrate for application in industrial, scientific, medical, high-Performance Radio Local Area Network, unlicensed national information infrastructure, and worldwide interoperability for Microwave Access’, *IET Microwaves, Antennas & Propagation*, 2014, 8(4), pp. 272–277.
- [13] Farooq U. et al. ‘Design of a 1×4 CPW microstrip antenna array on PET substrate for biomedical applications’, *2019 IEEE International Symposium on Antennas and Propagation and USNC-URSI Radio Science Meeting*, 2019.
- [14] Y. Mood and R. Pandeewari, “A Novel SRR Metamaterial Inspired CPW-Fed Dual Band MIMO Antenna for Sub-6 GHz 5G Application,” *Wireless Personal Communications*, vol. 130, no. 2, pp. 1277–1293, Apr. 2023, doi: 10.1007/s11277-023-10331-5.

Thermodynamics of a confined macromolecule: An analytical approach

P. K. Mishra

Department of Physics, DSB Campus, Kumaun University, Nainital Uttarakhand-263002 (INDIA)

Volume 1, Issue 3, May 2024

Received: 28 April, 2024; Accepted: 14 May, 2024

DOI: <https://doi.org/10.63015/5C-2429.1.3>

Corresponding Author Email: pkmishrabhu@gmail.com

Abstract: We consider a fully directed self-avoiding walk model on a cubic lattice to mimic the conformations of an infinitely long flexible polymer chain and also to mimic conformations of a short flexible chain under confined conditions. The confinement conditions is achieved using two parallel impenetrable plates. The confined chain is under good solvent conditions and we revisit this problem to solve the real (self avoiding) polymer's model for any length of the chain and also for any given separation in between the confining plates. The equilibrium statistics of the confined polymer chain are derived using analytical approach of the generating function technique. The force of the confinement, the surface tension and the monomer density profile of the confined chain are obtained analytically. We propose that the methods of calculation are suitable to understand thermodynamics of an arbitrary length confined polymer chain under other possible conditions of the confinement.

Keywords: Real polymer; Confinement; Monomer density; Generating function technique

1. Introduction: A lattice model of a self-avoiding walk (SAW) has been widely used for the past a few decades to understand the conformational statistics of a confined short polymer chain under various geometries, and the lattice models were also used to understand the equilibrium statistics of a polymer chain in the bulk [1-3]. Therefore, there are a variety of interesting results on thermo-dynamical aspect of a short and an infinitely long flexible polymer chain in the bulk, and also for a short and an infinitely long polymer chain under various geometries [4-7]. Such studies revealed a wealth of information regarding scaling behavior/universal properties and phase transitions in the polymer macromolecules. These reports gave us understanding of the steric stabilization of the polymer dispersions, colloidal solutions, thin films, and such studies were relevant for surface coatings and sensors [3,5,7-9].

Though, there are a couple of facts that are not well understood regarding an infinitely long as well as a short polymer chain for their three-dimensional confined geometries, *e. g.*, variations of thermo-dynamical properties (force of the confinement, entropic surface tension, monomer density profile, etc.) of a confined self-avoiding flexible polymer chain; and hence it requires an investigation to understand a few such aspects which we shall discuss for three-dimensional confinements here.

We have chosen a directed walk model [3] for a self-avoiding polymer chain to understand the thermo-dynamical properties of an infinitely long flexible chain. Also, we report results for a short flexible polymer chain to understand the thermodynamics of the chain under the proposed confined geometry. The confinement condition is achieved around the polymer chain using a pair of impenetrable flat plates (as shown in figure 1); the plate's

separation is measured in a unit of a monomer length. Thus, the separation of the confining plates is varied from one monomer length to the size of the polymer chain.

2. Model and method: We use theory of critical phenomenon to understand the Physics of a single polymer chain merely because a linear polymer chain is a critical object [3,5,7]. Therefore, there are several reports on the thermodynamics of a single polymer chain. These reports on the statistics of the single polymer chain and chain's statistics so obtained correspond to a condition that the chain is under very dilute solution [1,3,7,10-13]. We confine our discussion to the model of a fully directed walk of a confined flexible polymer chain.

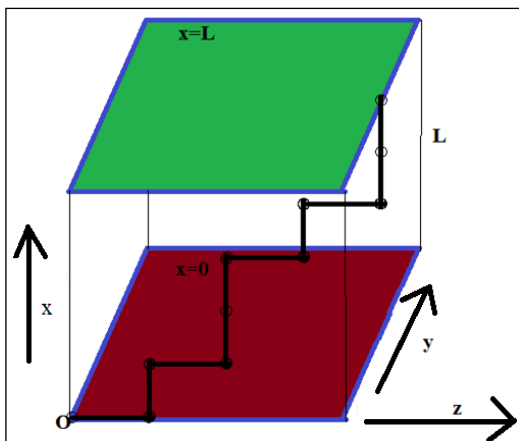


Figure 1: An N monomers long confined flexible polymer chain is shown in figure 1. A pair of impenetrable parallel plates confine the self-avoiding/real polymer chain. The lower plate is located at $x = 0$, and the upper plate is located at $x = L$; one end of the polymer chain is grafted at a point O on the lower plate, i.e., on the plate located at $x = 0$.

It is also to be highlighted that there are several reports on the adsorption-desorption phase transitions of a confined chain and there are reports on conformational statistics of a confined polymer chain under various geometries; the author tried his best to refer to some of the results for the sake of literature survey on the issue of confined polymer chain under specific geometries.

2.1 Fully Directed Self Avoiding Walk (FDSA) Model: A lattice model of the fully directed self-avoiding walk [3] is widely used to understand the thermodynamics of an infinitely long polymer chain under various geometries. Since a directed walk model is solvable analytically; therefore, we have exact results on single-chain statistics using a directed walk model. It is well known that the qualitative nature of the phase diagram for a directed walk model is the same as to that of its isotropic version [10]. It is assumed that the first impenetrable plate is placed at $x = 0$ and another impenetrable parallel plate is placed at $x = L$, where the value of $L = 1, 2, 3, \dots, \infty$; and the parameter L is measured in the unit of a monomer length; and the confined real/self-avoiding polymer chain is schematically shown in figure 1. A condition of $L \geq N$ corresponds to a polymer chain in the bulk.

In the case of a fully directed walk model in three dimensions, it is known also that the walker is allowed to take steps only along $+x$, $+y$, and $+z$ directions in between two parallel plates, and along $+x$ direction walker can take the maximum $L (\leq N)$ steps while the walker can take any number of steps (N) along remaining other two directions, i.e., along $+y$ and $+z$ directions. We have conformations (C_N^L) of an N monomers long polymer chain in between two parallel plates, where one end of the chain is grafted at the corner (O) of the lower plate ($x = 0$). Thus, we have a condition of the confinement provided $L < N$. A general expression of the grand canonical partition function for an infinitely long confined self-avoiding flexible chain is written as:

$$G(g, z) = \sum_{N=1}^{\infty} \sum_{\text{All walks of } N \text{ monomers}} g^P z^{N-P} \quad (1)$$

A symbol g refers to the step fugacity of the walker along a direction parallel to the plane of the confining plates. At the same time, z is the step fugacity perpendicular to the plane of the confining plates. There are P monomers of the chain lying in the plane of the parallel plates, and remaining $(N-P)$ monomers are located perpendicular to the plane of the plates for an N

monomers long confined polymer chain.

3. Results: A lattice model is often used to obtain an equilibrium statistics of an infinitely long confined flexible polymer chain and a short-confined polymer chain [3,5,7]. We obtained the exact results on the conformational statistics of a flexible self-avoiding polymer chain for its confinement using two parallel impenetrable plates; the analytical calculations are **given** below for a short-confined chain and an infinitely long confined flexible polymer chain, separately.

3A. The equilibrium statistics of a confined Self Avoiding flexible polymer chain using Grand Canonical Ensemble (GCE) approach:

An exact expression of the grand canonical partition function for an infinitely long confined flexible polymer chain is obtained for different possible values of the plate **separation (L)**; and also, for the bulk case, the partition function of the chain may be written as ($N \geq L$ and $L < N$),

$$G(g, z) = \sum_{P=1}^{N \rightarrow \infty} [(2g)^P + \sum_{K(\leq P)=1}^{L(\leq P) \rightarrow \infty} z^K \left\{ \frac{\prod_{Q=1}^K (P-Q+1)}{K!} (2g)^{P-K} \right\}] \tag{2}$$

We were able to recover an expression for the grand canonical partition function of the chain for the bulk case [10] by substituting $z = g$ (when $L \geq N$ and $N \rightarrow \infty$) in equation 2. The first term on the right-hand side of equation 2 corresponds to the conformations of the chain lying on the lower plate (*i.e.*, at $x = 0$). A simple form of the expression for the grand canonical partition function for the bulk case (*i.e.*, for an infinite separation between the parallel plates and the chain length infinity) may be written as:

$$G(g, z, L = \infty) = \frac{z+2g}{1-z-2g} \tag{3}$$

The partition function of an infinitely long polymer chain is obtained for a finite

separation (L) in between the confining plates. Accordingly, we calculate the thermodynamical properties of the confined chain. It is well known that the critical value of the step fugacity is 0.5 for a finite separation (L) in between parallel plates, and the critical value of the step fugacity is 0.33 for $L \geq N$ and $N \rightarrow \infty$.

We use canonical ensemble formalism to obtain an exact number (C_N^L) of a real flexible polymer chain conformation, and accordingly, the **equilibrium** statistics of the chain are **obtained** for a case when a pair of impenetrable parallel plate confines the polymer chain; an exact number of the conformations is written as follows for a case when $L < N$,

$$C_N^L = 2^N + \sum_{L=1}^{N-1} 2^{N-L} \frac{N(N-1)(N-2)\dots(N+1-L)}{L!} \tag{4}$$

We have many conformations (C_N^B) of a chain for a case when this short flexible chain is in the bulk ($L \geq N$), and the number of the conformations for the bulk ($L \geq N$) case is written as:

$$C_N^B = \sum_{i=1}^{N-1} C_i^L + 1 = 3^N \tag{5}$$

3B. Equilibrium statistics of a confined Self Avoiding flexible polymer chain using Canonical Ensemble approach:

An effect of the confinement is shown in figure 2, where a fraction of the polymerized (C_N^L) and a fraction of non-polymerized ($1 - C_N^L$) short polymer chain conformations are demonstrated for a set of values of the plates separation (L); and the chain length is an N **monomers**. We have divided the terms C_N^L and $(1 - C_N^L)$ by 3^N to obtain the said fraction of the polymerized and non-polymerized chain conformations, respectively.

We have calculated the force [1,2,9] of the confinement (f_N^L) acting on a short polymer chain of an N monomers due to parallel plates, and the force is acting perpendicular to the plane of the plates while the separation in between the plate is L . While calculating the force, the free energy of the self-avoiding polymer chain is written in a unit of the thermal

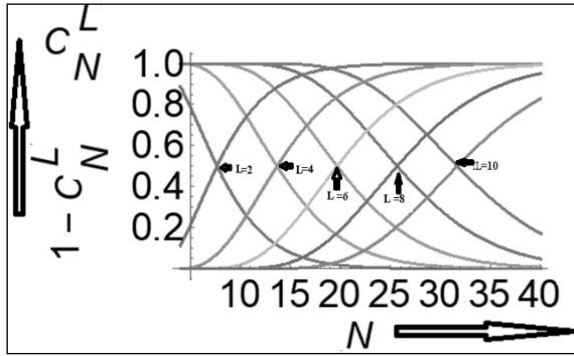


Figure 2: We have shown in figure 2, an average number of the polymer chain’s conformations ($1-CN^L$)/ $3N$ which were not polymerized due to a pair of an impenetrable plate’s confinement. The curves for $CN^L/3N$ and $(1-CN^L)/3N$ intersect at the 50% value of the

energy as $E(-k_B T \text{Log}[C_N^L])$, and thermal energy ($k_B T$) we have taken unity. Therefore, a graph between f_N^L versus L and for an N monomers length chain is shown using figure 3(a). The following equation gives the force of the confinement as:

$$f_N^L \cong -\text{Log}[2] + \frac{\partial \left\{ \frac{\text{Log} \prod_{l=1}^L (N-L+1)}{L!} \right\}}{\partial L} \tag{6}$$

The above equation (*i.e.*, equation 6) is simplified to the following relation to seeing that $f_N^L = -\text{Log}[2] - \text{Log}[L/N]$. Thus, the force bears logarithmic singularity provided $L < N$, $L \geq 1$, and $N \rightarrow \infty$ for an infinitely long chain.

$$f_N^L \cong \text{Log}\left[\frac{N}{2L}\right] \tag{7}$$

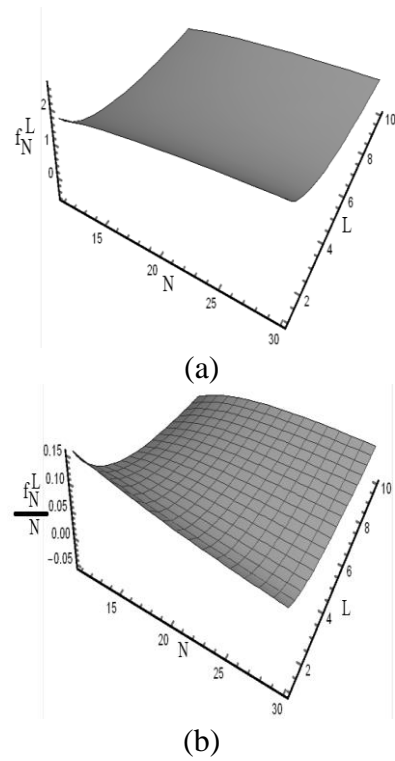


Figure 3: The force of the confinement which is acting perpendicular to the plane of the plates, and its nature of variation for a few sets of (N, L) has been shown in this figure 3(A) for a short chain of length an N monomers and we increase the separation in-between plates ($L=2, 4, 6, 8$ and 10) in a unit of monomer length. Figure 3(B) shows nature of variation of the confining force per monomer of the confined chain for set of N, L values.

The entropic surface tension (σ_N^L) of a short-chain and an infinitely long confined real polymer chain solution may be obtained using the following relation:

$$\sigma_N^L = \frac{\delta(E)}{\delta A} \tag{8}$$

Where $E(-k_B T \text{Log}[C_N^L])$ is the Helmholtz free energy of a short polymer chain under confined geometry; and, again, we have taken the value of the thermal energy ($k_B T$) equal to unity for the sake of mathematical simplicity. The maximum change in the area is $[(N-L+1)^2 - (N-L)^2]/2$ when the walker steps one unit along the x -direction, and the plate separation varies in the unit of one monomer length. For a confined chain, $L_{Max}=N-1$. It is to be noted

here that the surface tension for the present case has an entropic origin, and the value of the surface tension for a self-avoiding confined chain is written as:

$$\sigma_N^L = \frac{2\text{Log}\left[\frac{1}{2}\right]}{N-L} + \frac{2L\text{Log}\left[\frac{1}{N}\right]}{(N-L)^2} + \frac{2\text{Log}[L!]}{(N-L)^2} \tag{9}$$

The nature of variation of the entropic surface tension of a short polymer chain with confining plate separation is shown in figure 4.

We have also calculated the monomer number density (ρ_N^L) profile, **and a plot on the density profile for the confined flexible chain is shown in figure 5**; we have an exact expression for the number density of an N monomers long chain, and the density is written as follows:

$$\rho_N^L = [2^{N+1-L}] \frac{N(N-1)\dots(N-L+1)}{L!(N-L)} \tag{10}$$

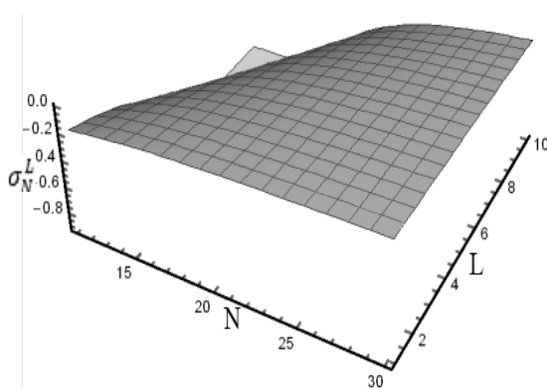


Figure 4: A plot on the entropic surface tension (σ_N^L) of a short polymer chain ($N = 11, 12, \dots, 30$ monomers) confined in between a pair of parallel plates is shown in this figure, and the plates are separated by a distance $L (= 1, 2, \dots, 10)$ monomers.

The monomer number density profile is shown in figure 5 for the confinement condition of a short flexible polymer chain for the given values of L . For $L=0$ and for a non-zero value

of L , and for a confined chain ($L < N$), the monomer density profile is written as equation 10.

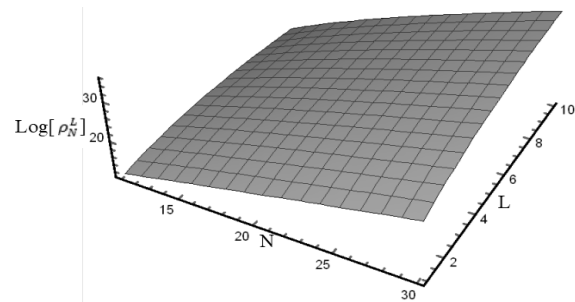


Figure 5: This figure shows the logarithmic value of the number density profile of a real flexible polymer chain. The length of the polymer chain (N) is varied from 11 to 30 monomers, and the separation (L) of the parallel plate is varied from 1 to 10 monomers.

4. Discussion: A lattice model of the fully directed self-avoiding walk is used to mimic the conformations of an infinitely long and a short confined flexible polymer chain, where the polymer chain is confined by a pair of impenetrable parallel plates (as shown schematically in figure 1). The confined regions **in** between a pair of parallel plates lead to different values of the step fugacity for the walker **along and perpendicular to** the plane of the confining plates. Therefore, along the plane of the plates, we have one value of step fugacity (*i.e.*, g), and in a direction perpendicular to the plane of the confining plates, we have another value (*i.e.*, z) of the step fugacity. We used the generating function method to solve the model analytically; and we obtained a general expression for the grand canonical partition function of an infinitely long self-avoiding flexible polymer chain for any given value of plate separation (L).

We have also obtained an exact expression of the canonical partition function for a short flexible self-avoiding polymer chain. The chain is made of an N monomers; the plate separation equals L monomers. We calculated an exact percentage of the polymer conformations which were not polymerized (suppressed) due to the confinement conditions imposed on the chain by the pair of parallel impenetrable plates. We derived expressions

for the force of the confinement, the entropic surface tension, and the monomer number density profile for a short-chain length of an N monomers and we derived a condition when an infinitely long chain is confined by the pair of plates for the plate separation L .

We have plotted $(C_N^L)/3^N$, *i.e.*, the number of a confined flexible polymer chain conformations of an N monomers long polymer chain along with the conformations, *i.e.*, $(1-C_N^L)/3^N$, which is suppressed due to the confinement, for different values of the plate separation (L); and we have shown the polymerized and suppressed fractions of the conformations in figure 2. It is seen from this figure that as we increase the length of the chain for a given value of the plate separation (L), the percentage of the polymerized chain's conformations decreases. Accordingly, the percentage of the non-polymerized/suppressed conformations increases due to the confinement. It is also found that the percentage of the polymerized conformations increases for a given length of the chain as the separation between the plates increases. The force of the confinement is a function of the chain length and the separation between the confining plates. It is found from analytical calculations that the force of confinement decreases logarithmically as we increase the plate separation for a given length of the confined chain. While the force of confinement increases logarithmically as we increase the length of the confined chain, provided the plate separation is retained constant. We have shown the nature of confining force which acts on a short polymer chain, in figure 3 for a set of N and L values.

The entropic surface energy per unit surface area (*i. e.* the entropic surface tension) for a confined flexible chain is shown in figure 4; it is seen that the surface tension of the confined chain increases for a given length of the chain as we increase the length of confinement, and it starts decreasing after a particular value of L . The surface tension of a confined chain also increases for a given value of L as we increase the number of monomers in the confined chain.

An actual dependency of the surface tension on N and L is shown in figure 4, and the mathematical form of the entropic surface tension is given by equation 9. Though we have a very dilute chain concentration, therefore, the entropic surface tension of a self-avoiding confined flexible polymer chain vanishes in the thermodynamic limit. The monomer number per unit areal extension of the confined flexible chain is shown in figure 5. It is seen from this figure that the monomer density increases as the length of the chain increases and L remains fixed, and also the monomer density increases as we increase L for a given length of the confined chain. The nature of the free energy curve for a confined short chain is also shown in figure 6 for the completeness. It is seen from figure 6 that in the thermodynamic limit, the free energy per monomer of the confined flexible chain is $\text{Log}[g_c(2D)]^{-1}$, where $g_c(2D) = 0.5$.

We have taken a factor $\alpha = (L/N)$ to report the confining force, the entropic surface tension, the monomer number density, and the free energy of a confined chain in terms of α (<1 , for a confined chain); and accordingly, we have plotted these thermo-dynamical parameters in the thermodynamic limit in figure 7 for the sake of completeness. Therefore, we have these thermo-dynamical parameters that may be written in the thermo-dynamical limit ($N \rightarrow \infty$) as (*i. e.* for an infinitely long confined chain):

$$f_{N \rightarrow \infty}^L = -\log[2] - \text{Log}[\alpha] \tag{11}$$

$$\sigma_N^L * N = -\frac{2\text{Log}[2]}{(1-\alpha)} + \frac{2(\text{Log}[\alpha]-1)}{(1-\alpha)^2} \tag{12}$$

$$\frac{\text{Log}[\rho_N^L]}{N} = (1-\alpha)\text{Log}[2] + \alpha(1-\text{Log}[\alpha]) \tag{13}$$

and finally, the free energy per monomer ($\epsilon = E_N^L/N$) of a confined chain is written as:

$$\varepsilon = -(1-\alpha)\text{Log}[2] + \alpha\text{Log}[\alpha] - \alpha$$

(14)

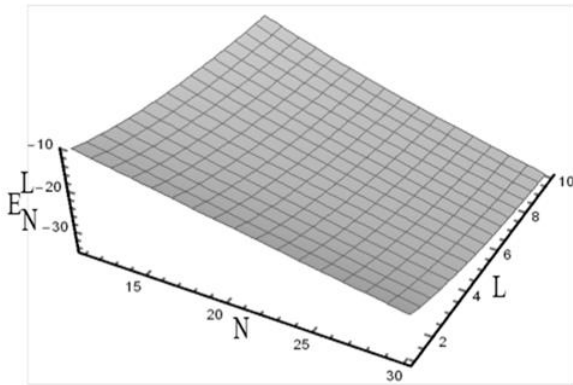


Figure 6: We have shown the free energy graph of a confined flexible polymer chain for the given values of L and N in this figure. The Helmholtz free energy is a function of N and L , and the free energy is approximated as $E_N^L \approx N\text{Log}[2] + L\text{Log}[2] - L\text{Log}[N] + L\text{Log}[L] - L$. The thermal energy is set to unity for the sake of mathematical simplicity.

A method of calculations reported in this manuscript may be easily extended to calculate the thermodynamics of an infinitely long and a short self-avoiding polymer chain confined to a length L for other versions of the directed/isotropic walk models on different possible lattices. It is also to be noted from reports that the qualitative nature of the phase diagram obtained for an isotropic self-avoiding walk model is the same as that of the phase diagram of a directed walk model of the problem [10], and therefore, our findings may be relevant to understand the thermodynamics of a confined three-dimensional polymer chain.

Our calculations include entropy of the confined chain where those conformations were chosen, which are in the form of polymer bridges or polymer trains, though we have not considered the loop-like conformations; However, the entropy of the confined chain has a monotonous variation with N and or L for other versions (*i.e.*, isotropic or partially directed walk model of the confined chain) of the confined polymer models; therefore physical insight will remain same for the confined chain when one includes polymer

loop like conformations for such studies. It is also to be noted that in the presence of another confining plate (*i.e.*, a plate located at $x = L$), the entropy of the chain is reduced due to excluded volume interaction among the monomers of the confined chain. Hence, many chain conformations are suppressed for any value of $L < N$, *i.e.*, not polymerized.

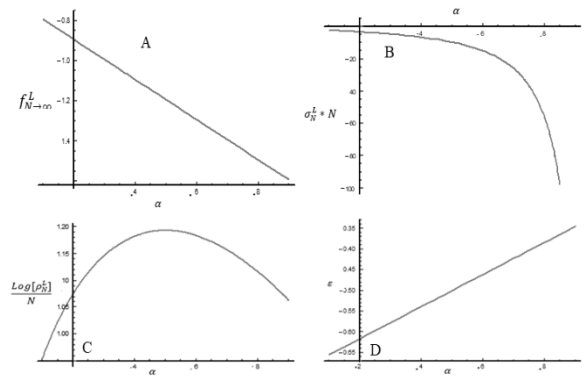


Figure 7: This figure no. 7A shows the force of the confinement acting on the chain as a function of α (as shown in the equation 11); the entropic surface tension of an N monomers long chain is shown in the figure (7B), and the equation 12; the logarithmic value of the monomer density per monomer is shown in the figure (7C), and the equation 13; and also, the free energy per monomer of the confined chain (ε) is shown in the figure (7D), and equation 14, as a function of α .

5. Challenges: There are limitations regarding visualizing a macromolecule in the restricted geometries, though we have reports on single macromolecule manipulations [11] and please also see the references quoted therein. Therefore, we can expect that it may be possible to track single macromolecule and measure its physical properties under the confined geometries soon.

6. Conclusion and Future Scope: The lattice model of a polymer chain has limitations, as the lattice model mimics discrete links of the monomers of a chain. Therefore, finite length fluctuations related physics of the system may have different results from real situations of the polymer Physics. Still, in the case of phase transitions, there are fluctuations of all length scales. Correlation length extends to the size of the confined chain length. Therefore, the phase

transitions which occur in the thermodynamic limit may not have any sensitivity regarding the finite and non-zero size of the monomers. Though there are studies based on continuum models of the polymer chain, it has been found that the Physics of polymer chain derived using continuum and discrete models have a qualitative similarity [1,3,5,11, 16].

Acknowledgements: The author is thankful to RAFM 2024 for providing the platform to present his research work.

Conflict of Interest: Authors declare No conflicts of interest.

References

- [1] E. A. DiMarzio and R. J. Rubin, Adsorption of a Chain Polymer between Two Plates, *J. Chem. Phys.* 55, 1971, 4318.
- [2] T. Ishinabe, Conformational properties of a polymer chain confined between two plates, *J. Chem. Phys.* 83, 1985).
- [3] Privman V., Svrakic, Directed models of polymers, interfaces, and clusters: scaling and finite-size properties, (Berlin Springer, 1989).
- [4] Hong Ji, D. Hone, P. A. Pincus, and G. Rossi, Polymer bridging between two parallel plates, *Macromolecules* 23(3), 1990, 698–707.
- [5] D'è Bell K. and Lookman T., Surface phase transitions in polymer systems, *Rev. Mod. Phys.*, 65, 1993, 87.
- [6] K. Shiokawa, Chain Dimensions of a Polymer Confined between Two Interacting Plates, *Polymer J.* 26, 1994, 688-693.
- [7] Vanderzande C., Peter G., Yeomans J. eds. Lattice models of polymers (Cambridge University Press, 1998).
- [8] J. de Joannis, J. Jimenez, R. Rajagopalan and I. Bitsanis, A polymer chain trapped between a thermal wall: Concentration profile and confinement force, *EPL* 51, 2000, 41.
- [9] P. K. Mishra and S. Kumar, Effect of confinement on coil-globule transition, *J. Chem. Phys.* 121 (17), 2004, 8642–8646.
- [10] O. Parreno, P. M. Ramos, N. Ch. Karayiannis and M. Laso, Self-Avoiding Random Walks as a Model to Study Athermal Linear Polymers under Extreme Plate Confinement, *Polymers* 12(4), 2020, 799; Brak, R., Owczarek, A.L., Rechnitzer, A., Whittington, S.G., A directed walk model of a long chain polymer in a slit with attractive walls, *J. Phys. A* 38, 2005, 4309-4325; Jansen, E.J., Rensburg, V., Orlandini, E.A.L., Owczarek, Rechnitzer A., Whittington, S.G., Adsorbed self-avoiding walks pulled at an interior vertex, *J. Phys. A* 38, 2005, 823-828.
- [11] P. K. Mishra, Kumar S. and Singh Y., A simple and exactly solvable model for a semiflexible polymer chain interacting with a surface, *Phys. A* 323, 2003, 453-465.
- [12] P. K. Mishra, *J. Phys: Cond. Matt.* 22, 155103 (2010).
- [13] P. K. Mishra, Equilibrium statistics of an infinitely long chain in the severe confined geometry: Exact results, *Phase Transitions* 88(6), 2015, 593-604.
- [14] P. K. Mishra, Effect of confinement and stiffness on the conformational change of a semiflexible homopolymer chain, *Ind. J. Phys.* 91, 2017, 1297-1304.
- [15] P. K. Mishra, A nano polymer aggregate on a substrate: A Theoretical study, *J. Phys: Conf. Ser.* 1644, 2020, 012033.
- [16] Arridge R.G.C., Barham P.J., Polymer elasticity discrete and continuum models, *Polymer.* 46, 2005, 67-117.

Farmers' Awareness of Millets in the Marathwada region

Indra Mani¹, P.S.Kapse^{2*}, and P.R.Deshmukh²

¹ Vasantrao Naik Marathwada Krishi Vidyapeeth, Parbhani (Maharashtra)

²Associate Professor, Dept. of Agricultural Extension Education, VNMKV, Parbhani

Volume 1, Issue 2, May 2024

Received: 30 January, 2024; Accepted: 28 March, 2024

DOI: <https://doi.org/10.63015/9S-2417.1.3>

*Corresponding Author Email: pravinkapse2016@gmail.com

Abstract: Historically, millets have been integral to diets, offering not only a plethora of health benefits but also contributing to environmental conservation through low water and input requirements. The International Year of Millets, declared by the United Nations for 2023 at the initiative of the Government of India, aims to raise awareness, increase production, and promote consumption of millets. This research explores the awareness and consumption of millets among the farmers of the Marathwada region. The study revealed that Great Millet and Pearl Millet garnered high awareness, while Little Millet, Proso Millet, and Kodo Millet exhibited lower awareness among the respondents. The data also showcased varying awareness of millet nutritional content, with 44.12 per cent having a medium overall awareness. Consumption behaviours unveiled diverse frequency patterns for different millets, with 40.91 per cent at a medium overall consumption level. Consumption patterns of the respondents depicted preferences for staple millet-based items. Reasons for consumption/non-consumption highlighted taste and health as major motivators. Respondents suggested measures like training programs, online resources, and awareness campaigns to boost millet usage. These findings provide a comprehensive understanding of the complex interplay between awareness, consumption patterns, and influencing factors, offering valuable insights for stakeholders aiming to promote millet adoption within communities.

(Keywords : Millets, Awareness, Consumption pattern, Marathwada)

Introduction: The Lancet Commissions underscore the imperative of identifying healthy and environmentally sustainable diets, emphasizing the enhanced utilization of underused plant species, such as millets and sorghum. These grains are recognized for their climate resilience and dense nutritional content. Despite the abundance of 14,000 edible plants, only three crops—rice, maize, and wheat—contribute a significant 60 per cent to caloric intake. The United Nations' Sustainable Development Goals for 2030 set an ambitious target of eliminating all forms of malnutrition, necessitating interventions that replace a substantial portion of the diet, currently

dominated by rice, wheat, and maize, with highly nutritious alternatives like millets.

Nutritional Importance of Millets: India, as the largest producer of various millets, plays a crucial role in food security due to the stability of millets under adverse climatic conditions. Once considered coarse grains, millets are now acknowledged as nutritious cereals, standing out as the least allergenic and most digestible grain. Millets boast unique attributes, including calcium richness, dietary fiber, polyphenols, and higher protein content compared to paddy rice. Their amino acid profile, particularly methionine and cystine, along with higher fat content than rice and corn, further highlight

their nutritional value. Millets exhibit nutraceutical properties as antioxidants, contributing to various health benefits such as lower blood pressure, reduced risk of heart disease, cancer prevention, and more [1].

Millets are more nutrient-dense and are a locally cultivated healthy food due to their added health benefits, which include being a source of gluten-free protein, being high in fiber, having a low glycemic index, and being rich in bioactive compounds [2]. Nutritional composition of millets is presented in Table 1 [3], the average carbohydrate content of millets and sorghum varies from 55.8 to 72.6 g/100 g, protein content from 7.3 to 12.5% and fat content ranges between 1.3 and 5 g/100 g.

Millets	Protein (g)	Fat (g)	Fiber (g)	Carbohydrates (g)	Minerals (g)	Iron (mg)	Calcium (mg)
Sorghum	10.40	1.90	1.6	72.6	1.6	4.1	25
Pearl Millet	11.60	5.00	1.2	67.5	2.3	8.0	42
Foxtail Millet	12.30	4.30	8.0	60.9	3.3	2.8	31
Finger Millet	07.30	1.30	3.6	72.0	2.7	3.9	344
Kodo Millet	11.00	3.60	10.0	66.6	1.9	0.5	27
Little Millet	07.70	-	7.6	-	1.5	9.3	27
Proso Millet	12.50	4.20	2.2	73.0	1.9	0.8	14
Barnyard Millet	12.20	3.85	10.1	55.8	3.2	1.4	24

TABLE 1: NUTRITIONAL COMPOSITION OF MILLETS (G/100G)

Millets are a rich source of calcium, especially finger millet or ragi (344 mg/100 g) contains 10 times more than that wheat or rice. The iron content of Pearl millet or Bajra (8.0 mg/100 g) and little millet (9.3 mg/100 g) is higher compared to other staple cereals. They are rich sources of crude fiber as well as dietary fiber and rich in vitamins and minerals [4]. Millets contain a good amount of nutrients like carbohydrates (Low GI), proteins with balanced amino acids, dietary fiber, good quality invisible fat, and have appreciably higher amounts of micronutrients like calcium, potassium, magnesium, iron, manganese, zinc, B complex vitamins and bioactive

phytochemicals, making them a superior choice over the cereal grains like rice and wheat [3]. Several research studies have endorsed the role of polyphenols in antioxidant, anti-carcinogenic, anti-inflammatory, antiviral and neuroprotective activities which in all have shown to be beneficial against diseases like cancer and cardiovascular disease, diabetes, high blood pressure, high cholesterol, inflammatory diseases, metabolic syndrome and Parkinson's disease [5]. Millets are rich in dietary fibre and resistant starch which help in weight regulation. Due to the slow release of glucose, millets are an excellent choice of food for diabetics. The non starch polysaccharides found in millets act as prebiotics and stimulate the lactic acid bacteria (LAB) of probiotic cultures and produce short chain fatty acid and antimicrobial agents in the digestive tract. Table 2 [3] represents the total production of millet, which includes Bajra, Sorghum, and Buckwheat, by the top five producing countries over a three-year period (2018, 2019, 2020). India is the largest producer of millet accounting for 17.68% of the total global production in 2020.

Sr. No.	Country	2018	2019	2020	% share in 2020
1	India	16436.46	13710.92	17260.57	17.68
2	USA	9615.75	9132.20	9772.91	10.01
3	Nigeria	8679.34	8590.08	8495.00	8.70
4	China	5744.18	5952.73	6283.50	6.44
5	Ethiopia	6060.00	6391.54	6276.62	6.43
	Total world	99449.87	92732.52	97614.00	100.00

TABLE 2: TOTAL PRODUCTION OF PRINCIPLE MILLETS (BAJRA + SORGHUM + BUCKWHEAT) (000 MT) (SOURCE: [HTTPS://APEDA.GOV.IN/MILLETPORTAL/PRODUCTION.HTML](https://apeda.gov.in/milletportal/production.html))

USA is the second-largest producer making up 10.01% of the world's production. Nigeria, the third-largest producer contributing 8.70% to the global production. The sorghum and pearl

millet are combined, they account for 92.6% of global millets production, followed by finger millet, foxtail millet, proso millet, little millet and kodo millet, which altogether account for 7.94% of global millet production. Unfortunately, witnessed a gradual decline in the area and production of millets globally. The area covered under millets declined from 74.6 million hectares in 2018 to 72.3 million hectares in 2020, while production decreased from 91.8 million metric tonnes to 89.2 million metric tonnes. The declining trend in area and production between 2010 to 2018 was also reported in recently published studies [7, 8]. Despite India being the world's largest producer of millets, more than 40% of millet consumption has been reported in African countries, particularly in Niger, Mali, Nigeria, Burkina, and Sudan. Global consumption has declined at a rate of 0.9% and is predicted to rise between 2019-2024 [9]. According to Food and Agriculture Organization (FAO), global millet production was estimated at 28.33 million metric tons in 2019, which increased to 30.08 million metric tons in 2021. India is the largest global producer, with a 43.0% global market share in 2021 with Sorghum(jowar), Pearl Millet (bajra), Finger millet (ragi), and other minor millets are grown in the country. According to the Ministry of Agriculture and Farmers Welfare, millet production in India has increased from 14.52 million tonnes in 2015-16 to 17.96 million metric tons in 2020-21.

State wise Scenario of Millets Production in India (2021-22): Table 3 to Table 6 provide a summary of the production and area under cultivation for different types of millets in India for the agricultural year 2021-22, showcasing the leading states in terms of production volume and area cultivated. Table 3 indicate that Jowar is cultivated on 3,800.81 thousand hectares (ha) in India with a total production of 4,150.60 thousand tonnes. Maharashtra leads in both area and production, followed by

State	Jowar (Sorghum)	
	Area (000 ha)	Production (000 tonnes)
All-India	3 800.81	4150.60
Maharashtra	1648.66	1558.00
Rajasthan	619.98	535.66
Karnataka	615.00	731.48
Tamilnadu	397.23	362.04
Uttar Pradesh	171.00	269.84

TABLE 3: TOP FIVE JOWAR PRODUCING STATES IN INDIA (2021-22) (SOURCE: DEPT. OF AGRICULTURE & FARMERS WELFARE, 2023)

Nadu, and Uttar Pradesh (Table 3). In case of Bajra (Pearl Millet) Production, bajra is cultivated on 6,840.80 thousand ha in India with a total production of 9,780.63 thousand tonnes. Rajasthan dominates bajra production, with Uttar Pradesh, Maharashtra, Haryana, and Gujarat also contributing significant volumes. Rajasthan and Uttar Pradesh together account for over half of India's bajra production. Regarding Ragi (Finger Millet) Production (Table 5), Ragi is cultivated on 1,218.43 thousand ha in the country with a production of 1,701.12 thousand tonnes. Karnataka is the largest producer by a substantial margin, followed by Uttarakhand, Maharashtra, Tamil Nadu, and Odisha. In case of small millets production of India, small millets cover an area of 428.92 thousand ha, with a total production of 367.44 thousand tonnes. Karnataka, Uttarakhand, Maharashtra, Tamil Nadu, and Odisha are leading in small millet production, with Karnataka having the largest area under cultivation.

Principle Millet Production in Maharashtra: Rabi Sorghum (19.417 lakh ha), Kharif Sorghum (3.787 lakh ha) and Bajra (6.875 lakh ha) as major crops in terms of area and production of Millet in Maharashtra (Table 4).

The Marathwada region consist of Aurangabad and Latur division, Aurangabad Division has significant cultivation of Rabi Sorghum (2.706 lakh ha) and Bajra (1.299 lakh ha) but does not cultivate Ragi.

State	Bajra (Pearl Millet)	
	Area (000 ha)	Production (000 tonnes)
All-India	6840.80	9780.63
Rajasthan	3736.10	3739.84
Uttar Pradesh	905.00	1951.18
Maharashtra	666.72	618.72
Haryana	483.10	1119.83
Gujarat	446.21	1089.64
Madhya Pradesh	343.00	868.82

TABLE 4: TOP FIVE BAJRA (PEARL MILLET) PRODUCING STATE IN INDIA (2021-22) (SOURCE: DEPT. OF AGRICULTURE & FARMERS WELFARE, 2023)

State	ragi (Finger Millet)	
	Area (000 ha)	Production (000 tonnes)
All-India	1218.43	1701.12
Karnataka	846.00	1126.87
Uttarakhand	86.00	127.11
Maharashtra	81.26	102.63
Tamilnadu	74.44	227.49
Odisha	54.98	43.65

TABLE 5: TOP FIVE STATE RAGI (FINGER MILLET) PRODUCING STATE (2021-22) (SOURCE: DEPT. OF AGRICULTURE & FARMERS WELFARE, 2023)

Whereas Latur Division has a 1.56 lakh ha area under Kharif Jowar, 3.281 lakh ha area under Rabi Sorghum, and 0.972 lakh ha area under Bajra cultivation. Although there is a considerable proportion of millet production and availability, consumption has declined over the years. A downward trend in per capita consumption of sorghum was seen in both rural

and urban India, with consumption dropping from 19.1 to 5.2 kg per year in rural India and from 8.5 to 2.7 kg per year in urban India, indicating 68 per cent and 70 per cent declines, respectively [9]. A similar study also stated that there was a decline in millet consumption and the difference in total millet consumption between rural and urban was 10 kgs in 2004-05 and 4 kgs in 2011-12 [11]. Historically, millets have been integral to diets, offering not only a plethora of health benefits but also contributing to environmental conservation through low water and input requirements. The International Year of Millets, declared by the United Nations for 2023 at the initiative of the Government of India, aims to raise awareness, increase production, and promote consumption of millets. As part of this context, this research explores the awareness of millets among the farmers of the Marathwada region, with specific objectives:

1. To assess the awareness of millets among the respondents.
2. To understand the consumption behaviour of millets among the respondents.
3. To gather suggestions from respondents for increasing the usage of millets.

Methodology: The current investigation aimed to assess the awareness of millets among the farmers of the Marathwada region. The study encompassed all eight districts within the Marathwada region and adopted an ex-post facto research design. A questionnaire was employed as the primary tool for data collection, formulated in Google Form. The Google form link was directly distributed among the farmers, with additional support provided through SMS from Krishi Vigyan Kendras (KVKs) to facilitate participation. A total of 402 responses were received through the Google Form, with 28 incomplete responses excluded from the analysis. Therefore, 374 complete and valid responses from the

Marathwada region constituted the respondent sample for this study. District-wise breakdowns of responses from the people of the Marathwada region are presented in Table 6. The independent variables such as age, education, gender, main occupation, family background, family size, family annual income, and source of information about millets were taken for the study. To gauge the awareness of millets among the respondents, factors such as awareness of different millets,

State	Small Millets	
	Area (000 ha)	Production (000 tonnes)
All-India	428.92	367.44
Karnataka	89.00	23.87
Uttarakhand	60.26	73.27
Maharashtra	52.35	26.03
Tamilnadu	47.00	29.83
Odisha	38.37	19.61

TABLE 6: TOP FIVE SMALL MILLETS PRODUCING STATES (2021-22) (SOURCE: DEPT. OF AGRICULTURE & FARMERS WELFARE, 2023)

knowledge about the nutritional content of millets, awareness of the importance of millets in the human diet, and general awareness about millets were considered for calculating the overall awareness level. Awareness responses of the respondents were recorded on two-point continuum i.e. assigning a score of 1 for "Yes" and 0 for "No.". The total awareness score for each respondent was derived by summing up

individual scores. Subsequently, mean scores

Sr. No.	Agriculture Division of Maharashtra	Kharif Jowar		Rabi Sorghum		Bajra (Pearl Millet)		Ragi (Finger Millet)	
		A	P	A	P	A	P	A	P
1	Konkan Division	00.00	00.00	00	00	00	00	318.61	23.29
2	Nashik Division	821.50	1338.79	758.76	1141.18	1719.95	2479.14	227.51	162.75
3	Pune Division	57.31	35.38	9582.42	6791.74	2486.90	3280.23	25.85	20.31
4	Kolhapur Division	726.81	1053.44	2799.27	2686.41	1248.52	1174.91	244.28	426.83
5	Aurangabad Division	87.16	60.70	2706.05	2954.67	1298.59	2064.82	00.00	00.00
6	Latur Division	1560.17	953.11	3281.84	4171.26	97.23	45.90	0.10	0.08
7	Amravati Division	503.73	356.21	214.94	258.62	23.78	11.23	0.00	0.00
8	Nagpur Division	30.72	16.73	73.64	45.00	0.00	0.00	0.00	0.00
	Total	3787	3814	19417	18049	6875	9056	816	939

TABLE 7: AREA AND PRODUCTION OF PRINCIPLE MILLETS IN THE MAHARASHTRA DURING 2020-21 (AGRICULTURE DIVISION WISE) ('00' HA AREA & '00' TONNES PRODUCTION) (SOURCE: APEDA – E – CATALOGUE FOR EXPORT OF MILLETS & VALUE ADDED PRODUCTS: MAHARASHTRA, 2022)

were computed, serving as a basis to categorize respondents into low awareness, medium awareness, and high awareness categories, determined by Mean + Standard Deviation.

Sr. No.	Districts	Frequency	Percentage
1	Ch. Sambhaji Nagar	85	22.72
2	Jalna	43	11.50
3	Beed	47	12.57
4	Dharashiv	25	06.68
5	Parbhani	64	17.11
6	Hingoli	39	10.43
7	Latur	30	08.02
8	Nanded	41	10.96
	Total sample (respondents)	374	100.00

TABLE 8: DISTRICT WISE RESPONSES GIVEN BY THE FARMERS OF MARATHWADA REGION (N=374 RESPONDENT FARMERS)

Regarding calculation of frequency of consumption of millet based products among the respondents, nine millets viz., great millet, pearl millet, barnyard millet, finger millet, amaranthus, foxtail millet, little millet, proso millet, kodo millet were selected for the study. The frequency of consumption was measured on a 9-point continuum: daily consumption (8 score), 2-3 times a week (7 score), once a week (6 score), once a fortnight (5 score), once a month (4 score), once every three months (3 score), once every six months (2 score), rarely in a year (1 score), and never consumed millets (0 score). The mean score was calculated from respondents' consumption scores, and respondents were categorized into low consumption, medium consumption, and high consumption based on Mean \pm SD. The statistical tools employed for the study included frequencies, percentages, arithmetic mean, standard deviation, and correlation coefficient.

Results

1. Awareness of millets among the respondents

1.1 Awareness of different millets among the respondents: Table 9 reveals the awareness levels of various millets among the

Sr. No.	Name of the millet	Frequency	Percentage
1	Great Millet (Sorghum / Jowar)	374	100.00
2	Pearl Millet (Bajra)	374	100.00
3	Barnyard Millet (Barti / Bhagar)	367	98.13
4	Amaranthus (Rajgira)	366	97.86
5	Finger Millet (Nachni / ragi)	281	75.13
6	Foxtail millet (Rala)	190	50.80
7	Little Millet (Sava)	55	14.70
8	Proso Millet (Varai)	54	14.44
9	Kodo Millet (Kudra)	49	13.10

TABLE 9: AWARENESS OF DIFFERENT MILLETS AMONG THE RESPONDENTS (N=374 RESPONDENT FARMERS)

respondents; it is noted that all respondents were fully aware of Great Millet (sorghum) and Pearl Millet (bajra), followed by high

awareness for Barnyard Millet (98.13%), Amaranthus (97.86%), Finger Millet (75.13%), Foxtail Millet (50.80%). Whereas low awareness about Little Millet (14.70%), Proso Millet (14.44%), and Kodo Millet (13.10%).

1.2 Awareness of nutritional content of millets among the respondents:

The awareness of the respondents regarding the nutritional content of millets is presented in Table 10. It is reported that the majority of the respondents (80.48%) were aware that millets are a source of iron, while 72.46 per cent of them were aware that millets contain calcium.

Sr. No.	Name of the nutrient content	Frequency	Percentage
1	Iron	301	80.48
2	Calcium	271	72.46
3	Magnesium	149	39.84
4	Zinc	127	33.96
5	Protein	127	33.96
6	Fibre	89	23.70

TABLE 10: AWARENESS ABOUT THE NUTRITIONAL CONTENT OF MILLETS(N=374 RESPONDENT FARMERS)

Whereas, 39.84 per cent of them were knowledgeable about the magnesium content in millets, 33.96 per cent knew about the zinc content, 33.96 per cent were aware of the protein content, and only 23.70 per cent of them were aware about the fibre content in millets.

1.3 Awareness of importance of millets in human diet:

The awareness of the respondents about the importance of millets in the human diet is presented in Table 11. The data from Table 11 indicates that the majority of respondents (88.77%) were aware that millets are a healthy diet and can increase the resistance power of human beings, while 79.14 per cent of them perceived that 'millets are easy to digest.' Whereas, 78.07 per cent of them

were aware that 'millets are good for increasing

Sr. No.	Statement	Frequency	Percentage
1	Easy to digest	296	79.14
2	Healthy diet / increase resistance power	332	88.77
3	Good for Diabetics	276	73.80
4	Good for cholesterol control	247	66.04
5	Manage the body weight	228	60.96
6	Good for increase the haemoglobin	292	78.07
7	Good for bone health	235	62.83
8	Beneficial in winter season	217	58.02

TABLE 11: AWARENESS ABOUT IMPORTANCE OF MILLETS IN HUMAN DIET (N=3)

haemoglobin,' followed by awareness that millets are good for diabetics (73.80%), millets are good for cholesterol control (66.04%), millets are good for bone health (62.83%), millets manage body weight (60.96%), and millets are beneficial in the winter season (58.02%).

1.4 Overall awareness of millets: Table 12 reports the overall awareness of millets among the people, indicating that the majority of respondents (44.12%) had a medium level of overall awareness of millets, followed by a low level (31.55%) and a high level (24.33%) of

Sr. No.	Awareness	Frequency	Percentage
1	Low (upto 8.40)	118	31.55
2	Medium (8.41 to 16.24)	165	44.12
3	High (16.25 & Above)	91	24.33
	Mean = 12.32 S.D. = 3.92	374	100.00

TABLE 12: OVERALL AWARENESS OF MILLETS AMONG THE PEOPLE (N=374 RESPONDENT FARMERS)

awareness of millets among the respondents. Table 13 reveals the mean overall awareness of millets among respondents categorized by various profiles. Notably, individuals aged 50 and above show the highest mean awareness score (14.05), indicating a stronger awareness in this age group. Females exhibit a higher mean awareness score (13.11) compared to males (12.23). Regarding family income, respondents with incomes up to Rs. 1,00,000/- have the highest mean awareness (12.70),

Sr. No.	Profile / Characteristics	Frequency	Mean of overall awareness
1	Age		
	Young (Upto 29 yrs)	143	12.03
	Middle (30 to 49 yrs)	179	12.04
	Old (50 & Above)	52	14.05
2	Gender		
	Male	336	12.23
	Female	38	13.11
3	Family Annual Income		
	Upto Rs. 1,00,000 /-	131	12.70
	Rs. 1,00,001 to 2,00,000/-	71	12.60
	Rs. 2,00,001 to 3,00,000/-	28	12.68
	Rs. 3,00,001 to 4,00,000/-	46	11.67
	Rs.4,00,001 & Above	98	11.81

TABLE 13: MEAN OF OVERALL AWARENESS OF MILLETS ACCORDING TO PROFILE OF RESPONDENTS (N=374 RESPONDENT FARMERS)

followed by those with incomes between Rs. 1,00,001 to 2,00,000/- (12.60). These findings offer valuable insights for tailoring targeted awareness campaigns to specific demographic groups with lower awareness levels, contributing to more effective dissemination of information about millets.

2. Consumption Behaviour of Millets among the Respondents

2.1 Frequency of consumption of millet-based products among respondents: The

consumption behavior of millets among the respondents was investigated and is presented in Table 14. The results from Table 14 indicate that 56.95 per cent of the respondents consumed sorghum daily, followed by rarely in a year (15.77%), 2-3 times a week (10.96%), once a week (5.88%), never consumed (4.81%), once in six months (1.87%), once in a fortnight (1.60%), once a month (1.60%), and once in three months (0.53%). This detailed breakdown sheds light on the diverse consumption frequencies of sorghum, providing valuable insights into the dietary habits of the surveyed population. Regarding Pearl millet, majority of the respondents rarely consumed it in a year (50.00%), followed by 34.76 per cent of them were consumed once in six months. While 6.15 per cent of the respondents were never consumed pearl millet. In case of Barnyard millet, 39.57 per cent of the respondents rarely

consumed it, while 25.40 per cent of them were consumed it once in a week, followed by once in three months and once in six months (i.e.9.36%). Whereas 7.49 per cent of respondents were never consumed barnyard Regarding Pearl Millet, the majority of the respondents rarely consumed it in a year (50.00%), followed by 34.76 per cent who consumed it once in six months. Whereas, 6.15 per cent of the respondents never consumed pearl millet. In the case of Barnyard Millet, 39.57 per cent of the respondents rarely consumed it, while 25.40 per cent consumed it once a week, followed by once in three months and once in six months (i.e., 9.36%). Only 7.49 per cent of respondents never consumed Barnyard Millet. This analysis provides insights into the infrequent consumption patterns of these specific millet types among the respondents. Regarding Finger Millet,

Sr. No	Name of the millet	Daily	2-3 times a week	Once in a week	Once in a fortnight	Once in a month	Once in a three monthly	Once in a six monthly	Rarely in a year	Not at all
1	Sorghum (Jowar)	213 (56.95)	41 (10.96)	22 (5.88)	06 (1.60)	06 (1.60)	02 (0.53)	07 (1.87)	59 (15.77)	18 (4.81)
2	Pearl Millet (Bajra)	00 (00.00)	01 (0.27)	06 (1.60)	05 (1.34)	07 (1.87)	15 (4.01)	130 (34.76)	187 (50.00)	23 (6.15)
3	Barnyard Millet (Barti/bhagar)	00 (00.00)	15 (4.01)	95 (25.40)	06 (1.60)	12 (3.21)	35 (9.36)	35 (9.36)	148 (39.57)	28 (7.49)
4	Finger Millet (Nachni / Ragi)	17 (4.55)	12 (3.21)	26 (6.95)	08 (2.14)	26 (6.95)	17 (4.55)	16 (4.28)	195 (52.14)	57 (15.24)
5	Amaranthus (Rajgira)	00 (00.00)	15 (4.01)	120 (32.08)	55 (14.71)	15 (4.01)	09 (2.41)	16 (4.28)	246 (65.77)	33 (8.82)
6	Foxtail millet (Rala)	00 (00.00)	00 (00.00)	00 (00.00)	00 (00.00)	15 (4.01)	21 (5.61)	36 (9.63)	81 (21.66)	221 (59.09)
7	Little Millet (Sava)	00 (00.00)	00 (00.00)	00 (00.00)	00 (00.00)	00 (00.00)	00 (00.00)	00 (0.00)	00 (00.00)	374 (100.00)
8	Proso Millet (Varai)	00 (00.00)	00 (00.00)	00 (00.00)	00 (00.00)	00 (00.00)	00 (00.00)	00 (0.00)	05 (1.34)	369 (98.66)
9	Kodo Millet (Kudra)	00 (00.00)	00 (00.00)	00 (00.00)	00 (00.00)	00 (00.00)	00 (00.00)	00 (0.00)	00 (0.00)	374 (100.00)

TABLE 14 : FREQUENCY OF CONSUMPTION OF MILLET BASED PRODUCTS AMONG RESPONDENTS (N=374 RESPONDENT FARMERS)

52.14 per cent of respondents rarely consumed Finger Millet in a year, followed by 15.24 per cent who never consumed it. Whereas, 6.95 per cent of the respondents reported consuming it once a week and once a month, while 4.55 per cent consumed it daily and with the same percentage once in three months. Concerning the consumption of Amaranthus, the majority of respondents (65.77%) rarely consumed it, followed by once a month (32.08%), and once a fortnight (14.71%). However, 8.82 per cent of respondents never consumed Amaranthus at all. This detailed breakdown provides insights into the diverse consumption patterns of Finger Millet and Amaranthus among the respondents. Majority of the respondents were never consumed foxtail millet (63.10%), followed by 21.06 per cent of the respondents were consumed it rarely in a year, once in a six monthly (9.63%), and once in a three monthly (5.61%). Table 9 further reported that majority of the respondents were never consumed little millet (100.00%), proso millet (98.66%) and kodo millet (100.00%). Most of the respondents never consumed Foxtail Millet (63.10%), followed by 21.06 per cent who rarely consumed it in a year, once in six months (9.63%), and once in three months (5.61%). Table 7 also shows that a significant portion of the respondents refrained from consuming Little Millet (100.00%), Kodo Millet (100.00%), and Proso Millet (98.66%). This data underscores the prevailing tendency of non-consumption of these millet within the respondents.

2.2 Overall Consumption of Millets among the Respondents

Table 15 reports the overall consumption of millets among the respondents, indicating that the majority of the respondents (40.91%) had a medium level of overall millet consumption. This is followed by a low level (35.83%) and a high level (23.26%) of overall millet consumption among the respondents. Table 16 indicate the mean of overall

consumption score of the respondents according their profile. It is reported that mean of overall consumption score of the

Sr. No.	Consumption	Frequency	Percentage
1	Low (upto 20.79)	134	35.83
2	Medium (20.80 to 27.64)	153	40.91
3	High (27.65 & Above)	87	23.26
	Mean = 24.22 S.D. = 3.42	374	100.00

TABLE 15: OVERALL CONSUMPTION LEVEL OF MILLET AMONG THE RESPONDENTS (N=374 RESPONDENT FARMERS)

respondents in the category of old age (26.14), female gender (26.85), farming as a main occupation (25.13), rural family background (24.90) and annual family income upto Rs. 1,00,00 /- (24.98) were higher as compare to other respondents. Table 9 presents the mean overall consumption levels of millets based on demographic profiles of the respondents. The data indicates that respondents in the older age

Sr. No.	Profile / Characteristics	Frequency	Mean of overall consumption
1	Age		
	Young (Upto 29 yrs)	143	22.82
	Middle (30 to 49 yrs)	179	24.78
	Old (50 & Above)	52	26.14
2	Gender		
	Male	336	23.92
	Female	38	26.85
3	Family Annual Income		
	Upto Rs. 1,00,000 /-	131	24.98
	Rs. 1,00,001 to 2,00,000/-	71	24.92
	Rs. 2,00,001 to 3,00,000/-	28	24.57
	Rs. 3,00,001 to 4,00,000/-	46	22.04
	Rs.4,00,001 & Above	98	23.71

TABLE 16: MEAN OF OVERALL CONSUMPTION LEVEL OF MILLETS ACCORDING TO PROFILE OF RESPONDENTS (N=374 RESPONDENT FARMERS)

group (50 & above) have the highest mean consumption score of 26.14, while females exhibit a higher mean consumption score (26.85) compared to males (23.92). Regarding

family annual income, respondents with mean consumption score (24.98), followed closely by those with incomes in the range of Rs. 1,00,001 to 2,00,000/-. The data provides valuable insights into the varying consumption patterns of millets among different age groups, genders, and income brackets, aiding in understanding dietary preferences and facilitating targeted interventions for promoting millet consumption.

2.3 Consumption pattern of millet based products among the respondents: Table 17 illuminates the consumption patterns of millet-based products among the respondents,

Sr. No.	Name of millet-based product	Aware about it	Like to eat
1	Bhakar	374 (100.00)	266 (71.12)
2	Khichadi / Bhagar	366 (97.86)	206 (55.08)
3	Kharudya / Kurudya	364 (97.33)	227 (60.69)
4	Chapati	102 (27.27)	98 (26.20)
5	Shevai / khir	119 (31.82)	101 (27.00)
6	Halva	98 (26.20)	89 (23.80)
7	Laddu	356 (95.19)	204 (54.54)
8	Upma	112 (29.95)	101 (27.00)
9	Dosa	109 (29.14)	98 (26.20)
10	Papdi	297 (79.42)	251 (67.11)
11	Papad	303 (81.02)	293 (78.34)
12	Cake	56 (14.97)	46 (12.30)
13	Pops snakes (Lahya)	368 (98.40)	277 (74.06)
14	Bread / toast	51 (13.64)	24 (6.42)
15	Noodles	48 (12.83)	41(10.96)
16	Biscuit / cookies	183 (48.93)	155 (41.44)
17	Pasta	13 (3.48)	04 (1.07)

TABLE 17: CONSUMPTION PATTERN OF MILLET BASED PRODUCTS AMONG THE RESPONDENTS (N=374 RESPONDENT FARMERS)

offering a comprehensive view of their awareness and preferences. The findings highlight that staple items such as Bhakar and Khichadi/Bhagar enjoy widespread recognition, with 100.00 per cent and 97.86 per cent

incomes up to Rs. 1,00,000/- have the highest awareness, respectively. The data further reveals a notable inclination towards these products, with 71.12 per cent expressing a preference for Bhakar and 55.08 per cent for Khichadi / Bhagar. Similarly, Kharudya / Kurudya also demonstrates substantial awareness (97.33%) and liking, with 60.69 per cent expressing a preference for this millet-based product. In contrast, certain millet-based products like Chapati and Halva exhibit moderate awareness levels (27.27% and 26.20%, respectively), with corresponding liking percentages of 26.20 per cent and 23.80 per cent. Table 10 also reported the popularity of millet-based sweets, particularly Laddu, which boasts high awareness (95.19%) and a substantial liking rate of 54.54 per cent. Moreover, the inclusion of various millet-based products, ranging from traditional choices like Papdi and Papad to modern options like Noodles and Pasta, showcases the diversity in respondents' consumption habits. The data serves as a valuable resource for stakeholders, allowing them to tailor marketing strategies and educational campaigns to enhance awareness and foster positive attitudes toward millet-based products. Understanding the varying levels of awareness and liking for these products aids in the promotion of healthier dietary choices and the integration of millets into the regular diet of the surveyed population.

3. Major Reasons for Consumption / Non-Consumption of Millets among the Respondents

3.1 Major reasons for consumption of millet based product: Table 18 offers a detailed exploration of the key motivations driving the consumption of millet-based products among the respondents, with a breakdown for each millet type. The first notable trend is the widespread perception that millet-based products are "Easy to Digest." Great Millet (Sorghum) leads in this category, with an impressive 85.56 per cent, suggesting that the

digestibility factor is a significant influencer across all millet varieties. Taste emerges as a

Sr. No.	Statement	Great Millet (Sorghum)	Pearl Millet (Bajra)	Barnyard Millet (Bhagar)	Amaranthus (Rajgira)	Finger Millet (Nachni)	Foxtail Millet (Rala)
1	Easy to digest	320 (85.56)	210 (56.15)	44 (11.76)	280 (74.87)	263 (70.32)	23 (6.15)
2	Tasty	230 (61.50)	258 (68.98)	139 (37.16)	284 (75.93)	152 (40.64)	17 (4.54)
3	Healthy diet / increase resistance power	301 (80.48)	232 (62.03)	136 (36.36)	192 (51.34)	183 (48.93)	24 (6.42)
4	Good for Diabetics	201 (53.74)	102 (27.27)	28 (7.49)	54 (14.44)	53 (14.17)	23 (6.15)
5	Good for cholesterol control	181 (48.40)	113 (30.21)	33 (8.82)	73 (19.52)	65 (17.38)	26 (6.95)
6	Manage the body weight	159 (42.51)	108 (28.88)	37 (9.89)	74 (19.79)	158 (42.25)	28 (7.49)
7	Good for increase the haemoglobin	114 (30.48)	130 (34.76)	25 (6.68)	188 (50.27)	167 (44.65)	19 (5.08)
8	Good for bone health	98 (26.20)	119 (31.82)	33 (8.82)	86 (22.99)	80 (21.39)	23 (6.15)
9	Beneficial in winter season	110 (29.41)	279 (74.60)	15 (4.01)	15 (4.01)	52 (13.90)	17 (4.54)
10	Main food in fasting	00 (00.00)	00 (00.00)	302 (80.75)	235 (62.83)	00 (00.00)	00 (00.00)

TABLE 18: MAJOR REASONS FOR CONSUMPTION OF MILLET BASED PRODUCT (N=374 RESPONDENT FARMERS)

crucial factor, notably for Pearl Millet (Bajra), which scores a high percentage of 68.98 per cent under "Tasty." This underscores the importance of flavor in influencing food choices, highlighting that taste plays a pivotal role in the consumption of certain millet-based products. Finger Millet (Nachni) also registers a noteworthy 40.64 per cent under this category, indicating that a sizable portion of respondents associates this millet type with a palatable eating experience. The findings are in line with [12]. Moreover, the data reveals that respondents perceive millets as a "Healthy Diet/In. crease Resistance Power," with Great Millet (Sorghum) leading at 80.48 per cent. This points to a prevalent belief among respondents that millets offer health benefits, aligning with a broader trend of conscious and nutritious eating. Furthermore, health-related reasons such as being "Good for Diabetics," "Good for Cholesterol Control," and "Managing Body Weight" demonstrate substantial

percentages across various millet types. This suggests that respondents are not only aware of the potential health benefits of millets but also consider these factors when incorporating millet-based products into their diets. The Table 18 also highlights specific health outcomes associated with millet consumption, such as being "Good for Increase in Haemoglobin" and promoting "Bone Health." These findings signify that respondents perceive millets as contributing to specific aspects of their well-being. The association of certain millets, particularly Pearl Millet (Bajra), with being "Beneficial in Winter Season" reflects a seasonal dietary preference among respondents. The recognition of Barnyard Millet (Bhagar) and Amaranthus (Rajgira) as the "Main Food in Fasting" emphasizes the cultural and ritualistic significance of these millets during fasting periods. Table 18 provides a nuanced understanding of the multifaceted motivations

behind millet-based product consumption, encompassing taste preferences, health

3.2 Major reasons for non-consumption of millets despite having awareness: Table 19 elucidates the factors hindering the

Sr. No.	Reasons	Frequency	Percentage
1	Lack of proper knowledge about all millets	290	77.54
2	Lack of proper knowledge about preparation of millet based products	219	58.86
3	Non-availability of millet-based products	285	76.20
4	Taste is not preferred by child	67	17.91
5	High price of millet based product	144	38.50

TABLE 19: REASONS FOR NON-CONSUMPTION OF MILLETS DESPITE HAVING AWARENESS (N=374 RESPONDENT FARMERS)

consumption of millets among the respondents, despite their awareness of these grains. The predominant reason, highlighted by 77.54 per cent of respondents, is the "Lack of proper knowledge about all millets," indicating a substantial gap in comprehensive understanding about different millets and their benefits. Following closely, "Lack of proper knowledge about preparation of millet-based products" stands as a significant barrier at 58.86 per cent, suggesting that respondents may struggle with incorporating millets into their diets due to uncertainties about how to prepare millet-based dishes. Furthermore, the Table 19 underscores the practical challenges faced by respondents, with "Non-availability of millet-based products" cited by 76.20 per cent of respondents. This signals a potential accessibility issue, emphasizing the importance of making millet products more readily available in the market. Whereas, taste considerations play a role, as "Taste not preferred by child" is noted by 17.91 per cent of respondents, indicating the influence of family preferences on millet consumption. The "High price of millet-based products" emerges as a

consciousness, and cultural practices among the surveyed population.

notable concern for 38.50 per cent of the respondents, highlighting the economic aspect as a critical factor influencing dietary choices. The findings underscore the multifaceted challenges that need to be addressed, ranging from knowledge gaps to practical accessibility and affordability issues, to promote widespread adoption of millets in the surveyed population's diets.

4. Suggestions of the respondents about increasing the usage of millet in diet: Table 20 provides the suggestions put forth by the

respondents to enhance the incorporation of millets into their diets. The most prominent suggestion, voiced by 77.00 per cent of respondents, is that "Extension agencies should organize training programs on millet-based value-added products/ready-to-eat products." This underscores the perceived importance of educational initiatives in equipping farmers with the knowledge and skills necessary to incorporate millets into their dietary routines. The second most prevalent suggestion, expressed by 68.98 per cent of respondents, is "Upload videos on the preparation of various recipes related to millet-based value-added products on YouTube/social media." This indicates a recognition of the power of visual content and online platforms in disseminating information and promoting the culinary versatility of millets. "Awareness/Publicity campaigns coupled with advertisements about the importance of millets in the diet should be organized at retailers' shops, malls, etc." emerges as the third most frequent suggestion, with 57.49 per cent of respondents endorsing this idea. This underscores the significance of targeted awareness campaigns to influence consumer perceptions and choices. Other noteworthy suggestions include an increase in the Minimum Support Price (MSP) of millets

(45.72%), advocating for the availability of millets in public distribution systems/ration

Sr. No.	Suggestions	Frequency	Percentage
1	The extension agency should organize training programs on millet-based value-added products/ready-to-eat products.	288	77.00
2	Upload videos demonstrating the preparation of various recipes related to millet-based value-added products on YouTube/social media.	258	68.98
3	An awareness / publicity campaign, along with advertisements emphasizing the importance of millets in the diet, should be organized at retailers' shops, malls, etc.	215	57.49
4	MSP of millets should be increased	171	45.72
5	Availability of millets in public distribution system / ration shop	166	44.38
6	An awareness program about millet-based products should be organized in schools and colleges.	162	43.31
7	Millet-based products should be included in midday meals at schools.	155	41.44
8	Guidance on the use of millets tailored to different diseases.	121	32.35

TABLE 20: SUGGESTIONS OF THE RESPONDENTS ABOUT INCREASING THE USAGE OF MILLET IN DIET (N=374 RESPONDENT FARMERS)

shops (44.38%), organizing awareness programs about millet-based products in the schools / colleges (43.31%), proposing the inclusion of millet-based products in midday meals in schools (41.44%), and seeking guidance on the use of millets tailored to different diseases (32.35%).

In summary, Table 20 reflects the diverse perspectives of the respondents on how to enhance millet consumption, ranging from educational initiatives and online resources to awareness campaigns, policy interventions, and targeted programs for specific demographics like school children. These suggestions collectively provide valuable insights for stakeholders aiming to promote millet consumption in the community.

The findings of the study are consistent with the previous studies [13, 14 and 15].

Conclusions:

1. The study found that respondents were highly aware of Great Millet (sorghum) and Pearl Millet (bajra). However, in case of other minor millets viz., Little Millet, Proso Millet, and Kodo Millet having lower awareness levels. This information can guide targeted awareness campaigns to bridge knowledge gaps for specific millets.

2. The results revealed that a significant proportion were aware of millets as a source of iron and calcium, whereas low awareness levels for other nutrients. This underscores the need for comprehensive nutritional education to enhance awareness of millets' health benefits.

3. The study indicated a medium level of awareness among respondents, with variations based on age, gender, and income. Tailoring

awareness campaigns to specific demographic groups may improve overall awareness levels.

4. Consumption patterns revealed that sorghum was consumed most frequently, daily (56.95%) by the respondents. While millets, such as Little Millet, Proso Millet, and Kodo Millet, were rarely or never consumed by the majority. Understanding these consumption trends is crucial for promoting diverse millet varieties.

5. Consumption patterns of specific millet-based products were explored, emphasizing the popularity of staples like Bhakar and Khichadi/Bhagar. This information is valuable for promoting certain millet-based products based on consumer preferences.

6. Reasons driving millet-based product consumption were explored, including taste, health benefits, and cultural practices. These insights aid in tailoring marketing strategies to align with consumer preferences and health-conscious choices.

7. Barriers to millet consumption, despite awareness, were identified in the study. Lack of knowledge about millets and their preparation, non-availability of millet-based products, taste preferences, and pricing were highlighted as significant challenges. Addressing these barriers is essential for promoting millet consumption. Respondents provided valuable suggestions to increase millet consumption. Recommendations included organizing training programs, leveraging digital platforms for recipe promotion, conducting awareness campaigns, increasing Minimum Support Prices, and advocating for millet inclusion in school meals. Implementing these suggestions can contribute to enhancing millet adoption.

In conclusion, the study provides a comprehensive understanding of millet awareness, consumption behavior, and influencing factors among farmers of the Marathwada region. The insights can inform targeted interventions to promote millet consumption and address existing barriers,

contributing to improved dietary diversity and overall health outcomes.

Reference

[1] Sujata Bhat, Nandini, C., and Tippeswamy, V. (2018). Significance of small millets in nutrition and health-A review. *Asian Journal of Dairy and Food Research*, 37(1), 35-40.

[2] A Poshadri, Y Praveen Kumar, G Shiva Charan, M Raghuvver, M Sunil Kumar and A Ramadevi (2020). Good Practices: Promoting women empowerment and nutritional diversity in Tribal hamlets of Adilabad. 33: June 2020. <https://www.aesanetwork.org/promoting-women-empowerment-and-nutritional-diversity-in-tribal-hamlets-of-adilabad/>. Accessed on 04.01.2023.

[3] Longvah T, Anathan R, Bhaskarachary K, and Venkaiah K (2017). Indian Food Composition Tables (2017). Published by National Institute of Nutrition, ICMR, India.

[4] Poshadri, A., Y. Praveen Kumar, G. Shiva Charan, M. Raghuvver, M. Sunil Kumar and Rama Devi, A. (2019). Energy Rich Composite Millet and Soybean based Malted Weaning Mix: A Complementary Food in Tribal Areas of Adilabad District, India. *International Journal of Current Microbiology and Applied Sciences*. 8(02): 2058-2064.

[5] Anitha S, Kane-Potaka J, Botha R, Givens DI, Sulaiman NLB, Upadhyay S, Vetriventhan M,

[6] Tsusaka TW, Parasannanavar DJ, Longvah T, Rajendran A, Subramaniam K, Bhandari RK. 2021. Millets Can Have a Major Impact on Improving Iron Status, Hemoglobin Level, and in Reducing Iron Deficiency Anemia-A Systematic Review and Meta-Analysis. *Frontiers Nutrition*. 14;8:725529.

[7] ASSOCHAM, 2021. Millets 2021: Status Way forward. https://www.assocham.org/uploads/files/Report_Millets2021_FINAL.pdf

- [8] Dayakar Rao, B., Gill, M.S., Thakur, S., Manjula, D., Ghoora, S., Kowsalya., Pant, K.K and Tonapi, V.A. 2022. Millet International Recipes: A Culinary Journey of Tradition and Innovation, ICAR – Indian Institute of Millet Research, Rajendranagar, Hyderabad, Telangana, India.
- [9] APEDA (2024). Market Intelligence Report for Millets. https://agriexchange.apeda.gov.in/Weekly_eReport/Millets_Report.pdf
- [10] Rao, P.P, Basavaraj, G., Ahmad, W., and Bhagavatula, S. 2010. An analysis of availability and utilization of sorghum grain in India. *Journal of SAT Agricultural Research*. 8: 1– 9.
- [11] Umanath, M., Balasubramaniam, R and Paramasivam, R. 2018. Millets consumption probability and demand in India an application of heckman sample selection model. *Economic Affairs*. 63: 1033–1044. doi: 10.30954/0424-2513.4.2018.29.
- [12] Lakshmy Priya, Krishnamurthy; Shobana, Shanmugam; Sudha, Vasudevan; Gayathri, Rajagopal; Beatrice, D Annette; Anjana, Ranjit Mohan; Krishnaswamy, Kamala; and Mohan, Viswanathan (2024). Consumption pattern of millets among south Indian adults *Journal of Diabetology* 15(1):p 63-69, January-March 2024. | DOI: 10.4103/jod.jod_90_23.
- [13] Kane-Potaka J, Anitha S, Tsusaka TW, Botha R, Budumuru M, Upadhyay S, Kumar P, Mallesh K, Hunasgi R, Jalagam AK and Nedumaran S (2021) Assessing Millets and Sorghum Consumption Behavior in Urban India: A Large-Scale Survey. *Front. Sustain. Food Syst*. 5:680777.doi: 10.3389/fsufs.2021.680777.
- [14] Ch. Hemamalini, Susan Sam and TSSK Patro (2021). Awareness and Consumption of Small Millets. *The Pharma Innovation Journal*, SP 10 (7) : 34-37.
- [15] Alekhya P, Shravanthi AR (2019) Buying behaviour of consumers towards millet based food products in Hyderabad district of Telangana, India. *Int J Curr Microbiol App Sci* 8(10):223–236.
- [16] APEDA (2022). APEDA – E – Catalogue for Export of Millets & Value added Products : Maharashtra, 2022. Retrieved from <https://apeda.gov.in/milletportal/>

A short review on toughened epoxy based nanocomposites for EMI shields

Ravi Kant¹ and M. Fahim^{2*}

¹ Department of Chemistry, Zakir Husain Delhi College, University of Delhi, New Delhi 110002 INDIA

² Department of Physics, Zakir Husain Delhi College, University of Delhi, New Delhi 110002 INDIA

Volume 1, Issue 3, May 2024

Received: 18 January, 2024; Accepted: 9 April, 2024

DOI: <https://doi.org/10.63015/5N-2416.1.3>

*Corresponding Author Email: fahim99@hotmail.com

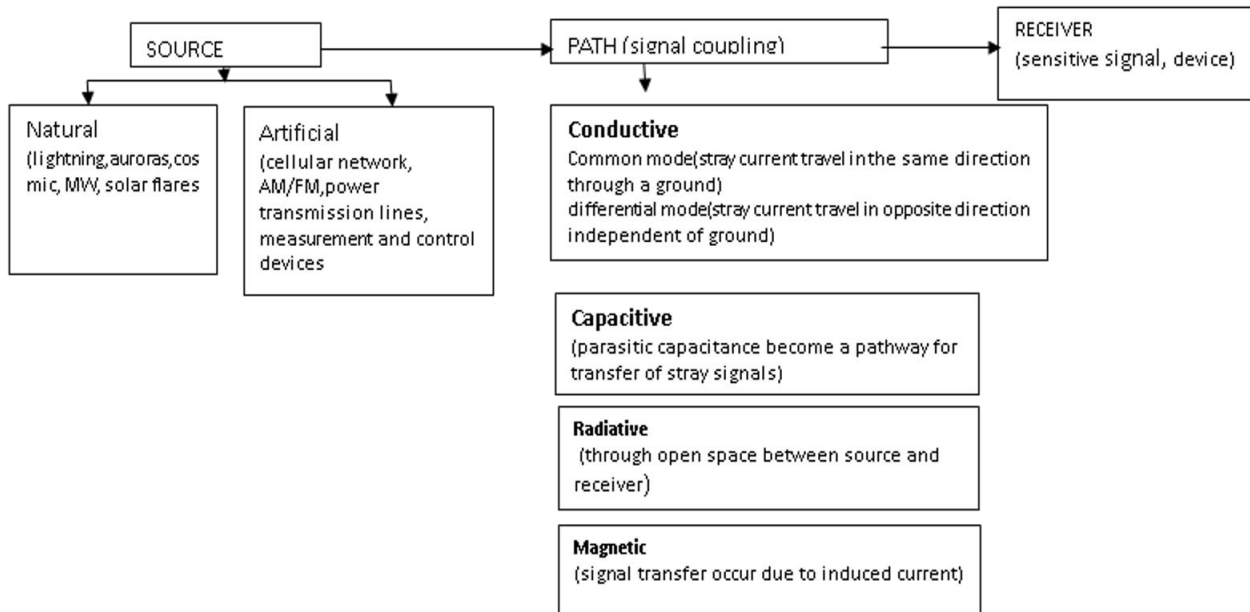
Abstract: Modern era devices and appliances require shielding from electromagnetic interference to ensure stable and efficient functioning. This is all the more pertinent in view of the safety and protection of electronic gadgets used in defence security equipment. It has been observed that the most prominent radiations of EMI fall in the range of microwave (GHz) and radio waves (MHz). Those materials which protect equipment from electromagnetic interference are called EMI shields, since they shield the equipment by either reflecting, absorbing or transmitting the electromagnetic radiation. However, not all materials can be used as EMI shields. The basic material requirement to be used as EMI shields include good magnetic permeability and dielectric properties as well as strong mechanical properties. Currently EMI shields made up of metals or silicones are used in the form of solid enclosures, cables, gaskets, O-rings, films, coatings, fabrics, tapes etc. With time and research new advanced lightweight materials have been developed which have shown potential for use as EMI shields. These include carbonaceous and ferrite nanofillers based polymer nanocomposites. These materials are unique because they provide shielding for a wide range of microwave frequency 2-18 GHz by a judicious choice of conductive, dielectric and magnetic nanofillers. The present review article provides an overview of the research work carried out on toughened epoxy (epoxy modified with other polymers) filled with multifunctional nanoparticles and their characterization for EMI shielding efficiency. Various factors and features have been critically analysed in this article. The entire focus of the article is aimed at Toughened epoxy as a base matrix which can support EMI shielding in the complete frequency range of 2-18 GHz and overcome inherent disadvantages of non-toughened epoxy.

Keywords: Electromagnetic interference, Toughened epoxy, EMI shielding, composites

1. Introduction and Literature Review:

Electromagnetic interference (EMI) shielding assumes paramount significance since EMI is one of the most undesirable by-products of telecommunication devices and high frequency electronics. Any device or technology which deduces, process, reflect and transmit or utilizes electrical energy of any form may emit radiations[1]. The performance and shell life of electronic gadgets is adversely affected due to EMI and is a major concern for defence security equipment [2]. It has been observed that the most prominent radiations of EMI waste stand in the range of microwave and radio waves. Hence, most of the research

work is focussed on developing EMI shields for this frequency range. Electromagnetic interference (EMI) shields are conventionally based on metals, silicones, ceramics and cements. They are used in the form of metallic enclosures, wire mesh and screens, gaskets, O-rings, cable shields and coatings. With time and research, however, the focus has shifted to composite materials which provide a spectrum of EMI shielding properties. These are achieved by adding desired fillers in the base matrix and making a judicious choice of processing

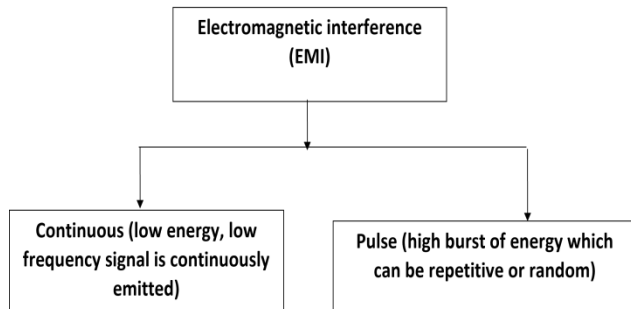


Scheme 1: Mode of electromagnetic Interference (EMI)

techniques. For instance, a composite material formed with polymer as base matrix (continuous phase) and ceramic/ferrites/conducting fillers as discontinuous phase, can be used to absorb a particular range of microwave frequency band. These frequency bands, identified as S (2 GHz to 4 GHz), C (4 GHz to 8 GHz), X (8 GHz to 12 GHz), Ku (12 GHz to 18 GHz), K (18 GHz to 26.5 GHz), and Ka (26.5 GHz to 40 GHz), still pose a challenge. However, same material cannot absorb all the frequency bands. In order to fabricate a material which can absorb all range of microwave frequency, multi layered/ mixed filler composites show a lot of promise. Hence, the main objective of this review is to critically analyse the current research and recent advancements in polymer composites materials which can absorb microwave frequency from 2 GHz to 18 GHz for applications in fields like telecommunication, microwave heating and health care sectors. The aim is to achieve a shielding effectiveness (SE_T) of greater than 60 dB. The subsequent section gives a review of the research work done in this field in the last five years. Electromagnetic interference (EMI) or radio frequency interference (RFI) shielding is a means by which leakage of strong electromagnetic fields is prevented using a shield or barrier, which if not prevented can

interfere with electronic devices and signals. Since electronic devices and circuits deal with small voltage and current, strong electromagnetic fields can either distort their performance or eventually damage them. EMI is basically the coupling of signals from one source to another (receiver) through a path as shown schematically in **scheme 1**. The source is a system that creates disturbance, receiver is the sensitive signal or device whose output signal is distorted by interference and path is the system where signal coupling occurs. EMI is of two types as shown in **scheme 2**. EMIs can also be categorised based on the bandwidth of incident disturbance. A narrowband disturbance has a bandwidth \leq receiver while for a broadband disturbance, bandwidth \geq receiver.

Basic Mechanisms of EMI shielding: An electromagnetic wave consists of oscillating electric (**E**) and magnetic fields (**B** or **H**) which are perpendicular to each other and to



Scheme 2: Types of Electromagnetic interference (EMI)

the direction of propagation of wave. Both the fields travel with the same frequency. When electromagnetic wave travels through a conductive medium, the electric component is blocked. Similarly, if the medium has high magnetic permeability, the magnetic component is blocked. Well known Maxwell's equations of electromagnetic theory are used to find the response of any material to the incident electromagnetic wave [3]. These equations have been derived for free space as well as the medium through which it is passing. Based on the dielectric, magnetic and conductive properties of the medium, these equations are changed. For dielectric or low conductivity materials, their dielectric permittivity (ϵ) and magnetic permeability (μ) are expressed as complex numbers viz. ($\epsilon = \epsilon' - j\epsilon''$) and ($\mu = \mu' - j\mu''$). These parameters govern the interaction of any material with the electric and magnetic field vectors of electromagnetic wave. The real part denotes stored energy while the imaginary part denotes loss or dissipation of energy as heat when em wave is absorbed within the material. The ratio of magnetic permeability and dielectric permittivity, defined as impedance matching ($\sqrt{\mu/\epsilon}$), and reciprocal of their product [$1/\sqrt{\mu\epsilon}$] which gives the velocity of em wave, eventually determine how the em wave will propagate in that medium. In free space, this impedance is equal to 377 ohms and velocity = 3×10^8 cm/s using the universal constants μ_0 and ϵ_0 for free space. An impedance mismatching occurs at the interface of media with different impedances and the wave is reflected. If the impedance mismatch is higher more reflection takes place at the interface[4].

From these equations it is imperative that when any base polymer matrix is dispersed with dielectric, conductive or magnetic fillers of nanosize, its interactions significantly change. EMI shielding mechanism is largely based on this concept wherein either of the electric or magnetic component is filtered out by shields using reflection, absorption (due to multiple internal reflection) or transmission mechanisms. In the reflection mode, the electric field vector is attenuated since the mobile charge carriers of shield interact with incoming EM wave and are redistributed along the conductor which eventually creates an opposing electromagnetic field. The two opposing EM fields cancel out each other. The higher the conductivity, the better is the shielding efficiency. However, for high frequency electromagnetic wave (low wavelength) there is a limitation due to the size of the holes of shielding enclosure and skin effect which lowers the conductivity in the inner section as charges accumulate on the top surface of the conductor. In such a case either the surface area of conductor can be increased, or the surface is coated with highly conductive material. Contrary to reflection, absorption of EMI acts on the magnetic field vector of electromagnetic wave. Due to the external magnetic field of incident electromagnetic wave, the magnetic lines of force travelling through the material are intercepted and eventually absorbed. Thus, a shield material absorbs the magnetic and electric lines of force by creating a path within itself. However, in such a material conductivity is very low which do not provide protection from electric component of incident electromagnetic wave. Secondly, the oscillating em wave at higher frequencies generate eddy currents which possess their own magnetic field opposite to the external magnetic field. Thus, if a material is chosen whose electrical conductivity is high it creates stronger eddy currents. Absorption due to multiple reflections occurs by either scattering of electromagnetic waves or having multiple reflection boundaries. Thus, the desired properties of EMI shielding material are (i) electrical conductivity and (ii) magnetic permeability. Metals are the preferred choice

because they have higher electric conductivity, magnetic permeability, strength and ductility. However, they are expensive. Carbon steel alloys, mild carbon steel and ferrite stainless steel and Fe-Ni alloys such as Mu-metal are used for EMI shielding because they have high relative permeability of 10^4 at 1 kHz. Carbon allotropes such as exfoliated graphite, graphene, carbon fibres and carbon nanotubes are used as fillers in composites that can be used for EMI shield. All the fillers can be dispersed in a polymer matrix, metal, ceramic or cement. They have high conductivity; high aspect ratio and high porosity and they can operate through multiple reflection mechanism. For high frequency shielding applications, graphene and CNTs are mostly used because the dimension of the materials is less than the skin depth., which makes them better conductors than metals in GHz region. Conducting polymers (PANI, Polypyrrole etc) conduct electricity between atoms due to the conjugated bonds. This enables the delocalization of π -electrons which act as mobile charges. However, their use is still being explored. Silicone embedded with Nickel or graphite is effective at shielding radio frequency between 20 Hz and 10^4 Hz without any metal component. Foil and fabric (nylon, polyester interwoven with metals also provide protection as EMI shields.

Common materials used for EMI shielding:

Metal based advanced materials have always been the choice for EMI absorption. However, polymer based materials have shown lot of promise to replace metals for EMI shielding applications. Largely two types of polymer based EMI shielding materials have been identified 1) Intrinsic and 2) compound type. Intrinsic polymers have poor mechanical and processing aspect which limit their utilization in EMI absorption. While compound type material provides ease of modification, designing and fabrication as per desired range of EMI absorption. Polymer-based composites are being designed so as to achieve high dielectric constants, good electric conductivity and magnetic permeability which are required for low EMI permeation. Many polymers are

used today for their property of absorbing radiations including polyurethane, epoxy, polyaniline etc. Both biodegradable and non-biodegradable polymers have been explored for such application.

Material requirement for EMI shielding:

Different criteria have been used to synthesize materials for EMI shielding applications. These include versatile surface chemistry, high aspect ratios, addition of electromagnetically charged particles, excellent mechanical and electrical properties, conductivity, reflection losses and multiple internal reflections which play a key role in EMI shielding. In general, two regions of EMI shielding are identified. If the distance between the radiations source and the shield is $> \lambda/2\pi$, it is known as far field shielding region while it is known as near field shielding region if the distance is $< \lambda/2\pi$ [1].EMI plane wave theory is applied in the far field shielding region while theory based on contribution of electric and magnetic dipoles is applied for near emi shielding[2].The two major pre-requisites for EMI absorption are dielectric and magnetic losses. Secondly, impedance matching (i.e. matching of complex permittivity and permeability), interfacial polarization, attenuation capability and multiple reflection are equally desirable. The ratio of E to H is called wave impedance and for free space intrinsic impedance is equal to 377 ohms. In order to design materials possessing these properties, multifunctional polymer nanocomposites (PNCs) filled with ferrite and carbonaceous nanofillers have been developed and characterized for their ferromagnetic resonance and hysteresis loss, reflection loss (RL), shielding effectiveness (SE) and absorption bandwidth. It has been observed that single layer absorbers have their own limitation such as narrow absorption bandwidth. Hence double-layer absorbers have been suggested for achieving a wider bandwidth.

In effective absorbing material, firstly the intrinsic impedance value of the material is made to approach impedance of the free space in a matching layer and, $E_A = KV \sin^2\theta$

secondly, the incident EM wave is attenuated rapidly in the second absorbing layer [5]. These layers are made up of material having better dielectric and magnetic permeability and their functions can be interchanged [6]. In absorbing layer maximum absorption can occur when normalised impedance (Z_0) and input impedance is equal to one. In such an ideal situation, EM wave can penetrate and get absorbed completely within the material [7,8]. In real situation, attempts are being made to achieve over 90% absorption by making input impedance almost equal to normalised impedance. A term Reflection loss (RL) can indicate absorbing capacity of the shield material and is evaluated as [9],

$$RL(dB) = 20 \log \left| \frac{z_{in}-z_0}{z_{in}+z_0} \right| \text{ (for single layer microwave absorber) } \dots\dots (1)$$

where z_{in} and z_0 are the input impedance and vacuum impedance respectively,

$$z_{in} = z_0 \sqrt{\frac{\mu_r}{\epsilon_r}} \tanh \left[j \frac{2\pi f t}{c} \sqrt{\mu_r \epsilon_r} \right] \dots\dots(2)$$

(t = thickness of specimen, f = frequency of the incident EM wave, c = EM wave velocity in vacuum). For double layer

$$Z_{in} = \frac{\sqrt{\frac{\mu_2}{\epsilon_2} \left(\sqrt{\frac{\mu_1}{\epsilon_1}} \tanh \left[j \left(\frac{2\pi f d_1}{c} \right) \sqrt{\mu_1 \epsilon_1} \right] + \sqrt{\frac{\mu_2}{\epsilon_2}} \tanh \left[j \left(\frac{2\pi f d_2}{c} \right) \sqrt{\mu_2 \epsilon_2} \right] \right)}{\sqrt{\frac{\mu_2}{\epsilon_2} + \sqrt{\frac{\mu_1}{\epsilon_1}} \tanh \left[j \left(\frac{2\pi f d_1}{c} \right) \sqrt{\mu_1 \epsilon_1} \right] \tanh \left[j \left(\frac{2\pi f d_2}{c} \right) \sqrt{\mu_2 \epsilon_2} \right]} \dots(3)$$

Absorption of EM wave can be quantified in terms of percentage as:

$$\text{Absorption (\%)} = 100 - \left[10^{(RL/10)} \times 100 \right]$$

Ferromagnetic properties namely coercive field (H_c), saturation (M_s) and remanent magnetization obtained using B-H hysteresis loop can be used to find anisotropy constant (K) and energy (E_A) as

(for a single domain nanocrystalline material)(4)

where K, V and θ are the anisotropy constant, volume of nanocrystal and orientation of applied field induced magnetization with respect to easy axis, respectively

$$K = \frac{\mu_0 M_s H_c}{2} \dots\dots(5)$$

where $\mu_0 = 4\pi \times 10^{-7}$ H/m is the permeability in vacuum. The dissipation or tangent loss is obtained using following equations,

$$\mu^* = \mu' - j\mu'' \text{ and } \epsilon^* = \epsilon' - j\epsilon'' \dots(6a,b)$$

$$\tan \delta_e = \epsilon'' / \epsilon' \text{ (dielectric loss tangent)} \dots(7)$$

$$\tan \delta_m = \mu'' / \mu' \text{ (magnetic loss tangent)} \dots(8)$$

$$\tan \delta = \tan \delta_e + \tan \delta_m \text{ (total loss tangent)} \dots(9)$$

The complex permeability (μ^*) and permittivity (ϵ^*) values of the samples can be calculated from the reflected (S_{11}) and transmitted (S_{21}) signals measured using a waveguide technique [10]. Using these shielding parameters, shielding effectiveness can be measured as,

$$SE_{\text{Total}} = SE_A + SE_R + SE_M \dots(10)$$

which is the sum of absorption (SE_A), Reflection (SE_R), and multiple reflections (SE_M) and is obtained using following equations discussed below.

$$SE_{\text{Total}} = 10 \log(P_i/P_t) = 20 \log(E_i/E_t) = 20 \log(H_i/H_t) \dots\dots(11)$$

$$SE_R = -10 \log_{10}(1 - S_{11}^2) = 10 \log_{10}(1 - R) \dots(12)$$

where $R = S_{11}^2$

$$SE_A = -10 \log_{10}(S_{21}^2 / (1 - S_{11}^2)) = 10 \log_{10}(T / (1 - R))$$

where $T = S_{21}^2$ (13)

where subscript i and t represent properties of incident and transmitted waves, respectively. S_{11} and S_{21} denote the scattering parameters of the forward reflection (R) and

backward transmission coefficients (T) respectively. The multiple reflection scattering parameter SE_M is calculated as

$$SE_M = 20 \log_{10}(1 - e^{-2t/\delta}) = 20 \log_{10}(1 - 10^{SE_A/10}) \quad \dots(14)$$

where t is the thickness of shielding material, δ is the skin depth. However, SE_M can be neglected for $SE_A > 10$ dB as amplitude of EM wave dies down with thickness. The attenuation constant (α) is related to the skin depth (δ) as $\alpha = \frac{1}{\delta}$ and $\delta = 1/\sqrt{(\pi f \mu \sigma)}$ where μ is the permeability and σ is the conductivity of the shield material. It is obtained using following relation,

$$\alpha = \frac{\sqrt{2\pi}f}{c} \left\{ \mu'' \varepsilon'' - \mu' \varepsilon' + [(\mu''^2 + \mu'^2)(\varepsilon''^2 + \varepsilon'^2)]^{1/2} \right\} \quad \dots(15)$$

Common methods by which shielding effectiveness is calculated/measured include (i) measurement through a waveguide and (2) through antenna and receiver. A free and enclosed environment is required to attenuate the external noise interference.

Toughened epoxy based nanocomposites:

Epoxy resin is a versatile thermoset polymer having numerous industrial applications. However, its intrinsic brittleness limits its engineering applications. To mitigate this disadvantage and increase its range of application, it is toughened using elastomers such as rubber with no compromise of its original properties. The, so called, rubber toughened epoxy resins when filled with nanofillers show further improvement in elastic properties as well as glass transition temperature T_g of base matrix [11,12]. The toughening may be attributed to shearing, debonding and cavitation of epoxy-rubber molecular chains [13]. For developing rubber toughened epoxy-based nanocomposites, generally butadiene-acrylonitrile based rubbers such as CTBN, ETBN, ATBN and VTBN have been used. The mechanism for the formation of carboxyl terminated butadiene acrylonitrile copolymer and triphenylphosphine toughened epoxy resin can be found elsewhere [14, 15]. In a research paper

published almost a decade back, it was reported that for C8 ether linked bismaleimide toughened epoxy filled with carbon black, a higher electrical conductivity and impact strength can be achieved with just 5 wt% of CB [16]. This was attributed to the covalent bonds between CB and C8 e-BMI/epoxy matrix. Ten years later, the same group reported on tuning the characteristics related to microwave absorption capability of rGO filled toughened epoxy composites via SiC- induced phase separation [17]. Using vector network analyzer (VNA) measurements it was observed that simple RGO-based composites show poor reflection loss (RL) characteristics. However, with SiC loading the same material gains excellent absorption with RL of -46.5 dB (effective absorption bandwidth of over 2 GHz) for a thickness upto 10 nm. Earlier the same authors had reported RL -51.6 dB (99.999% microwave absorption) at 9.51 GHz and an effective absorption bandwidth of 2.48 GHz for m-caproamine/imidazole toughened epoxy composites with 3 wt% r-GO composites compared to unfilled m-CA/ER composite [18]. Toughening of epoxy using rubber and filled with multifunctional nanoparticles has also been reported extensively in the literature. For instance, the treatment of epoxy with 10% recycled rubber increased its toughness that was confirmed through scanning electron microscopy and nanoindentation, static (3PB). Addition of Nano-magnetic iron oxide, Fe_3O_4 , Nickel and aluminium particles enhanced the magnetic permeability and dielectric properties of the resultant composites [19]. However, the material has not been characterized for their microwave absorption properties. An exhaustive literature on this topic can be found in a review published in 2020 [20]. Recently, EMI shielding properties of thermosetting epoxy foams modified with rubber (CTBN) and functionalised MWCNTs using supercritical carbon dioxide were reported [21]. It was observed that the alignment of oriented fMWCNTs (5 wt%) in foams may have caused an increase in electrical conductivity (0.43 S/m), EMI SE (22.90 dB) and specific EMI SE (37.54 dB/(g·cm³)) with better EMI shielding

performance rendered possible due to multiple reflections of microwaves and their eventual attenuation by conductive filler [20]. Wang et al. [22] has toughened one epoxy system using CTBN and filled it with MWCNT-COOH claiming that accelerated curing occurred because of bonding developed between COOH-functionalised MWCNT and epoxy resin. The same composite was made electrically conductive with the addition of CNT [23] having enhanced fracture toughness and thermal stability [24]. Jyotish kumar et al. [25] toughened DGEBA epoxy with ABS and MWCNT and reported enhanced stability of the material. It has been reported that nanocomposites based on toughened epoxy using carboxy-terminated butadiene acrylonitrile copolymer and filled with 5 wt% functionalised MWCNT can produce an EMI shielding effectiveness (22.90–37.94 dB) since EM waves are absorbed due to multiple reflection [26]. With 1 wt% graphene nanofiller, rubber toughened epoxy also produces an EMI shielding effectiveness in the same range (22–48 dB) [27].

Numerous studies are available in the literature wherein new polymer materials have been explored for microwave absorption of different ranges of frequency. However, other polymer systems are beyond the scope of this review. Recent studies for these polymer systems can be found in ref [28–30]. In one instance, Saini et al. [31] produced a nanocomposite based on polyaniline and MWCNT for microwave absorption in the range of 12.4 – 18 GHz. Dielectric characteristics and microwave absorption of graphene composite materials have been studied by Kevin et al [32] and reported the microwave absorption in different ranges of frequency. Sun et al. [33] developed a $\text{Fe}_3\text{O}_4/\text{CNFs}$ material synthesized by chemical co-precipitation and investigated its microwave absorption properties. Hong-Wen [34] studied the microwave absorption of materials over 9 GHz and reported the reflection loss more than -25 dB for specific frequencies. Microwave absorption properties of highly filled polymer composites with amorphous Fe-B Particles was studied by Kiyotaka et al. [35]. Yichao et al. [36] prepared

anisotropic Fe_3O_4 nanoparticle and a series of $\text{Fe}_3\text{O}_4/\text{RGO}$ nanocomposites and found that the materials exhibit high-performance microwave absorption properties over 2.0–18.0 GHz. The optimal reflection loss of the pure Fe_3O_4 composite was reported as – 38.1 dB at 14.8 GHz while it reaches to – 65.1 dB at 15.2 GHz with 3 wt.% of RGO of same thickness. Microwave absorption of ferrite-rubber composite at X-band frequencies has been reported by Kim et al [37]. Microwave absorption properties of honeycomb core structures coated with composite absorber was studied by Wang et al. [38] have reported the reflection loss in the range of 12 GHz to 18 GHz.. Young et al [39] have reported the microwave absorber properties of magnetic and dielectric composite materials in the range of 5.8 GHz. These studies show that work is still needed to develop such novel materials which are light weight, flexible and economical and that can be used to absorb microwave of frequency of all ranges from 2 GHz to 18 GHz. A comparison of the EMI shielding performance of Toughened epoxy based composites and Epoxy based composites is given in Table 1.

Table 1: A comparison of the EMI shielding performance of Toughened epoxy based composites and Epoxy based composites

Toughened Epoxy based composites		
rGO filled toughened epoxy composites with SiC loading	RL -46.5dB (effective absorption bandwidth of over 2GHz) for a thickness upto 10 nm.	[17]
mcaproamine/imidazole toughened epoxy composites with 3 wt%	RL -51.6 dB (99.999% microwave absorption) at 9.51 GHz and an effective absorption bandwidth of 2.48 GHz	[18]
Epoxy foams modified with rubber (CTBN) and functionalised MWCNTs using supercritical carbon dioxide	EMI SE (22.90 dB) and specific EMI SE (37.54 dB/(g·cm ³))	[20]
Toughened epoxy using carboxy-terminated butadieneacrylonitrile copolymer and filled with 5 wt% functionalised MWCNT	EMI SE (22.90–37.94 dB)	[26]
1 wt% graphene filled rubber toughened epoxy	EMI SE in the range (22–48 dB)	[27]
Epoxy based composites		
LSCO/epoxy	31.3 (8.2 GHz)	[40]
AlCoCrFeNi /epoxy	20 (26-40 GHz)	[41]
Ni coated Carbon Fibre mat/3D PLA mesh sandwiched/epoxy	45 (18 GHz)	[42]
PANI doped with PTSE/Fe-Ni coated epoxy	80 (8.2-12.4 GHz)	[43]
	40 (12.4 – 18 GHz)	
CB/MWCNT/Silver nanoflakes/silver nanoplates/GF/epoxy	43 (8.2-12.4 GHz)	[44]
Conductive CB/Glass fibre/ epoxy	20 (8.2-12.4 GHz)	[45]
Fe ₂ O ₃ /CFmat/epoxy	20 (8.2-12.4 GHz)	[46]
rGO/Fe ₂ O ₃ /CFmat/epoxy	51 (8-26.5 GHz)	[47]
Activated UD CF mat/epoxy	39 (1-1.5 GHz)	[48]
CF mat/epoxy	60 (8-12 GHz)	[49]
Graphene/epoxy foam	30 (10-20 GHz)	[50]
rGO/carbonyl iron/epoxy	36 (9.5 – 12 GHz)	[51]
MWCNT/epoxy sponge	33.9 (8.2-12.4 GHz)	[52]
MWCNT/foamed epoxy	21.3 (12-18 GHz)	[53]
MWCNT/Glass fibre/epoxy	18 (0.03 – 1 GHz)	[54]
MWCNT/MnZn Ferrite/epoxy	44 (10 GHz)	[55]
SWCNT/epoxy	49.2 (0.01-1.5 GHz)	[56]
SWCNT/epoxy	23-28 (8.2-12.4 GHz)	[57]
Electrified SWCNT/epoxy	12.8 ((8.2-12.4 GHz)	[58]
CNT/CB/exfoliated graphite/Epoxy	12 (26-27 GHz)	[59]
Plasticized CB/epoxy	SE _T 44 (1-11 GHz)	[60]

Concluding remarks: Nanocomposites based on rubber toughened epoxy and filled with carbonaceous nanofillers show enhanced mechanical, thermal, electrical and morphological characteristics due to synergistic effect of matrix and fillers. While nanofillers improve conducting and magnetic

properties, toughened epoxy matrix provides high strength, ductility, and fracture toughness. This synergistic effect results in better EMI shielding effectiveness. However, the current research advocates the use of rubber toughened epoxy foams filled with nanofillers for still better EMI shielding effectiveness. For

instance, EMI SE of 22.90 dB and specific EMI SE of 37.54 dB/(g·cm³) has been obtained in the epoxy composite foam with 5.0 wt% conductive filler loading which not only increased electrical conductivity but also rendered attenuation of em waves due to multiple reflections. These preliminary results appear to be promising and sets a direction for future research on Toughened epoxy based composites for EMI shielding [61].

Acknowledgement: Authors wish to acknowledge the financial grant sanctioned by DRDO India for carrying out this work.

Conflict of Interest: Authors declare No conflicts of interest

References:

- [1] I. Nam, H.-K. Lee, and J. Jang, Electromagnetic interference shielding/absorbing characteristics of CNT-embedded epoxy composites, *Compos. Part A Appl. Sci. Manuf.* 42 (9), (2011) 1110.
- [2] Banerjee, P., Bhattacharjee, Y. & Bose, S. Lightweight Epoxy-Based Composites for EMI Shielding Applications, *J. Electron. Mater.* 49, (2020). 1702–1720 <https://doi.org/10.1007/s11664-019-07687-5>
- [3] David J Griffiths, *Introduction to Electrodynamics*, Pearson, Cambridge University (1981) ISBN: 978-1108420419
- [4] J.D. Jackson, *Classical Electrodynamics*, Wiley, (1962), ISBN: 0-471-30932-X
- [5] Vineeta Shukla, Review of electromagnetic interference shielding materials fabricated by iron ingredients *Nanoscale Adv.*, 1, (2019), 1640.
- [6] J. Wang, J. Wang, B. Zhang, Y. Sun, W. Chen and T. Wang, Combined use of lightweight magnetic Fe₃O₄-coated hollow glass spheres and electrically conductive reduced graphene oxide in an epoxy matrix for microwave absorption, *J. Magnetism and Magnetic Mater.*, 401 (2016), 209–216
- [7] R. Che, C. Zhi, C. Liang and X. Zhou, Fabrication and microwave absorption of carbon nanotubes/CoFe₂O₄ spinel nanocomposite, *Appl. Phys. Lett.*, 88 (2006), 033105.
- [8] P. R. Agarwal, R. Kumar, S. Kumari and S. R. Dhakate, Three-dimensional and highly ordered porous carbon–MnO₂ composite foam for excellent electromagnetic interference shielding efficiency, *RSC Adv.*, 6 (103), (2016) 100713–100722.
- [9] Rusly, S.N.A., Matori, K.A., Ismail, I. et al. Microwave absorption properties of single- and double-layer coatings based on strontium hexaferrite and graphite nanocomposite *J Mater Sci: Mater Electron* 29, (2018) 14031–14045 <https://doi.org/10.1007/s10854-018-9535-9>
- [10] Ibrahim, I.R., Matori, K.A., Ismail, I. A Study on Microwave Absorption Properties of Carbon Black and Ni_{0.6}Zn_{0.4}Fe₂O₄ Nanocomposites by Tuning the Matching-Absorbing Layer Structures. *Scientific Reports* 10, (2020) 3135 <https://doi.org/10.1038/s41598-020-60107-1>
- [11] Yan, L.; Zhang, B.; Wang, Y.; Zhou, C.; Li, R.; Luo, W.; Chen, Y.; Zou, H.; Liang, M. The Improvement of Thermal Stability and Adhesion of Silicone Rubber Composites Modified by Phenolic Epoxy Resin *J. Macromol. Sci. A.* 56, (2019), 506–512. DOI: 10.1080/10601325.2019.1584858.
- [12] Wang, Y.; Chen, Z.; Yu, F. Preparation of Epoxy-Acrylic Latex Based on Bisphenol F Epoxy Resin. *J. Macromol. Sci. A.* 55, (2018), 205–212. DOI: 10.1080/10601325.2017.1410065
- [13] Thomas, S., Sinturel, C., Thomas, R. Eds., *Micro- and Nanostructured Epoxy/Rubber Blends*; Wiley-VCH: Hoboken, 2014.
- [14] Bajpai, A.; Wetzel, B.; Klingler, A.; Friedrich, K *Mechanical Properties and*

- Fracture Behavior of High-Performance Epoxy Nanocomposites Modified with Block Polymer and Core-Shell Rubber Particles. *J. Appl. Polym. Sci.* 137,(2020) 48471. DOI: 10.1002/app.48471.
- [15] Ramos, V. D.; Da Costa, H. M.; Soares, V. L.; Nascimento, R. S. Modification of Epoxy Resin: A Comparison of Different Types of Elastomer. *Polym. Test.* 24, (2005) 387–394. DOI: 10.1016/j.polymertesting.2004.09.010.]
- [16] M. Mandhakini, A. Chandramohan, K. Jayanthi, M. Alagar, Carbon black reinforced C8 ether linked bismaleimide toughened electrically conducting epoxy nanocomposites *Materials & Design*, 64, (2014), 706-713 (<https://doi.org/10.1016/j.matdes.2014.07.041>)
- [17] J.S. Santhosh Jeferson, S. et al..Tuning the microwave absorption characteristics of r-GO toughened epoxy composites via SiC-induced phase separation *Diamonds And Related Materials.* 132, 109625 (2023),<https://doi.org/10.1016/j.diamond.2022.109625>.
- [18] J.S. Santhosh Jeferson Stanley, Logesh Govind, Ariraman Mathivathanan, Bashaiah Sindam, James Raju K.C., Mandhakini Mohandas, Impact of reduced graphene oxide on microstructure evolution in m-caproamine/imidazole toughened epoxy composites – Synergia of viscoelastic and microwave absorption properties, *Synthetic Metals*,286, (2022), <https://doi.org/10.1016/j.synthmet.2022.117035>.
- [19] A.B. Irez, E. Bayraktar, I. Miskioglu, Recycled and devulcanized rubber modified epoxy-based composites reinforced with nano-magnetic iron oxide, *Fe₃O₄Composites Part B: Engineering*, Volume 148, (2018), 1-13, <https://doi.org/10.1016/j.compositesb.2018.04.047>.
- [20] Ayesha Kausar, Rubber toughened epoxy-based nanocomposite: a promising pathway toward advanced materials *Journal of Macromolecular Science, Part A*, (2020), DOI: 10.1080/10601325.2020.1730190
- [21] Xun Fan, Guangcheng Zhang, Jiantong Li, Zhengyang Shang, Hongming Zhang, Qiang Gao, Jianbin Qin, Xuetao Shi, Shi, Study on foamability and electromagnetic interference shielding effectiveness of supercritical CO₂ foaming epoxy/rubber/MWCNTs composite *Composites Part A* 121 (2019) 64–73
- [22] Wang, Y. T.; Wang, C. S.; Yin, H. Y.; Wang, L. L.; Xie, H. F.; Cheng, R. S. Carboxyl-Terminated Butadiene-Acrylonitrile Toughened Epoxy/Carboxyl-Modified Carbon Nanotube Nanocomposites: Thermal and Mechanical Properties *Exp. Polym. Lett.* 6 (2012)719–728. DOI: 10.3144/expresspolymlett.2012.77.
- [23] Salinas-Ruiz, M. D. M.; Skordos, A. A.; Partridge, I. K., Rubber-Toughened Epoxy Loaded with Carbon Nanotubes: Structure–Property Relationships. *J. Mater. Sci.* 45, (2010), 2633–2639.
- [24] Zewde, B.; Pitliya, P.; Karim, A.; Raghavan, D. Synergistic Effect of Functionalized Carbon Nanotubes and Micron-Sized Rubber Particles on the Mechanical Properties of Epoxy Resin. *Macromol. Mater. Eng.* 301 (2016),542–548.
- [25] Jyotishkumar, P.; Abraham, E.; George, S. M.; Elias, E.; Pionteck, J.; Moldenaers, P.; Thomas, S. Preparation, Properties of MWCNTs/Poly(Acrylonitrile-Styrene-Butadiene)/ Epoxy Hybrid Composites, *J. Appl. Polym. Sci.* 127 (2013), 3093–3103. DOI: 10.1002/app.37677.
- [26] Fan, X.; Zhang, G.; Li, J.; Shang, Z.; Zhang, H.; Gao, Q.; Qin, J.; Shi, X. Study on Foamability and Electromagnetic Interference Shielding Effectiveness of Supercritical CO₂ Foaming Epoxy/Rubber/MWCNTs Composite

- Compos. A: Appl. Sci. Manuf.121, (2019), 64–73. DOI: 10.1016/j.compositesa.2019.03.008.
- [27] Al-Ghamdi, A. A.; Al-Ghamdi, A. A.; Al-Turki, Y.; Yakuphanoglu, F.; El-Tantawy, F. Electromagnetic Shielding Properties of Graphene/Acrylonitrile Butadiene Rubber Nanocomposites for Portable and Flexible Electronic Devices Compos. B: Eng. 88 (2016), 212–219. DOI: 10.1016/j.compositesb.2015.11.010.
- [28] BedriyeUcpinarDurmaz, Alp Oral Salman, and Ayse Aytac.,Electromagnetic Interference Shielding Performances of CarbonFiber-Reinforced PA11/PLA Composites in the X Band Frequency Range, ACS Omega 8 (25) (2023), 22762-22773DOI: 10.1021/acsomega.3c01656
- [29] LekshmiOmana, Anoop Chandran, Reenu Elizabeth John, Runcy Wilson, Kalapurackal Cherian George, Nellippambil Viswambharan Unnikrishnan, Steffy Sara Varghese, Gejo George, Sanu Mathew Simon, and Issac Paul, Recent Advances in Polymer Nanocomposites for Electromagnetic Interference Shielding: A Review, ACS Omega 7 (30) (2022) 25921-25947 DOI: 10.1021/acsomega.2c02504
- [30] Junye Cheng et.al, Recent Advances in Design Strategies and Multifunctionality of Flexible Electromagnetic Interference Shielding Materials, Nano-Micro Lett. (2022) 14:80
- [31] Saini P; Arora M; Gupta G; Gupta B. K; Singh V. N; Choudhary V.. High permittivity polyaniline–barium titanate nanocomposites with excellent electromagnetic interference shielding response, Nanoscale. 5(10) (2013), 4330-4336
- [32] Rubrice K; Castel X; Himdi M; Parneix P. Dielectric Characteristics and Microwave Absorption of Graphene Composite Materials, Materials 2016, 9, 825; doi:10.3390/ma9100825
- [33] Dexiang Li; Xiaoweizhou; Keren Luo; Bo Yuan; Yongjun Liu; Li Sun; Zhu Liu. Investigation on the Microwave Absorbing Property of Fe₃O₄/CNFs Synthesized by Chemical Co-precipitation, Int. J. Electrochem. Sci., 10 (2015) 8097 – 8102
- [34] Sun Wanshuo; Li Hong; Liu Ying; Zhao Xiuchen; Cheng Jingwei; Wen Shulai, Preparation and Microwave Absorption Properties of Spherical Cobalt Particles, RareMetal Materials and Engineering, 45 (12), 2016, 3099-3103
- [35] KiyotakaFuruta; Kazuaki Shimba; Nobuki Tezuka; Satoshi Sugimoto, Microwave Absorption Properties of Highly Filled Polymer Composites with Amorphous Fe–B Particles, Materials Transactions, 53(9) (2012) 1665 -1668
- [36] Yichao Yin; Min Zeng; JueLiu; ukui Tang; Hangrong Dong; Ruozhou Xia; Ronghai Yu, Enhanced high-frequency absorption of anisotropic Fe₃O₄/graphene nanocomposites, Scientific Reports, 6, 25075 (2016). <https://doi.org/10.1038/srep25075>
- [37] Kim S-Y, Kim S-S. Design of Radar Absorbing Structures Utilizing Carbon-Based Polymer Composites. Polymers and Polymer Composites. 2018;26(1):105-110. doi:10.1177/096739111802600113
- [38] Yanfei He; Rongzhou Gong; Heng Cao; Xian Wang; Yi Zheng, Preparation and microwave absorption properties of metal magnetic micropowder-coated honeycomb sandwich structures, Smart Materials and Structurst, 16 (2007) 1501, DOI 10.1088/0964-1726/16/5/001
- [39] Young Joon An; Ken Nishida; Takashi Yamamoto; Shunkichi Ueda; Takeshi, Microwave absorber properties of magnetic and dielectric composite materials, Electronics and communication in japan, 93 (4) (2010) 18-26

- [40] K.S. Dijith, S. Pillai, and K.P. Surendran, Screen printed silver patterns on $\text{La}_{0.5}\text{Sr}_{0.5}\text{CoO}_{3-\delta}$ - Epoxy composite as a strategy for many-fold increase in EMI shielding, *Surf. Coat. Technol.* 330, (2017) 34-41
- [41] Y. Zhang, Y. Huang, T. Zhang, H. Chang, P. Xiao, and H. Chen, Broadband and Tunable High-Performance Microwave Absorption of an Ultralight and Highly Compressible Graphene Foam, *Adv. Mater.* 27, (2015) 2049.
- [42] S. Mishra, P. Katti, S. Kumar, and S. Bose, Macroporous epoxy-carbon fiber structures with a sacrificial 3D printed polymeric mesh suppresses electromagnetic radiation, Saswat Mishra, Prajakta Katti, S Kumar, Suryasarathi Bose, *Chem. Eng. J.* 357, (2019) 384
- [43] N.E. Kamchi, B. Belaabed, J.L. Wojkiewicz, S. Lamouri, and T. Lasri, Hybrid polyaniline/nanomagnetic particles composites: High performance materials for EMI shielding, *J. Appl. Polym. Sci.* 127, (2013), 4426-4432
- [44] W.-K. Jung, B. Kim, M.-S. Won and S.-H. Ahn, Fabrication of Radar Absorbing Structure (RAS) Using GFR-nano Composite and Spring-back Compensation of Hybrid Composite RAS Shells, *Compos. structures.*, 75 (1-4) (2006) 571-576
- [45] Oh J. H; Oh K. S; Kim C. G; Hong C. S. Design of radar absorbing structures using glass/epoxy composite containing carbon black in X-band frequency ranges *Composites B* 35 (2004) 49-56.
- [46] M. Gholampoor, F. Movassagh-Alanagh, and H. Salimkhani, Fabrication of nano- Fe_3O_4 3D structure on carbon fibers as a microwave absorber and EMI shielding composite by modified EPD method, *Solid State Sci.* 64, (2017) 51-61.
- [47] J. Wu, Z. Ye, H. Ge, J. Chen, W. Liu, and Z. Liu, Modified carbon fiber/magnetic graphene/epoxy composites with synergistic effect for electromagnetic interference shielding over broad frequency band, *J. Colloid Interface Sci.* 506, (2017) 217-226.
- [48] J. Wu and D. Chung, Increasing the Electromagnetic Interference Shielding Effectiveness of Carbon Fiber Polymer-Matrix Composite by Using Activated Carbon Fibers, *Carbon* 40, (2002) 445-447
- [49] Y. Ramadin, S. Jawad, S. Musameh, M. Ahmad, A. Zihlif, and A. Paesano, Electrical and electromagnetic shielding behavior of laminated epoxy-carbon fiber composite, *Polym. Int.* 34, (1994) 145
- [50] Y.-J. Wan, S.-H. Yu, W.-H. Yang, P.-L. Zhu, R. Sun, and C.-P. Wong, Tuneable cellular-structured 3D graphene aerogel and its effect on electromagnetic interference shielding performance and mechanical properties of epoxy composites, *RSC Adv.* 6, (2016) 56589.
- [51] Y. Chen, H.-B. Zhang, Y. Huang, Y. Jiang, W.-G. Zheng, and Z.-Z. Yu, Magnetic and electrically conductive epoxy/graphene/carbonyl iron nanocomposites for efficient electromagnetic interference shielding, *Compos. Sci. Technol.* 118, (2015) 178
- [52] Y. Chen, H.B. Zhang, Y. Yang, M. Wang, A. Cao, and Z.Z. Yu, High-Performance Epoxy Nanocomposites Reinforced with Three-Dimensional Carbon Nanotube Sponge for Electromagnetic Interference Shielding, *Adv. Funct. Mater.* 26 (3), (2016) 447-455
- [53] J. Li, G. Zhang, Z. Ma, X. Fan, X. Fan, and J. Qin, Morphologies and electromagnetic interference shielding performances of microcellular epoxy/multi-wall carbon nanotube nanocomposite foams, *Compos. Sci. Technol.* 129, (2016) 70-78

- [54] K.-Y. Park, S.-E. Lee, C.-G. Kim, and J.-H. Han, Application of MWNT-added glass fabric/epoxy composites to electromagnetic wave shielding enclosures, *Compos. Struct.* 81 (3), (2007). 401-406
- [55] C. Phan, M. Mariatti, and Y. Koh, J. Magn. Mater. Electromagnetic interference shielding performance of epoxy composites filled with multiwalled carbon nanotubes/manganese zinc ferrite hybrid fillers, *Journal of Magnetism and Magnetic Materials*, 401, (2016) 472-478
- [56] N. Li, Y. Huang, F. Du, X. He, X. Lin, and H. Gao, Electromagnetic interference (EMI) shielding of single-walled carbon nanotube epoxy composites, *Nano Lett.* 6, (2006) 1141-1145.
- [57] Y. Huang, N. Li, Y. Ma, F. Du, F. Li, and X. He, The influence of single-walled carbon nanotube structure on the electromagnetic interference shielding efficiency of its epoxy composites, *Carbon* 45, (2007) 1614-1621.
- [58] S.A. Hashemi, S.M. Mousavi, M. Arjmand, N. Yan, and U. Sundararaj, Electrified single-walled carbon nanotube/epoxy nanocomposite via vacuum shock technique: Effect of alignment on electrical conductivity and electromagnetic interference shielding, *Polym. Compos.* 39, (2018) E1139-1148
- [59] P.Kuzhir, A. Paddubskaya, A. Plyushch, N. Volynets, S. Maksimenko, and J. Macutkevici, Epoxy composites filled with high surface area-carbon fillers: Optimization of electromagnetic shielding, electrical, mechanical, and thermal properties, *J. Appl. Phys.* 114, (2013) 164304
- [60] N.A. Aal, F. El-Tantawy, A. Al-Hajry, and M. Bououdina, New antistatic charge and electromagnetic shielding effectiveness from conductive epoxy resin/plasticized carbon black composites, *Polym. Compos.* 29, (2008) 125-132.
- [61] R.M. Neves, H.L. Ornaghi Jr, A.J. Zattera, S.C. Amico, Toughening epoxy resin with liquid rubber and its hybrid composites: A systematic review, *J Polymer Research*, 29 (2022), 340

CNS&E

Current Natural
Sciences &
Engineering

www.cnsejournals.org

e-ISSN
3048-460X

**Retains India's
Intellectual Property**

**Globally
Visible**

**Peer
Reviewed**



**A Comprehensive
Interdisciplinary
Partially Open
Access
Journal**

**Easy
Submission,
Quick
Publication
in 40 days**

CNS&E Associated with
Crossref (USA) to use its
Global Network for DOI in
Google Scholar & other
citation platforms.

**CNS&E Editorial Board Comprises of Globally Renowned S & T
Luminaries & Advisory Support from World Top Institutes' Leaders**

Current Natural Sciences &
Engineering (CNS&E), a bimonthly
journal, publishes new, innovative
and cutting-edge research in:

- Natural Sciences
- Health Science
- Nuclear science
- Agricultural Science
- Environmental Science
- Nanomaterials
- Hydrogen Energy
- Net Carbon Zero
- Industrial R&D
- Engineering & AI

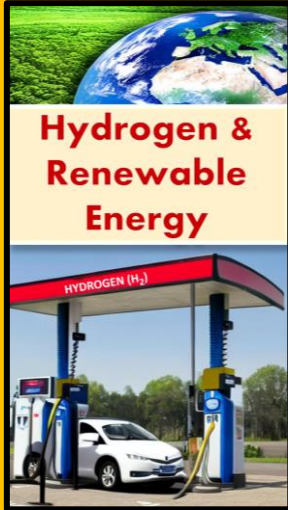
**No Article Processing
Charges !!!
For 3 months**

**The Most
Valuable & Biggest
Journal on
New Science
from India**

A Unique Platform to Boost your Research Impact Globally !

CNS&E

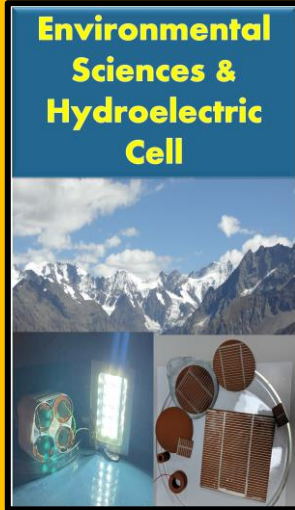
Current Natural
Sciences &
Engineering



Hydrogen & Renewable Energy

HYDROGEN (H₂)

A collage featuring a green globe, a hydrogen fuel station with a car, and a blue hydrogen tank.



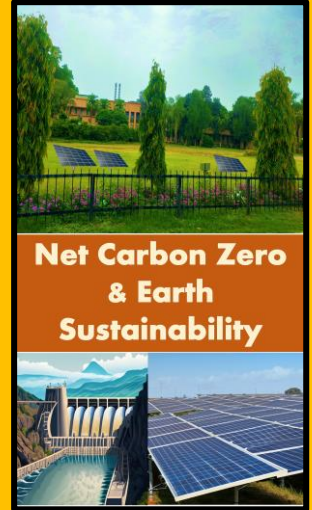
Environmental Sciences & Hydroelectric Cell

A collage showing a mountain range, a hydroelectric dam, and various scientific equipment like a microscope and a fan.



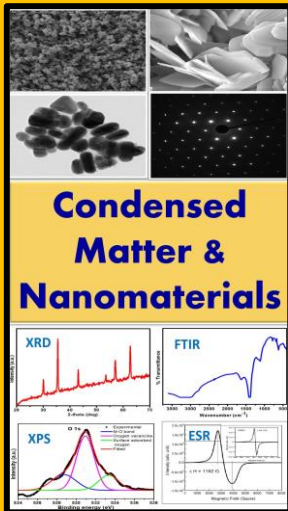
Artificial Intelligence Convergence in S&T

A collage featuring a robotic hand, a futuristic cityscape, and a glowing human head with neural connections.



Net Carbon Zero & Earth Sustainability

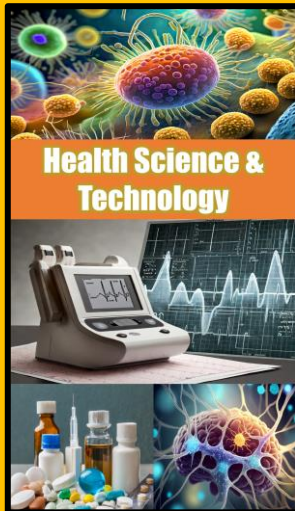
A collage showing a green landscape with solar panels, a dam, and a large solar farm.



Condensed Matter & Nanomaterials

XRD FTIR XPS ESR

A collage of microscopic images, chemical structures, and scientific graphs.



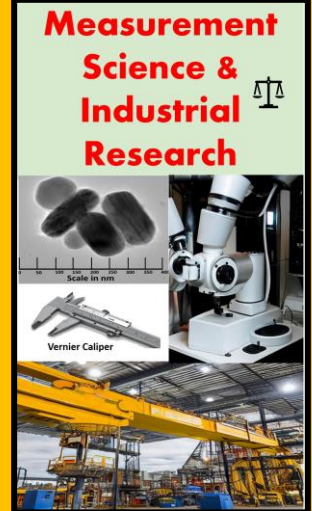
Health Science & Technology

A collage of colorful cells, a medical monitor, and various pharmaceutical bottles.



Nuclear Science: Health & Society

A collage of a nuclear explosion, a particle detector, and a medical scanner.



Measurement Science & Industrial Research

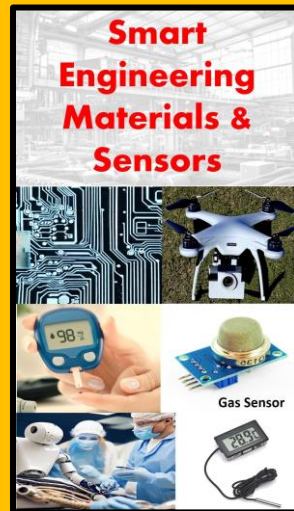
Scale in mm Vernier Caliper

A collage of industrial machinery, a microscope, and a vernier caliper.



Digital & Sustainable Agriculture

A collage of a farm with digital icons, a tractor, and a field with irrigation equipment.



Smart Engineering Materials & Sensors

Gas Sensor

A collage of a circuit board, a drone, a gas sensor, and a person in a lab.